Assessing and Enhancing the Functional and Structural Maturation of Human Pluripotent Stem-Cell Derived Cardiomyocytes with Engineered Microenvironments

Marita Lynn Rodriguez

A dissertation submitted in partial fulfillment of the requirements for the degree of

Doctor of Philosophy

University of Washington
2015

Reading Committee:
Nathan J. Sniadecki, Chair
Charles E. Murry
Per G. Reinhall

Program Authorized to Offer Degree:
Mechanical Engineering

University of Washington

Abstract

Assessing and Enhancing the Contractile and Structural Maturation of Human Stem-Cell Derived Cardiomyocytes with Engineered Microenvironments

Marita Lynn Rodriguez

Chair of Supervisory Committee:

Professor Nathan J. Sniadecki

Department of Mechanical Engineering

There is great potential for human pluripotent stem cell derived cardiomyocytes (hPSC-CMs) to serve as a test bed for developmental, pharmacological, and regenerative studies. These cells can serve as therapeutic agents, which can be implanted into damage heart tissue to supplant dead cells. They can be used to assess new pharmacological treatments for heart disease. Moreover, they can be used as model systems to study the progression of developmental and pathological states of the heart. However, upon differentiation into cardiomyocytes, these cells are distinctly immature i.e. their cell size, shape, cardiac-specific markers, ploidy, nucleation, calcium handling properties, action potentials, contractility, metabolism, etc. more closely mimic that of an embryonic-stage cardiomyocyte. Therefore, in order for these cells to serve as a valid replacement or model for more developed cardiomyocytes, their structural and functional maturation must be assessed and enhanced. One of the most important functional characteristics of a cardiomyocyte is its ability to produce contractile forces. Therefore, having the ability to quantify this contraction would provide a powerful assessment tool for hPSC-CMs. Arrays of micropost have previously been employed as a means to measure the isotonic contraction of cardiomyocytes. In this work, a new micropost

technique was developed in order to allow for real-time measurements of hPSC-CM contractility, to enable contractile assessment under various different culture conditions. Previous studies with immature cardiomyocytes have shown that a number of different methods are able to enhance their contractile and structural maturation. Here, hPSC-CM maturation was achieved via: i) prolonged cell culture, ii) cell alignment, iii) controlling cell-cell contact between adjacent cells, iv) altering substrate stiffness, v) electrically-stimulating the cells, and vii) treating the cells with various different biochemical agents. Assessment of hPSC-CM structural maturation was achieved by immunofluorescent analysis, while high speed imaging of micropost deflections and fluorescent calcium transients was used to quantify functional maturation. Through these studies, I found that the micropost assay is capable of accessing the contractile state of immature human cardiomyocytes, which makes it a powerful tool for developmental studies, pharmacological screening, and disease modeling applications. Furthermore, the pro-maturation environment that I developed was able to elicit cardiomyocyte maturation in the absence of any biochemical cues. Ultimately, I believe that these novel culture and analysis techniques will provide future researchers with a means to culture large populations of rapidly matured stem cell-derived cardiomyocytes, in order to effectively perform developmental, pharmacological, and therapeutic studies in a more rapid and high-throughput manner.

This dissertation is dedicated to the members of my family, and my dear friends, whose unwavering support was integral to its completion.

TABLE OF CONTENTS

LIST OF FIGURES

LIST OF TABLES

AIMS OVERVIEW

AIM 1 Development & Optimization of Engineered Platforms

1.1 Development of a Platform to assess hPSC-CM Contractility

A micropost bioreactor that enables the measurement of single-cell hPSC-CM contractility was designed and fabricated. As an initial assessment of this system, human iPSC-CMs were seeded onto microposts stamped with laminin, fibronectin, or collagen IV, to determine differences in their attachment, cytoskeletal structure, and contractility on different ECM proteins.

1.2 Development of Pro-Maturation Tissue Culture Environment for hPSC-CMs

A tissue culture environment capable of producing large populations of mature hPSC-CMs was developed using standard laboratory practices and equipment. This environment was designed to allow for studies assessing the simultaneous effect of substrate stiffness, cell alignment, cell-cell contact, and electrical stimulation on hPSC-CMs. To determine the ability of this system to effectively deliver each of these stimuli, the structural and functional properties of hESC-CMs cultured within this environment were assessed following a week of culture.

AIM 2 Studies on the Effect of Biomechanical Manipulations on hPSC-CM Maturation

2.1 Prolonged Cell Culture

To determine the effect of prolonged culture on hPSC-CM maturation, cells that were growing in culture for 20, 70, and 100 days post-differentiation, were seeded onto arrays of microposts for contractile analysis. These cells were also fixed and stained to determine differences in their cytoskeletal structure. This data was then investigated for temporal trends in maturation, to assess the rate of hPSC-CM development in stagnant culture.

2.2 Stiffness

To determine the effect of substrate stiffness on hPSC-CM maturation, flat PDMS surfaces with stiffnesses spanning the range of 5 kPa to 101 kPa were fabricated and stamped with unpatterned regions of laminin. Human ESCs were then seeded onto these surfaces and cultured for one week. Following this, the cytoskeletal structure of single cells was assessed to determine the optimal stiffness for promoting the structural maturation of hPSC-CMs. Additionally, live calcium

transients of single cells were analyzed to assess the effect of substrate stiffness on their calcium handling properties.

2.3 Alignment

The effect of forced alignment on hPSC-CM maturation was assessed by microcontact printing optimal-stiffness PDMS surfaces (determined in Aim 2.2) with 12 μm, 18 μm, and 24 μm wide lines of laminin. The same cell line used in Aim 2.2 was utilized here. Following a week of culture, the structural characteristics and calcium transient properties of single cells were assessed to determine the optimal pattern width for promoting hPSC-CM maturation.

2.4 Cell-Cell Contact

A high seeding density was used to obtain one cell-wide strips of aligned cells on top of soft PDMS surfaces with the optimal stiffness and ECM pattern width (discovered in Aims 2.2 and 2.3, respectively). After one week of culture, groups of cells were analyzed for the same properties listed in Aim 2.3, to determine whether cell-cell contact led to improvements in cardiomyocyte maturation.

AIM 3 Studies on the Effect of Biochemical Manipulations on hPSC-CM Maturation

3.1 Thyroid Hormone Supplementation

The effect of triiodothyronine (T3) treatment on the contractile maturation of hiPSC-CMs was determined by culturing the cells on top of arrays of microposts, in T3-doped medium. After allowing the cells to culture in T3 for a week, they were transferred to the micropost bioreactor for contractile analysis. To determine differences in contractile properties, the total twitch force, time to peak contraction, time to 90% relaxation, and total twitch duration were analyzed.

3.2 AMPK Activation

The effect of AMPK activation on the contractile maturation of hiPSC-CMs was determined by culturing the cells on top of arrays of microposts in AICAR-doped medium for one week. Following these treatments, the cells were transferred to the micropost bioreactor for contractile analysis. The effect of AICAR treatment was determined by quantifying total twitch force, twitch force per post, passive tension, beating frequency, and cell spread area.

3.3 Let-7 Overexpression

The micropost assay developed in Aim 1.1 was used to assess the contractile properties of hESC-CMs that were matured via viral-mediated overexpression of the let-7 family of miRNAs. To achieve this, the hESCs were transduced with a lentrivirus containing an empty vector, let-7i, or let-7g during the differentiation process. These cells were then seeded onto arrays of microposts for contractile assessment. Here, differences between treated and non-treated cells were determined based on total twitch force and twitch frequency.

INTRODUCTION

Heart Disease

Heart disease is currently the number one cause of death worldwide [3]. In the United States alone, 83 million Americans receive treatment for cardiovascular diseases annually, and over 600,000 of these patients die each year [4, 5]. Furthermore, the collective cost to treat patients with heart disease is estimated to be over $312 billion per year, and this number is expected to reach $1.48 trillion by 2030 [4]. Heart failure is the general name given to a wide variety of disease phenotypes associated with the cardiovascular system, and can be defined as a state in which the heart is unable to provide sufficient cardiac output to the rest of the body, in order to maintain unassisted life.

The primary cause of heart failure is a myocardial infarction i.e. heart attack. A myocardial infarction occurs when the coronary arteries that supply blood, oxygen, and nutrients to the heart, become obstructed. The resulting ischemic environment often triggers cell death [6], and due to the low regenerative capacity of myocardial tissue, this damage is generally too severe to be naturally remedied. Instead, mechanisms to restore heart function involve the hypertrophy of surviving cardiomyocytes, proliferation of fibroblasts, and replacement of the damaged area by a fibrotic scar, which has high electrical and mechanical resistance. Normal synchronous heart function relies upon the uninterrupted flow of ions from one cardiomyocyte to another, as well as a strong mechanical connection between adjacent cells. However, the presence of this scar often interrupts cell-cell signaling within the fibrotic region of the heart, which can result in heart arrhythmia. This scar also reduces the pumping efficiency of the heart, because its high stiffness resists wall motion and takes the place of healthy cardiomyocytes [7]. Ultimately, these properties often lead to irreversible heart failure.

Genetic cardiomyopathies are another source of heart failure. These cardiomyopathies are caused by inherited mutations, and can result in one of a number of different cardiovascular disease phenotypes. In general, these phenotypes can be roughly classified: as dilated cardiomyopathy (DCM), hypertrophic cardiomyopathy (HCM), arrhymogenic cardiomyopathy, restrictive cardiomyopathy (RCM), left ventricular noncompaction cardiomyopathy (LVNC), a cardiomyopathy associated with muscular dystrophy, or as one of the many unclassified cardiomyopathies [8]. Although there are some distinct differences between these phenotypes, they can all eventually lead to heart failure.

Currently, the only completely effective treatment for heart failure is a heart transplant, but the number of donor hearts is highly limited. Furthermore, heart transplants from donors that are not genetically related to the patient necessitate the use of immunosuppressive drugs to prevent rejection, which are not always effective. Additionally, while advances in pharmacological and interventional approaches for treating heart diseases have significantly reduced the number of associated morbidities, these treatments are unable to directly reverse injury to the heart. Consequently, the underlying damage or source of damage is still present, likely to necessitate prolonged treatment, and could eventually lead to further malicious health events. Therefore, there is a great need for innovative platforms to investigate the mechanisms that govern the progression of heart disease, as well as novel therapeutic means for reversing the damage caused by its progression.

Human Stem Cell Derived Cardiomyocytes

Investigators have used human cardiomyocytes derived from stem cells as a model system to study the developmental and pathological states of the heart at the cellular level [9-

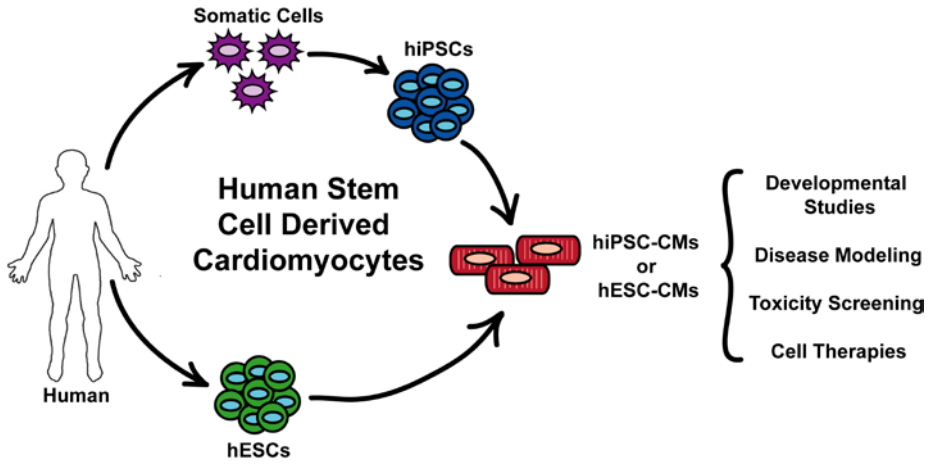

Figure 1 Uses for hSC-CMs.

13]. hSC-CMs have also been used to screen new pharmacological treatments for heart disease [9, 10, 14]. In addition, recent findings suggest that hSC-CMs, when infused or injected into damaged heart tissue, can partially restore heart function by supplanting the dead or diseased tissue [13, 15-21]. Therefore, the applications for hSC-CMs in cardiovascular medicine are vast (Figure 1). The following sections of this work go into further detail on this subject.

Developmental Studies

During human embryonic development, the heart is the first organ in the body to form [22]. This process is initiated when stem cells within the body commit to one of the three major germ lines i.e. endoderm, mesoderm, and ectoderm. Heart progenitor cells committed to the mesoderm line differentiate into embryonic cardiomyocytes, which then form a linear heart tube [23-25]. Subsequent looping of this tube forms the primitive heart structure. The heart then forms its septum, valves, and chambers, as well as it grows in size to accommodate the pumping demands of the developing heart [23]. This growth continues to occur until the heart has reached its fully developed adult state. Many of these processes are governed by mechanical stimuli, as well as they result in changes to the mechanical properties of cardiomyocytes within the heart.

Mechanical stress, strain, fluid shear, and pressure have all been found to contribute to the formation of the heart. In the early stages of cardiac development, there are rapid increases in blood flow and pressure in order to meet the demands of the growing embryo [26]. At the same time, a number of structural changes occur, which impart stresses and strains to the cells [27, 28]. In fact, bending of the heart tube is thought to be driven by mechanical forces [25]. Additionally, heart valve formation has been shown to coincide with increased fluid shear stress and mechanical strain [29-31], as well as hemodynamic forces play an important role in ventricular separation [24]. Alternatively, in the mature heart, mechanical stimuli can result in changes to overall heart function. Experimental results indicate that pressure overload results in an increased wall thickness, while volume overload leads to an enlarged ventricular cavity [23]. Therefore, determining the direct relationship between these stimuli, and corresponding changes to the heart, would lead to important insights regarding the environmental and genetic perturbations that govern normal heart development, as well as those that lead to cardiac remodeling.

During the process of heart development, individual cardiomyocytes grow in size, remodel, and undergo shape changes [23]. Therefore, assessing the mechanical properties of these cells gives

insight into their current developmental state, and this information could be used to distinguish between populations of hSC-CMs from different developmental backgrounds i.e. cells of different ages, cells from different differentiation protocols, cells originating from different cell lines, etc.

Disease Modeling & Disease Risk Assessment

The direct observation of cardiomyocyte structure and function on the microscale is essential to understanding the underlying causes and eventual outcomes of genetic heart diseases. However, biopsies from the diseased human heart can only be obtained via an invasive surgery, and because these cells do not multiply in culture, they can only be used for a limited number of experiments. Alternatively, the end-state of the heart can be investigated following patient death in autopsy. But, neither of these routes allows for sequential assessment of resident cardiomyocytes, which is required in order to expose temporal changes in cell properties.

Previous research has found that iPS derived cardiomyocytes from patients with cardiovascular diseases bear disease traits [32-37]. Therefore these cells could be used as a “disease in a dish” platform, to determine differences in the mechanical, biochemical, and electrical properties of cardiomyocytes with genetic mutations. Additionally, if researchers are able to determine early indicators of a pathogenic mutation, then it is possible that these markers could be screened for, and used to determine one’s risk of developing heart disease, years prior to the appearance of obvious symptoms. Using this technique, if a patient is determined to have a moderate to high risk of developing heart disease, precautionary steps could be taken in order to maintain the health of this patient’s heart.

Toxicity Screening

Toxicity testing is a common practice used in clinical testing to reveal all the potential side effects of a treatment, prior to its dissemination to the general population. This kind of testing is generally performed in vitro on small scale model organisms i.e. cells or small tissues, prior to being tested in a whole body. This is due to the lower cost, higher availability, and higher throughput of these platforms. Specifically, when testing the effect of a treatment on heart function, these studies are often initially performed on individual cardiomyocytes, since they are the primary functional building block of the heart. However, there is a very limited number of human cardiomyocytes available for these studies, as healthy human cardiomyocytes are only available via tissue biopsy

from an invasive heart procedure, or in the very rare case that a donor heart is not being used for transplant. Additionally, cells taken from a patient with impaired heart function are unlikely to act the same way in culture as those taken from a healthy human heart. Depending on how the donor patient died, cells taken from a donor heart may not either.

Due to this lack of human models, testing is most commonly performed in animals, or on animal organs/tissues/cells. However, since there are differences in the normal function and genetic makeup of these cells, as compared to human cardiomyocytes, it is unlikely that will respond to treatments in the same way. Therefore, determining the precise effect of candidate drugs or treatments on human heart or cardiomyocyte function is nearly impossible with animal models. Alternatively, mature cardiomyocytes derived from human cells could serve as a potentially unlimited source of human cardiomyocyte models, which could be used as a test bed to screen potential new drugs or treatments.

Recent reviews have discussed the utility of hSC-CMs for drug screening applications [38]. Overall, these studies have found that hSC derived cardiomyocytes are able to consistently respond to a large panel of therapeutic compounds, in a similar manner as has been seen on a larger scale in the whole heart. However, certain responses in hSC-CMs do not recapitulate those found for mature heart tissue. Therefore, these cells must first be matured to a developmental state more akin to those found in the adult human heart, in order to serve as a better test platform for treatment screenings.

Cell Therapies

A stem cell therapy can be defined as the injection, implantation, or infusion of stem cells, or cells derived from a stem cell source, into the myocardium; with the aim of improving heart repair and function. In general, the cell therapies used to treat heart disease are intended to elicit therapeutic paracrine signaling within the host myocardium, or to supplant cells that were killed during the progression of the disease. Thus, the optimal cell population for treating heart disease will be obtainable in a non-invasive manner, easy to isolate, abundant in source, able to proliferate in culture, efficiently differentiated along the myocyte lineage, able to survive in the ischemic environment of the heart, etc.

Studies which have assessed the therapeutic effect of implanting or infusing human stem cells into the myocardium have found that when used in models of myocardial infarction, these cells can result in enhancements to local cardiomyocyte cell survival, heart function, wall thickness, and microvessel densities [39-41]. However, there has also been some evidence that both human embryonic and iPS derived stem cells can lead to tumor formation if delivered to the heart in their stem cell state [42, 43]. Alternatively, if these cells are first differentiated into cardiomyocytes, and then implanted into an MI animal model, they have been shown to engraft with the host myocardium, mature within the heart, reduce the size of the fibrotic scar, attenuate ventricular remodeling, and lead to enhancements in cardiac function [44-50]. However, these results were found to be time-dependent – with the therapeutic benefits decreasing over time – likely due to large-scale death of the implanted cells over time. Studies that have examined the long-term effect of hSC therapies have found that functional improvement is generally only sustained for a period up to around 12 weeks [46].

In order for cell therapies to be truly effective, the rate of functional engraftment of the cells into the host tissue must be improved. Functional engraftment entails the biochemical and biomechanical coupling between implanted stem cells and native host cells. Without adequate cell-to-cell integration, implanted stem cells can only deliver improvements to heart performance via paracrine mechanisms, which are generally transient in nature, and unlikely to be adequate enough to alleviate the damage caused by extensive cell death [51, 52]. Furthermore, the presence of non-fully-integrated cells could lead to heart arrhythmias. Therefore, an effective cell therapy requires a cell type that is able to differentiate into a cardiomyocyte, and electromechanically couple with other cardiomyocytes within the myocardium.

It has been hypothesized that improved engraftment requires a closer match between the mechanical characteristics of the implanted hSC-CMs and the host cardiomyocytes [53, 54]. Adult cardiomyocytes are rigid, elongated, brick-shaped cells that have a high level of cytoskeletal organization and produce strong, unidirectional contractile forces. Alternatively, hSC-CMs are malleable, round, poorly spread, have highly unorganized cytoskeletons, and produce weak, unaligned contractile forces [53, 55]. Therefore, in order for hSC-CMs to serve as an effective treatment for heart disease, it is suggested that these cells first be matured to an optimal level of structural and contractile maturation, prior to implantation. However, dissociated adult

cardiomyocytes have proven to have problems reforming cell-cell contacts [56], which makes them a poor therapeutic for treating damage to the heart. Therefore, these cells should malleable enough that they are able to attach and engraft with their new host environment, but mature enough that they are able to meet its functional demands.

Sources of Human Stem Cells

There are various different sources of human stem cells, including: bone marrow mononuclear cells, skeletal myoblasts, cardiac stem cells, embryonic stem cells, induced pluripotent stem cells, and cells resident within the heart itself. The benefits and downsides to each of these potential cell sources are discussed in this section of the dissertation.

Bone Marrow Mononuclear Cells

Bone marrow mononuclear cells (BMMNCs) are cells that are derived from a patient's bone marrow cell aspirate. This aspirate contains hematopoietic stem cells, mesenchymal progenitor cells, endothelial progenitor cells, and various other cell types [57]. Hematopoietic stem cells are multipotent, and can differentiate along the myeloid lineage (blood cells), or the lymphoid lineage (lymphocytes) [58]. Similarly, mesenchymal stem cells are also multipotent, but have a broader range of different cell types that they can differentiate into i.e. bone, cartilage, marrow, muscle, adipose tissue, and connective tissue [59]. Alternatively, endothelial progenitor cells – which could come from either of these multipotent lines – generally only differentiate into endothelial cells [60]. Treatments that use a combination of these cell types, or these individual cell components, have both been used to treat MI.

In vitro, researchers have demonstrated that hematopoietic and mesenchymal stem cells can be induced to develop protein structures and exhibit genes that are specific to the cardiac lineage, spontaneously and synchronously contract, and demonstrate action potentials [61-64]. In vivo, BMMNCs have been shown to differentiate along the myocyte lineage, electromechanically couple with host cardiomyocytes, lead to new capillary formation, improve regional wall motion, and prevent remodeling of the heart wall when implanted into an animal model of MI [65-75]. However, in other in vivo studies, haematopoietic stem cells [76] and mesenchymal stem cells [77] were unable to differentiate into cardiomyocytes within the heart. Overall, these results imply that

BMMNCs are able to deliver some level of benefit in animal models but have yet to be proven as a good model of adult human cardiomyocytes.

Skeletal Myoblasts

Skeletal myoblasts, also known as satellite cells, are a population of quiescent stem cells that can be found under the basal lamina of muscle tissue [78]. Upon muscle injury, these cells have been found to proliferate, in order to help remuscularize the damaged tissue [79]. Therefore, it is possible that these cells could be differentiated along the cardiac lineage and used as a model for adult cardiomyocytes.

In vitro, these cells have been found to become elongated, striated cells, which resemble both skeletal and cardiac cells [80]. However, in general, these cells do not electrically couple with cardiomyocytes – as evidenced by a lack of gap junction proteins – nor do they differentiate into cardiomyocytes [81]. However, if skeletal myoblasts are induced to overexpress connexin 43, then the electrical coupling between these cells and other cardiomyocytes can be enhanced, albeit to a fairly small degree [82]. Therefore, on the positive side, skeletal myoblast derived cardiomyocytes are available in abundance from autologous sources and can be expanded in vitro. However, the retrieval of skeletal myoblasts necessitates an invasive procedure, as well as subsequent purification steps lead to an overall small number of total harvested cells.

Cardiac Stem Cells

Up until a decade ago, it was assumed that the heart lacks any form of regenerative capacity. However, since then, a group of cardiac stem cells has been discovered within the myocardium of the heart. These cells are identified by the positive expression of c-kit, which is an indicator of steminess [83, 84]. Upon injury or the progression of pathological states, these cardiac stem cells have been found to increase their proliferation rates in order to provide some amount of myocardial regeneration [85]. Therefore, it is likely that these cells can be differentiated into cardiomyocytes. These cells can be isolated from the myocardium via antigenic selection using antibodies for c-kit and can be expanded in culture [57, 86].

In vitro, these cells have been shown to self-renew, form cell-cell junctions, and have differentiated into both the cardiomyocyte and vascular lineages [78, 87]. Additionally, cardiac stem cells are autologous, are already committed to cardiac cell differentiation, and are a natural replacement for

cardiomyocytes. However, obtaining these cells involves an invasive operation, there is a limited supply of these cells within the heart, and it is currently unclear whether these cells add any beneficial treatment over other cell types.

Embryonic Stem Cells

Embryonic stem cells (ESCs) are found within the inner cell mass of the embryo during the blastocyst stage of development [88]. These cells are pluripotent, meaning that they can differentiate into all of the adult cell types [78]. In culture, ES cells are maintained in an undifferentiated pluripotent state by growing them on an embryonic fibroblast feeder layer [89]. In the absence of this feeder layer, ES cells will spontaneously-differentiate into an assortment of cell types. There are various different compounds that have been shown to enhance the cardiomyocyte differentiation of pluripotent stem cells, including: ascorbic acid, transforming growth factor-β1 (TGF-β1), bone morphogenic protein-2 (BMP-2), BMP-4, insulin-like growth factor-1, fibroblast growth factors, Notch, FGF, and Activin A [53, 90-92].

These cardiomyocytes have been shown to express major cardiac transcription factors and cardiac-specific genes, demonstrate myofibrillar architecture, spontaneously contract, exhibit action potentials, and electromechanically couple with cardiomyocytes in vitro [93-96]. However, there are ethical and legal issues surrounding the use of embryonic stem cells. Nonetheless, because these cells have the ability to divide infinitely, can differentiate into all of the cardiac cell types, and have already been shown to have therapeutic benefits, they still remain a viable candidate cell type to serve as a model for adult cardiomyocytes.

Induced Pluripotent Stem Cells

Induced pluripotent stem cells (iPSCs) are essentially somatic cells that are reprogrammed to a pluripotent state. The first successful demonstration of this reprogramming was performed by the Yamanaka group out of Japan in 2006 [97]. In this study, mouse embryonic and adult fibroblasts were dedifferentiated to a pluripotent state via retroviral induction of transcription factors that are known to play important roles in the maintenance of pluripotency and the embryonic stem cell phenotype (Oct3/4, Sox2, c-Myc, and Klf4). Following this initial study, another group demonstrated successful reprogramming human somatic cells to the pluripotent state (hiPSCs) via lentiviral induction of OCT4, SOX2, NANOG, and LIN28 [98]. More recently, other groups have

shown the ability to perform this reprogramming non-virally [99-101]; however, these techniques generally result in much lower differentiation efficiencies than the previously-mentioned viral methods. Since these pioneering studies, various different groups have demonstrated successful reprogramming of human somatic cells from various different sources, including other cells in skin [102], blood [103-105], fat [106], urine [107, 108], and mucosa [109], to a pluripotent state.

When differentiated into cardiomyocytes in vitro, human iPS-derived cardiomyocytes demonstrate similar cardiac gene expression, sarcomeric structure, and action potential characteristics as ESC-derived cardiomyocytes and immature cardiomyocytes, and they are able to electromechanically couple with other cardiomyocytes [110-112]. Additionally, iPS cells have a number of advantages over the previously mentioned types of stem cells. Namely, the number of different potential sources that can be used to create these cells is abundant, they can be obtained non-invasively, and they can serve as an autologous source of replacement cells. Additionally, because these cells capture the entire genetic profile of their host genome, they can be used to model genetic cardiomyopathies, and if implanted into the same host, it is unlikely that they will illicit immune responses. Despite their many advantages, methods for enhancing the purity and yield of iPS derived cardiomyocytes, for reducing the amount of time that it takes to perform this differentiation, and for classifying these cell lines will first need to be developed before iPS stem cells can meet their potential as a potential model or replacement for human cardiomyocytes.

Assessing hPSC-CM Maturation

Due to the higher number of beneficial properties of hESC-CMs and hiPSC-CMs over the other reviewed cell types, for this dissertation work I chose to focus my studies on these human pluripotent stem cell lines (hPSCs).

Cell Size and Morphology

As a cardiomyocyte matures from the embryonic to the adult state, its spread area increases, and its shape transitions from a circular to an elongated anisotropic morphology, both of which contribute to higher contractile forces (Table 1). This increase in cell size is accompanied by an increase in the number of contractile proteins within the cell [113], while the shape transition leads to an enhanced alignment and organization of these proteins [114].

Table 1 Reported morphological properties for cardiomyocytes.

Cell Age	Single or Multi	Spread Area (μm^2)	Circularity	Aspect Ratio	Sarcomere Length	REFs
Early-Stage hPSC-CMs	S M	480-1625 65-90	0.38-0.7 -	1.25 – 3.66 1.75 – 1.9	1.44-1.68 1.77 – 2.09	[115-124]
Mid-Stage hPSC-CMs	S M	~1500 ~180	- -	1.3-3 3 - 3.5	- -	[118, 119, 125]
Late-Stage hPSC-CMs	S M	1716-2500	0.28	1.35	1.81	[115, 118]
rNeonate	S M	195-2512 300 - 1280	0.3-0.55 -	1.2 - 5 1.25 – 9.2	1.69 - 2.27 2.05	[125-142]
Non-Human Adult	S	1000-4800	-	1.3-5	1.75 - 2.4	[130, 143-148]

In general, the average spread area measured for early stage stem cell-derived cardiomyocytes [115-118] is lower than that measured for an adult cardiomyocytes [143-146, 149]. Reported values for hPSC-CM spread area fall within the range of 480-2500 μm^2, while adult cardiomyocytes have average spread areas between 1000 and 4800 μm^2 (17-29 μm in diameter, and 60-140 μm in length). However, these values are dependent on the age of the cells being measured, and the environment in which they are being grown. This topic is discussed in further detail in the Aims 2 and 3 of this work.

Cell shape can be quantified via aspect ratio or circularity. The aspect ratio of a cell is simply a ratio of the cell's length to its width, while circularity measures the roundness of a cell i.e. how close the cell's projected two-dimensional shape is to a circle. Therefore, the lower the circularity value for a cell, the more elongated it is, which implies that the cell is more mature. The average circularity of early stage, stem cell-derived cardiomyocytes has previously been measured to vary from 0.38 to 0.7 [115, 117]. In general, adult cardiomyocyte morphology is reported as an aspect ratio, rather than a circularity, and has found to fall between 1.3 and 5 in vitro, depending on the stiffness of the underlying substrate [130]. In vivo measurements are closer to 7 [150].

Cardiac-Specific Structures and Markers

As a cardiomyocyte transitions from its early stages of differentiation to an adult cardiomyocyte, its transcriptional profile and protein expression panel change substantially. Transitioning from an early cardiomyocyte to a mature adult cardiomyocyte requires down regulation of pluripotent pathways and upregulation of cardiac developmental pathways, as well as the development of new protein structures, the conversion of proteins from their fetal to their adult isoform, and the reorganization of these proteins into a mature network [151, 152].

During this transition, cardiomyocytes also lose their ability to divide, which results in an increased number of binucleated cells. Previous work has found that the multinucleation percentage of early-stage stem cell-derived cardiomyocytes is around 4.2% [73], while the percentage of multinucleated cells in the adult human heart is closer to 26% [153]. Nuclei within the remaining cells, which are mononucleated, take up approximately 5% of the cellular volume [154], leaving the majority of the space for mitochondria and sarcomeric proteins.

In an adult cardiomyocyte, myofibrils comprise 50-60% of the cell volume and are arranged in parallel, giving the cardiomyocyte its rod-like shape. Myofibrils are composed of aligned sarcomeres, which are the fundamental units of contraction within a muscle cell (Figure 2). A sarcomere is composed of actin thin filaments, myosin thick filaments, and a Z-disc at either end (also referred to as Z-line or Z-band). During contraction, the overall length of a sarcomere shortens, as a result of myosin heads binding to and pulling on its neighboring actin thin filaments. This action causes the actin thin filaments to slide over the thick filaments, and generate tension in the muscle. Z-discs separate adjoining sarcomeres and are cross-linked by α-actinin proteins. Actin thin filaments are directly connected to the Z-disc, and myosin thick filaments are tethered to the Z-disc via the spring-like protein titan, which provides sarcomere elasticity.

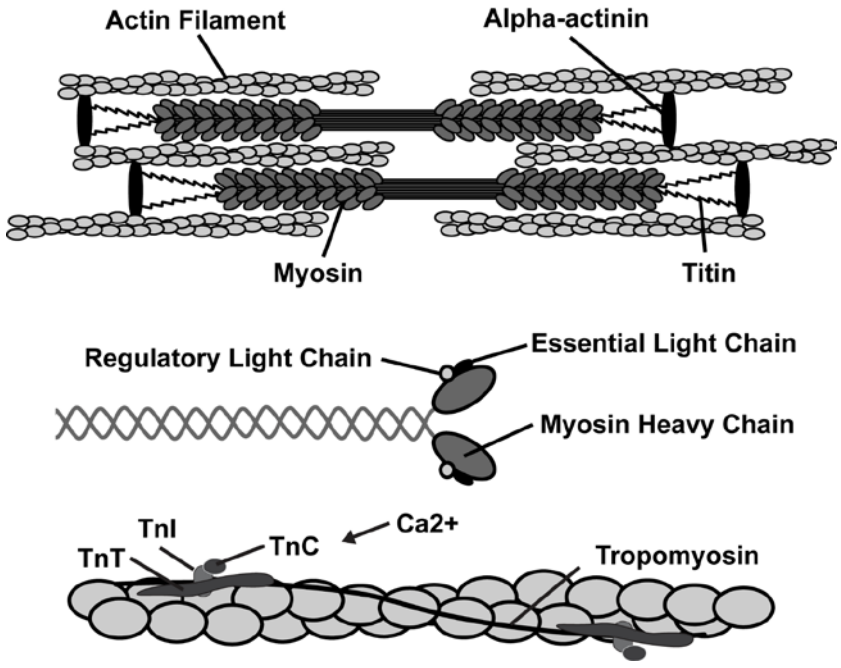

Figure 2 Cardiomyocyte sarcomeric structures.

In order to keep up with the demand of the growing heart, a number of these proteins undergo isoform switches. In the human heart, there are two isoforms of myosin heavy chain (MHC), α-

MHC and β-MHC. During all stages of development, β-MHC is the primary myosin isoform in the human ventricles, but during development the relative amount of α-MHC increases to compose approximately 35% of the mRNA levels found in the normal adult human heart [155, 156]. This isoform switch is associated with increased cardiomyocyte power output, due to an increased rate of shortening and relaxation [157]. Additionally, titin switches from its compliant form (N2BA), to a stiffer form (N2B) [158-160]. This switch increases the passive stiffness of the myocardium, which in turn leads to an increased the stroke volume [161]. Also, cardiac troponin, which governs myosin crossbridge formation, switches from slow skeletal troponin I (ssTnI) to cardiac troponin I (cTnI) during cardiomyocyte maturation, which leads to a decreased Ca^{2+} sensitivity [162-164].

During development, sarcomeres grow in length and align in the direction perpendicular to the long-axis of the cell, and the distance between parallel Z-bands increases. The increased length of these sarcomeres indicate an elevated probability of actin-myosin cross-bridge formation [165], and increased Z-band widths indicate enhanced coupling between adjacent sarcomeres [166]; both of which contribute to higher actomyosin forces. These proteins are generally qualitatively assessed via electron microscopy or immunofluorescent staining, which have found that the average sarcomere length for an early stage stem cell-derived cardiomyocytes on a flat, gelatin-coated surface is approximately 1.65 μm [115], while those measured for an adult rat fall within the range between 1.53 to 2.4 μm [143-146, 167-169].

Cardiomyocyte function is also highly dependent on the effective coupling of adjacent cardiomyocytes. In the heart, connexin-43 (Cx43) is the primary cell-cell junction responsible for transmitting electrical signals between the short ends of cardiomyocytes, while N-cadherin is the primary structural linkage between them, and serves to maintain tensional integrity and alignment of the cell cytoskeleton. In addition to being spatially co-localized, these protein structures have also been found to be functionally linked. A loss of N-cadherin interactions has been found to result in decreased conduction velocities, a loss of Cx43 expression, as well as sudden death [170]. Upon investigating the Cx43 expression in hPSC-CMs, researchers have found that it is homogeneously distributed along the cell borders between cells, and appears to have no preferential orientation [93].

In addition to these structural changes, the global mRNA expression profile of cardiomyocytes has been found to change from the pluripotent state, to a fetal cardiomyocyte, and then a mature

cardiomyocyte (Table 2). These markers can be quantified via western blotting, flow cytometry, immunofluorescence a PCR technique, or microarray analysis [171, 172]. Large-scale analyses of these mRNA profiles in adult and immature cardiomyocytes have revealed that there are over 1,311 genes that are significantly upregulated in mature cardiomyocytes when compared fetal and hSC-derived cardiomyocytes [171].

Table 2 Markers of pluripotency, fetal cardiomyocytes, and adult cardiomyocytes.

Pluripotency	Fetal	Adult
NANOG Oct4 Lin28 Sox2	Nkx2.5 GATA4/5/6 MEF2C HAND1 Isl1/2 Tbx5/20 Titin N2BA ssTnI	RYR2 βMHC >> αMHC cTnI α-actinin Titin N2B SERCA MLC2v >> MLC2a CASQ2 PLN

Calcium-Handling Properties

Cardiomyocyte contraction within the heart is primarily regulated by the synchronized storage, release, and removal of calcium from the cell. This is achieved by a spatially organized group of ion channels and exchangers, receptors, and organelles [22]. In an adult cardiomyocyte, the calcium cycle is initiated by a depolarization wave, which originates at pacemaker cells in the sinoatrial node, propagates to the atrial cardiomyocytes, and then passes to the ventricular cardiomyocytes. This depolarization causes a small influx of Ca^{2+} into the cytosol through the voltage-dependent L-type calcium channels located in transverse tubules (T-tubules) (Figure 4). This influx then triggers a larger release of Ca^{2+} from the sarcoplasmic reticulum (SR) through the ryanodine receptors (RyR2), which travels to the sarcomeres [173].

At low levels of cytosolic Ca^{2+}, the tropomyosin-troponin complex blocks the myosin-binding site on actin, which restricts cross-bridges from forming. However, high levels of cytosolic Ca^{2+} promote the binding of Ca^{2+} ions to the TnC subunit of troponin, which induces a conformal change in TnI and exposes the myosin-binding site. This allows for the initiation of the cross-bridge cycle, which progresses in a series of four steps (Figure 3). (i) ATP attached to the myosin head is

hydrolyzed, which causes the head to cock. (ii) The cocked head binds to actin and the inorganic phosphate (P_i) is released. (iii) The power stroke ensues, during which the myosin head returns to its bent (low energy) position, and thereby displaces the attached actin filament. During this process, ADP is released. Lastly, (iv) a new ATP binds to myosin, allowing it to release from actin and restart the cross-bridge cycle.

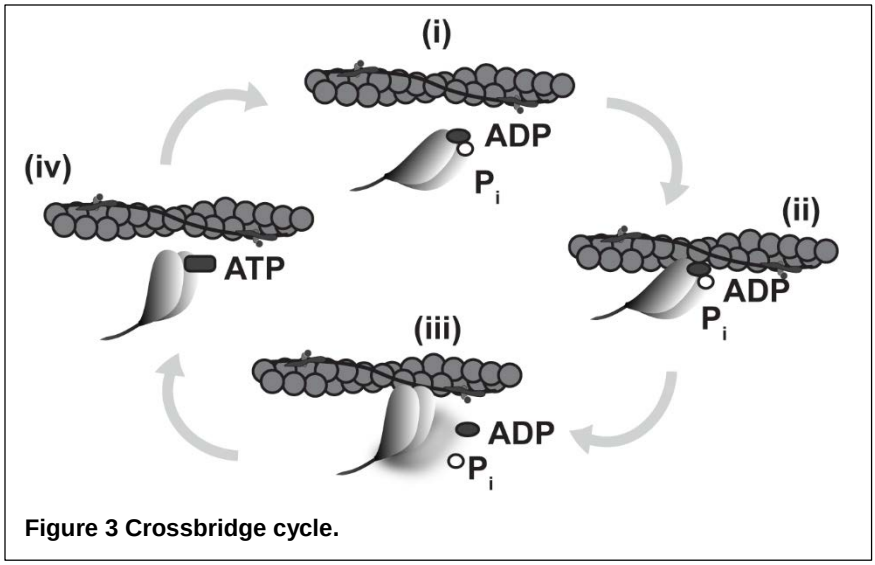

Figure 3 Crossbridge cycle.

Following contraction, a portion of the calcium is removed from the cell and returned to the SR via sarcoendoplasmic reticulum Ca^{2+} ATPases (SERCA2a), some is sent outside the cell via the Na^+/Ca^{2+} exchanger (NCX), and a small amount goes into the mitochondrial calcium uniport (Figure 4) [22]. As a consequence, Ca^{2+} concentration drops and troponin returns to its cross-bridge blocking state until the next depolarization wave occurs. Within the SR, calcium-binding proteins, such as calsequestrin, store the calcium until the next stimulation is triggered [174].

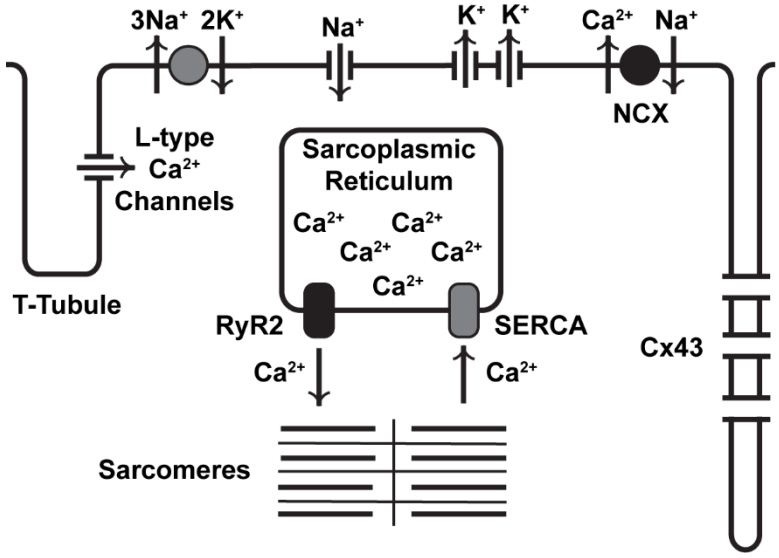

Figure 4 Cardiomyocyte ion fluctuations.

In an immature cardiomyocyte, the sarcoplasmic reticulum is not completely developed, so the cell primarily relies upon fluxes of calcium into the cell from an extracellular fluid [174-176]. Following contraction, rather than being taken up by the SR, the majority of this calcium leaves the cell through Na^+/Ca^{2+} exchangers [177].

During the progression of cardiomyocyte development, the sarcoplasmic reticulum matures, and the primary calcium source for contraction switches to the SR. Additionally, increases in cell size are accompanied with additional SERCA2a protein production, which leads to more rapid removal of calcium during the diastolic phase of contraction. Furthermore, the formation of t-tubules enable more efficient calcium transients, because these invaginations allow for depolarizations to quickly travel to all regions of a cardiomyocyte, which results in more uniform calcium wavefronts across the transverse cross-section of the cell [178].

The calcium handling properties of human cardiomyocytes can be assessed by a number of different techniques. Qualitatively, immunohistochemistry or electron microscopy can be used to visually assess the presence of calcium-associated proteins within the cell, while a western blotting or polymerase chain reaction (PCR) technique can be used to quantify the relative expression of these structures. Alternatively, calcium transients can be visualized by fluorescently tagging the calcium and imaging them via confocal microscopy, or by using a microelectrode array.

An increased presence of calcium-associated proteins and ion channels i.e. the sarcoplasmic reticulum, ryanodine receptors, SERCA2a, t-tubules, phospholamban, and calsequestrin, and a decreased presence of NCX within a cardiomyocyte suggests improvement in the cell's calcium-handling properties [177]. Studies which have qualitatively and quantitatively assessed the presence of these structures in hPSC-CMs and adult cardiomyocytes have revealed substantial differences in the prevalence of some structures, while others seem to be equally prevalent in both immature and mature cells. It has previously been reported that the expression of RyR2 in adult cardiomyocytes is approximately 1000 times that found in hPSC-CMs [179], that the expression of SERCA2a and NCX in hPSC-CMs is similar to that reported for adult cardiomyocytes [174, 180, 181], calsequestrin is either not expressed or expressed in very small quantities in hPSC-CMs [174, 180-182], and t-tubule expression is practically absent in hPSC-CMs [178].

In general, these studies have found the average amplitude, conduction velocity, as well as upstroke and decay velocities measured for hPSC-CMs (Table 3) [93, 178, 183, 184] are much lower than those previously found for adult ventricular cardiomyocytes [185]. Additionally, the calcium waveforms of hPSC-CMs are generally U-shaped while those for adult cardiomyocytes are uniform across the cell cross-section [178]. This is typical for immature cardiomyocytes with few or no t-tubules.

Table 3 Reported calcium-transient properties for cardiomyocytes.

Cell Age	Single or Multi	Amplitude (F/Fo)	Upstroke Velocity (F/Fo/s)	Decay Velocity (F/Fo/s)	TPeak (ms)	Time to 50% Decay (ms)	Time to 90% Decay (ms)	REFs
Early-Stage hPSC-CMs	S M	0.16 – 0.24 0.68	1.5 – 3.75 4.2 – 7.36	0.3 - 0.75 -	342 403 - 511	446 -	- 315 - 380	[115, 180, 182, 186]
Mid-Stage hPSC-CMs	S M	1.85 - 2.96 0.75 – 0.81	-	-	- 150 - 275	- 225 - 310	- 500 – 700	[34, 178, 182, 187-189]
Late-Stage hPSC-CMs	S M	0.24 – 0.43 -	5 – 9 6	0.8 - 1.1 -	102 -	227	-	[115, 186, 190]
rNeonate	S M	0.25 – 6 0.75 – 3.55	-	-	70 - 100 36 - 62	- 75 - 80	200 - 300 225 - 230	[114, 126, 127, 129, 134, 138, 191, 192]
Non-Human Adult	S	5.5	-	-	30 - 34	99 - 190	-	[193]

Action Potentials

The action potential cycle in cardiomyocytes consists of four stages (Figure 5). In the zero stage, a high influx of positive sodium (and some calcium) ions causes the cardiomyocyte to depolarize, and consequently, its membrane potential changes from its resting negative value to a positive one. In stage 1, the sodium channels close, and positive potassium ions begin to leave the cell. This results in a short transient repolarization and a lower positive membrane potential. Shortly thereafter, a slightly less positive plateau is reached when a large influx of positive calcium ions begins to enter the cell. The plateau is caused by a balance in the positive potassium ions leaving the cell, and the positive calcium ions entering the cell. In stage 3, the calcium ions close, and the membrane potential repolarizes back to its negative resting membrane potential, due to the continued efflux of potassium ions. And, in stage four, the resting state, the cell remains at this negative potential in until another action potential is triggered. This process has been reviewed in more detail in Nerbonne et al. [194]. There are a number of different qualitative and quantitative characteristics that can be obtained from the action potential properties of a cardiomyocyte, including: the maximum diastolic potential (MDP), the upstroke velocity, the action potential duration (APD), and the depolarization velocity. Based on these values, a cardiomyocyte can be classified as atrial, nodal, or ventricular-like.

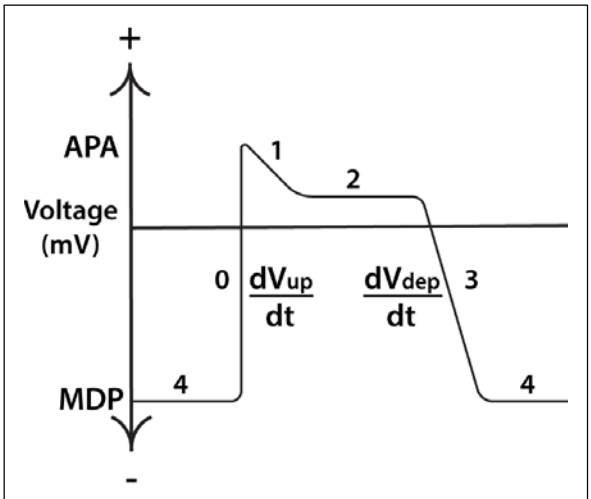

Figure 5 Action potential cycle.

Previous research has found that there are also distinct differences in these values when comparing immature cardiomyocytes to adult ones.

The action potential properties of cardiomyocytes can be measured on individual cells with a patch clamp technique [115], on cell aggregates using a microelectrode array approach [195], or on either using optical mapping. In patch clamping a micropipette is attached to the cell surface and is used to measure ion channel currents. Alternatively, a microelectrode array uses electrodes to measure changes in electrical field potential data. Lastly, in optical mapping studies, the cells are stained with a voltage-sensitive dye, contraction is inhibited to prevent signal distortion, and action potentials are imaged with a high-speed camera.

In general, these studies have found that, in comparison to adult ventricular cardiomyocytes, immature cardiomyocytes have lower negative resting potential, shorter action potential durations, and lower depolarization velocities (Table 4) [196, 197]. However, these values were also found to be highly dependent on whether the cells were isolated or in groups, whether they were spontaneously beating or paced, and the cell line studied [198].

Table 4 Action potential properties of hPSC-CMs.

Cell Age	Single or Multi	Action Potential Amplitude (mV)	Conduction Velocity (cm/s)	Upstroke Velocity (V/s)	Maximum Diastolic Potential (mV)	APD 50% (ms)	APD 90% (ms)	REFs
Early-Stage hPSC-CMs	S M	81-94.1 -	- 5– 23.6	7-44 -	-48.6 - -68.9 -	88.3-331.5 295.6	125.4 -534.6 300 - 550	[115, 120-124, 199-204]
Mid-Stage hPSC-CMs	S M	104 80 -87.9	-	- 7 - 40.5	-75.6 -48 - -64.3	- 224-241	414.7 299 - 436	[200, 205]
Late-Stage hPSC-CMs	S	113.2	-	188.7	-68.2	87	188.9	[110, 115]
rNeonate	M	-	15 – 37.2	-	-	25 - 170	60 - 175	[114, 129, 136, 206, 207]
rAdult	S	96.8 – 140	-	200-300	60 – 85	-	211.1– 513.6	[184, 208-214]

Bioenergetics and Metabolism

The primary chemical energy substrate used by cells is ATP. ATP can be generated by glycolysis, via fatty acid oxidation, or by the direct oxidation of lactate, ketone bodies, and amino acids [215-217]. In glycolysis, glucose derived from carbohydrates, amino acids, glycerol, and lactate metabolism, are converted into pyruvate. The pyruvate can then be converted into acetyl-coenzyme A (Acetyl-CoA) in the mitochondria, and metabolized into NADH by the Krebs cycle.

Electrons from NADH then activate ATP synthesis in the electron transfer chain. Alternatively, fatty acids are derived from lipids and metabolized into Acetyl-CoA via β-oxidation. Following the fatty acid oxidation pathway, 1 mol of glucose can generate a maximum of 38 mol of ATP, whereas glycolysis can only generate 2 mol of ATP from 1 mol of glucose, making fatty acid oxidation a much more efficient energy conversion process [215].

Adult cardiomyocytes primarily obtain their energy from the oxidation of fatty acids, while immature cardiomyocytes, including stem cell derived cardiomyocytes, derive the majority of their energy from glycolysis [218]. This discrepancy has been attributed to differences in the overall number and maturity of mitochondria within adult cardiomyocytes when compared to immature cardiomyocytes. In mature cardiomyocytes, 20-30% of the cell volume is occupied by mitochondria, whereas this percentage has been observed to be much lower in immature stem cell derived cardiomyocytes [152, 154]. Furthermore, adult mitochondria are elongated and have well-developed cristae, while the mitochondria in stem cell derived cardiomyocytes tend to have a globular shape and poorly developed cristae [215]. Additionally, the mitochondria in adult cardiomyocytes are co-localized with sarcomeric α-actinin, which enhances the transfer of ATP to the contractile apparatus, while those in immature cardiomyocytes are concentrated around the perinuclear area [219, 220].

Contractility

One of the most important functional characteristics of a cardiomyocyte is its ability to produce contractile forces; therefore, the ability to quantify this contraction would provide a powerful assessment tool for performing studies with stem cell-derived cardiomyocytes. There are currently a number of different tools that have the ability to resolve micro or even nanonewton forces produced by cells. The following sections review some of these techniques which have been employed to measure cardiomyocyte contractility.

Traction Force Microscopy

Traction force microscopy was developed as a means for measuring cell traction forces in a quantitative manner. In traction force microscopy (also known as particle tracking), the cell of interest is seeded onto or within a polymeric gel substrate, along with a large number of micro-scale fiduciary beads [221]. Given a value for the elastic stiffness of the substrate, traction forces

can be estimated by tracking the displacement of the beads [222]. Assuming that an elastic, homogenous, isotropic and linear material is used as the particle substrata, the relationship between the displacement field and traction field can be determined from the material properties of the substrate material using Green's function [223].

Traction force microscopy has a number of advantages over other force-sensing assays. Because the cells of interest can be seeded on top or within the gel material, this technique can be used with both adherent and non-adherent cell types. Additionally, the material properties of the gel can be altered to expose the cells to testing environments of different stiffness. Furthermore, the variety of different bead types and sizes available for these experiments allows researchers to control the area over which the force is applied, as well as the vast range of different bead coatings that can be used for these experiments allows for strict control over cell-bead attachment. However, there are also a number of negative aspects associated with particle tracking. Namely, the accuracy of this technique is limited by a number of different properties. First, force resolution is based on optical resolution; therefore, forces that are resolved using a low resolution imaging technique will be inherently inaccurate. Second, determined cell forces are based on the accuracy of the cell's assumed stiffness, which is often based on indirect measurements. Third, resolved forces are strongly influenced by the size of the particle and fluctuations in temperature. And lastly, since bead deflections are due to the summation of multiple different point forces, traction force microscopy only gives an estimation of the directionality and magnitude of a cell's traction force at one particular point in space [224].

Cantilevers

Microneedles and the atomic force microscope (AFM) are both force measurements techniques that rely upon cantilever deflections to determine magnitudes of force. In microneedle experiments, a thin and flexible microscale cantilever is permanently attached to a cell [224]. When the cell contracts, the microneedle is deflected much like a cantilever spring. After determining this deflection, which can be done electrically [225] or optically [226], and calibrating the microneedle's bending stiffness, the applied force can be calculated from Hooke's Law.

Overall, this technique is fairly cheap and simple. However, the approach is somewhat data-limited because individual cells are tested serially and by hand, making it time-consuming for an experimentalist to reach a statistically significant set of data for their study. Development of

automated, high-throughput devices could provide a more data-rich approach [227]. Furthermore, this is a single-point and single-axis assay. That is, force information can only be determined at one location, and in a single direction.

Atomic force microscopy (AFM) is similar to the microneedle technique in that it also uses a flexible cantilever with a fine tip to measure deflections caused by cardiomyocyte contraction. However, in AFM systems, the tip is generally non-permanently attached to the cell via a protein coating, and vertical displacement of this tip is tracked by a laser with excellent measurement precision.

AFMs are sophisticated tools that can resolve piconewton forces and interrogate nanoscale structures of a cell. They can provide rich data at one discrete point of a cell at a time, but are limited in probing multiple points of a cell with high temporal resolution. Furthermore, the shape of the AFM tip, as well as the location of tip attachment, affect the nature of the force-deformation curve and biases the results of the test; therefore results are not easily transferable between experiments employing different AFMs.

Optical Detection

Perhaps the simplest of the methods used to analyze cardiomyocyte contraction is optical detection or optical tracking. In general, this is achieved by taking a phase contrast video of a contracting cell on a flat culture surface, and then manually or automatically tracking cell shortening based on the displacement of the cell extremities, sarcomeres, or inhomogenities within the cell, to infer information regarding the contractile stress produced by the cell [228]. Since its earlier uses, more robust methods for determining cell shortening throughout the entire cell have been developed to achieve results of higher accuracy [229, 230].

Due to its minimal requirements of a flat culture surface, optical tracking allows for contraction measurements in the presence of protein-mediated adhesion, cell patterning, and alterations in substrate stiffness. However, a number of assumptions must be made to calculate forces using this technique. First, unless you are using an algorithm that simultaneously tracks deflections within the entire cell, one must assume that cell is a uniform unit, which we know to not be the case, as a large portion of the cell volume is occupied by the nuclei and organelles. Second, one must assume that changes in myofilament overlap, sarcomere length, and cell length are similar throughout the

cell, which is also untrue. Third, that the contractile center of the cell, is located at the geometric center of the cell, which is only true for homogeneous cells with flat ends. And lastly, that cell motion only occurs in the longitudinal direction, which is likely not the case, especially in immature cells. Furthermore, if the culture surface is non-deformable, then the cells will undergo isometric contraction, which is not representative of their contraction in vivo.

Microposts

Micropost arrays, also known as microfabricated post array detectors (mPADs) or micropillars, are arrays of vertical cantilevers, which are used to measure traction forces at multiple locations beneath a cell. This is accomplished by tracking post deflections under a microscope, and repeating the calculations described for the cantilever systems, for each post beneath the cell.

Micropost arrays can be used to measure local traction forces, multicellular forces, cell-cell forces, and any changes to these forces due to externally applied stimuli. Furthermore, since cell structures can be visualized via fluorescence imaging, changes to these structures can be simultaneously investigated. With regard to their spatial resolution, microposts have dimensions that are on the microscale, which results in a high density of force sensors beneath a single cell. Additionally, these posts can be fabricated in a cost effective manner, as multiple identical arrays can be made from a single silicon master, and PDMS is a relatively cheap material.

However, since post deflections are optically observed using microscopy, the range of materials that the posts can be fabricated out of is limited to those that are transparent. Also, during experimentation, the researcher must choose between observing one cell with high accuracy or multiple cells with low accuracy, due to limited field of view with microscopy at high magnification. Furthermore, the non-physiological form of these substrates could stimulate cell responses that are elicited by the topology and adhesion area of the micropost landscape. Lastly, tapered side walls and/or top surfaces, posts sticking in the holes, and posts coming out of the molds with greatly reduced dimensions, are some of the difficulties that can arise during the fabrication of these microposts [231].

Cardiomyocyte Contraction

Previous studies that assessed the contractile characteristics of single stem cell-derived cardiomyocytes report twitch forces in the range of 0.1 nN to 144 nN, depending on the stiffness

of the underlying substrate, the technique used to acquire these values, the age of the cells, and whether or not the cells were electrically stimulated (Table 5) [125, 232-235]. In general, smaller twitch force are reported using an AFM, whereas the largest forces are found using traction force microscopy. Alternatively, adult rat cardiomyocytes have been found to produce twitch forces within the range of 0.73 μN to 12.6 μN [145, 146, 167, 168].

Table 5 Contractile properties of single cardiomyocytes. NR = not reported.

Assay	Pacing	Culture Surface	Stiffness (kPa)	Force (nN)	Stress (mN/mm^2)	Velocity (μm/s)	Freq. (Hz)	REFs
Early stage hSC-CMs (20-40 days)								
AFM	No	Glass	NR	0.097-0.3	-	1.06	0.95-1.5	[232, 233]
Microposts	Yes	PDMS	0.01 N/m	45-85	-	-		[234]
Optical	No	PA gel	4.4-99.7	-	3-35	-	0.28-0.6	[116]
Optical	No	Col I	NR	-	-	2	0.73	[236]
TFM	No	PA gel	NR	-	0.26-0.29	-	-	[120]
Mid Stage hSC-CMs (40-60 days)								
TFM	Yes	PA gel	4	144	0.22	6.9	-	[125]
Optical	No	Col I	NR	-	-	3	0.45	[236]
Optical	-	PEI gel		-	-	-	-	[115]
Late Stage hSC-CMs (60+ days)								
Optical	No	Col I	NR	-	-	4-7	0.73	[236]
Microposts	Yes	PDMS	0.01 N/m	45-85	-	-	-	[234]
Neonate Cardiomyocytes								
TFM	No Yes	PA gel	0.3 - 99 1-50	220-600 100-720	0.04-23 0.34	0.5-1.5 5-10	0.3-0.37 -	[116, 142, 191] [125, 126]
Microposts	No Yes	PDMS	3-15 0.065 N/m	16-189 18-146	-	3.3-5.9 -	-	[127, 128, 237] [234]
Adult Cardiomyocytes								
Cantilever	No Yes	N/A	N/A	100-5720 -	21-81 44	106-330 335-360	-	[143, 144, 148, 238, 239]
Optical	No Yes	TC dish	NR	-	-	210 – 330 330 – 360	- 0.25 - 2	[239]
Optical	Yes	PDMS	7 - 255	-	-	2.3 - 5	-	[134]

The velocity at which a cardiomyocyte can produce force is important in regulating cardiomyocyte twitch dynamics. The average twitch velocity of early stage (20-40 days post-differentiation) hiPSC-derived cardiomyocytes has previously been measured to be approximately 2 μm/s, based on optical edge detection, while the twitch velocity of mid-stage (40-60 days post-differentiation) cells was approximately 3 μm/s [236]. Alternatively, using traction force microcopy, the average twitch velocity of mid-stage hESC-derived cardiomyocytes on a 4 kPa gel was measured to be approximately 6.9 μm/s [125]. These values are compared to those obtained for adult cardiomyocytes using IonOptix (3-5 μm/s contraction velocity and 2-4 μm/s relaxation velocity),

but they are much lower than those found for adult cardiomyocytes using carbon fibers (~ 107 μm/s) (Table 5) [145]. Additionally, the twitch power produced by a cell is a measure of the heart's work rate during the ejection phase of systole. To the best of our knowledge, there have been no other previous studies that have investigated the power produced by stem cell-derived cardiomyocytes, however adult cardiomyocytes have been approximated to generate around 25 pW of power [240].

During maturation, the beating frequency of cardiomyocytes decreases from around 140 bpm to an average of 80 bpm, as well as they lose their ability to spontaneously beat [241]. This change has also been seen in older hiPSC-CMs, as compared to younger ones [118, 236]. An essential property of the adult human myocardium is also its ability to contract with more force in response to increased demands for blood supply i.e. an increased rate of stimulation [174, 242]. This property is commonly referred to as a positive force-frequency relationship. Alternatively hPSC-CMs have consistently been shown to have negative force-frequency relationships [182, 243]. It is hypothesized that this occurs because the SR releases more calcium than is acquires [174].

AIM 1: DEVELOPMENT OF ENGINEERED MICROENVIRONMENTS

1. Development of a Platform to assess hPSC-CM Contractility

1.1 Background

One of the most important functional characteristics of a cardiomyocyte is its ability to produce contractile forces; therefore, the ability to quantify this contraction would provide a powerful assessment tool for performing studies with stem cell-derived cardiomyocytes. However, assessing the contractile properties of hPSC-CMs is a difficult task. In vitro methods that have been previously used to measure the contractility of single cardiomyocytes include: magnetic beads [244], polyacrylamide gels [116, 126, 245, 246], carbon fiber deflection [145, 167, 247, 248], atomic force microscopy [233, 249, 250], optical edge detection [251, 252], flexible cantilevers [253], and strain gauges [254]. However, many of these techniques are two-point force assays, meaning that the cell is suspended between a surface and a force transducer, and twitch forces can be measured only along a single axis. Current protocols used to derive hPSC-CMs yield cells with relatively immature and unaligned cytoskeletons, which contract along multiple different directions. Therefore, two-point force assays are unable to fully capture the twitch force produced by immature cell types at each of their adhesion points. Furthermore, while adult cardiomyocytes

primarily attach to surfaces at their distal ends, immature cardiomyocytes like hPSC-CMs form integrin attachments along their basal surface [255]. Thus, a technique that limits the attachment of immature cells to two distinct regions of the cell also limits the amount of integrin attachments that these cells can form. Additionally, some of these techniques require clamping, gluing, or poking of the cell, which could affect its ability to produce force. Others are computationally complex or require mathematical estimations in order to determine twitch forces [116, 126, 245, 246].

The contractile properties of a population of cardiomyocytes have also been approximated by seeding these cells within a three-dimensional construct [256-262]. However, in this system, it is difficult to determine the actual contractile force produced by individual cells, since a portion of this contraction is lost to the rigidity of the bulk tissue and/or to through its cell-cell contacts. Moreover, due to the tightly-packed configuration of cells and extracellular matrix (ECM) within these constructs, it is only possible to determine the average mechanical properties of the cells, and the properties of unique subpopulations of cardiomyocytes are lost. Lastly, the non-planar, thick, three-dimensional environment of multicellular constructs makes it difficult to use microscopy to analyze individual cells within the construct.

Micropost arrays, also known as microfabricated post array detectors (mPADs) or micropillars, are arrays of vertical cantilevers, which are used to spatially track the traction forces produced by cells attached to their tips. Micropost arrays can be used to measure local traction forces, multicellular forces, cell-cell forces, and any changes to these forces due to externally applied stimuli, as well as they can be designed to elicit certain cell responses i.e. cell shape, cell-cell contact, [127, 128, 263-278]. Furthermore, since cell structures can be visualized via fluorescence imaging, changes to these structures can be simultaneously investigated. Therefore, in contrast to some of the previously-mentioned techniques, arrays of microposts have the ability to simultaneously assess the contractile and structural properties of cardiomyocytes, as well as the ability to control cell properties on top of the microposts.

Micropost arrays can be used to measure local traction forces, multicellular forces, cell-cell forces, and any changes to these forces due to externally applied stimuli. With regard to their spatial resolution, microposts have dimensions that are on the microscale, which results in a high density of force sensors beneath a single cell. Additionally, these posts can be fabricated in a cost effective

manner, as multiple identical arrays can be made from a single silicon master, and PDMS is a relatively cheap material. If a higher density is desired, arrays with nanoscale dimensions can be fabricated for a higher cost with e-beam lithography and reactive ion etching.

Micropost arrays have been shown to effectively measure the contractile forces produced by neonate [237] and adult rat cardiomyocytes [279, 280]. Furthermore, high speed imaging of individual post deflections by IonOptix systems has enabled the measurement of the contractile velocity and power produced by these cells [127, 281]. More recently, a modification on this platform enabled the measurement of the contractile forces produced by human embryonic stem cell-derived cardiomyocytes (hESC-CMs) [234]. These studies have established that the micropost platform is a viable means for assessing the contractile properties of various types of cardiomyocytes. Here, I demonstrate a significant improvement in micropost technology by simultaneously measuring the contractile force, velocity, and power produced by hiPSC-CMs at each of their adhesion points. This approach consists of culturing cells on arrays of silicone microposts, taking videos of their contraction, and assessing their contractile properties using a custom written MATLAB code that analyzes the position and velocity of the tip of the microposts. Cells adhered to the microposts can also be immunofluorescently stained to investigate structural markers of maturation.

Furthermore, as an initial assessment of this system, I investigated the effect that ECM protein coating has on the attachment, as well as the contractile and structural maturation, of hiPSC-CMs on microposts. The cardiac ECM is a dynamic structural entity, with the interstitium composed principally of types I and III collagens and proteoglycans; and the basement membrane surrounding the cardiomyocytes, primarily composed of fibronectin, collagen IV, laminin, entactin and proteoglycans [282, 283]. Previous studies have suggested that there are developmental differences between neonate and adult cardiomyocytes in regard to the recognition of these extracellular matrix proteins. Neonate rat cardiomyocytes have been found to attach and spread on collagen types I through V, fibronectin, and laminin [255, 284]. Alternatively, adult rat cardiomyocytes have been found to preferentially attach to laminin and type IV collagen whereas they weakly attach to fibronectin-coated surfaces and do not attach at all to interstitial collagens I and III [255, 284-286]. Furthermore, adult human cardiomyocytes, harvested from patient

biopsies, have also shown a preference for laminin-coated surfaces [287]. However, the influence that these matrix proteins have on hiPSC-CM attachment remains unclear.

2.1.2 Methods

Cell Culture

Human iPSCs derived from the IMR-90 lung fibroblast cell line (James A. Thomson, U.Wisconsin-Madison) [98] were propagated under feeder-free conditions, and high density monolayers of these stem cells were then differentiated into cardiomyocytes by sequential treatment of activin A and bone morphogenetic protein 4 (BMP4) [45], supplemented with the Wnt agonist CHIR 99021 and Wnt antagonist Xav 939. The cells were cultured on Matrigel-coated plates in RPMI medium: RPMI 1640 with L-glutamine (Gibco), supplemented with 1X B-27 (Gibco) and 1% penicillin/streptomyosin (Cellgro). This media was exchanged every other day. A large number of beating cardiomyocytes were observed in the culture approximately 14 days after induction and were studied between 40 and 70 days later. Prior to experimentation, these cells were dissociated from their culture surfaces with a solution of 0.25% trypsin EDTA (Cellgro) in Versene^{TM} (Gibco). Dissociated cells were then seeded onto the microposts in RPMI medium supplemented with 5% FBS. The following day, the media was removed and replaced with serum-free RPMI medium, which was exchanged every other day. Prior to imaging, the micropost coverslips were transferred into an Attoflour® viewing chamber (Life Technologies), and cell media was replaced with HEPES RPMI medium (Gibco). Dissociated cells were seeded onto micropost arrays at a density of approximately 500,000 cells.

Micropost Fabrication

Before making the silicone micropost arrays, master cantilever templates are made from silicon or photoresist using photolithography techniques. During this process, a photosensitive photoresist (generally SU-8) is exposed by UV light through a photomask (generally made out of chrome and glass). This UV treatment cross-links the exposed material, which makes it insoluble to the developer solution. Therefore, when the substrate is immersed in the developer, the remaining regions will wash away, leaving only the exposed structures. This master can be fabricated as either a positive (silicon microposts) or a negative replica (silicon substrate with micro-sized holes) of the post arrays.

After this silicon master, micropost arrays can be created by casting replicas of this master mold, using a silicone or thermoplastic material (Figure 6). Generally, micropost arrays are formed out of polydimethylsiloxane (PDMS), but they have also been fabricated out of polymethylmethacrylate (PMMA) [288]. When using a positive master, two casting steps are required. First, the silicone or plastic is cast off of the silicon master to create a negative mold. A second casting is then made from this negative mold to make the mPAD. Alternatively, when using a negative master, the silicone or plastic can be cast onto the silicon master to form the microposts in one step. While this single-step process eliminates the need for a second casting procedure, it has previously been found that the silicone material can become clogged within silicon holes, which leads to micropost arrays with defective posts. In order to prevent the casting material from sticking to the master wafer or negative mold, these structures must be silianized prior to these casting steps.

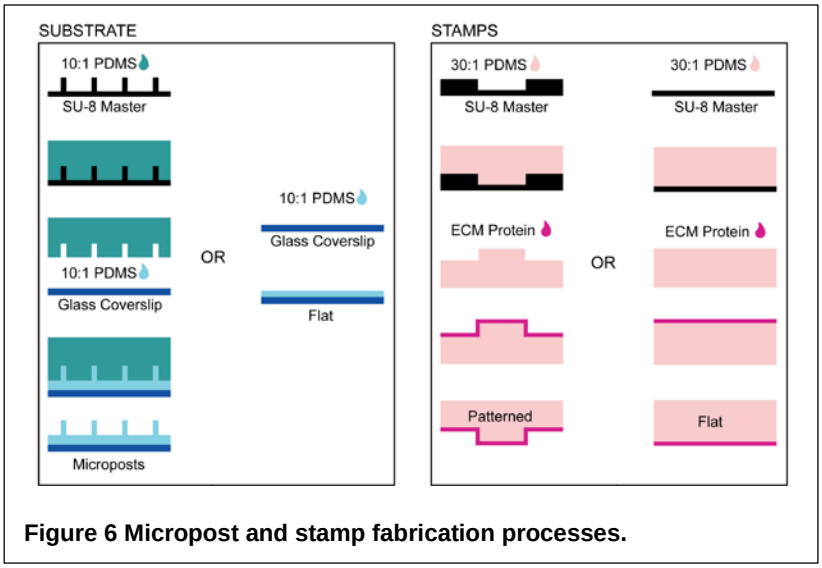

Figure 6 Micropost and stamp fabrication processes.

After making the micropost arrays, cells are attached to the tops of the posts by coating an extracellular matrix protein on their tips via a process called microcontact printing i.e. stamping (Figure 7). In the initial steps of this process, an ECM protein is allowed to absorb on a block of silicone material (called a "stamp"), while the micropost arrays are treated with UV ozone to make them hydrophilic. These stamps are fabricated in the same manner as the microposts (Figure 6). When these two surfaces are placed in contact, the protein is transferred from the stamp to the tips of the microposts. Once the ECM protein has been absorbed to the post tips, the posts are fluorescently stained such that their locations can be determined during fluorescence microscopy. After staining, the remaining surfaces of the microposts are treated with Pluronic to ensure that cell attachment is limited to the tips of the microposts, and

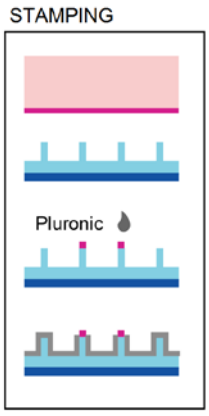

Figure 7 Stamping process.

not along their sides or base. At this point, the substrates are ready for cell seeding and experimentation [288].

For these studies, the arrays of PDMS microposts were cast onto #1 round glass coverslips, the post tips were coated via microcontact printing with either 50 μg/ml of mouse laminin (Life Technologies), human fibronectin (BD Biosciences), or human collagen IV (Millipore) [288]. Each micropost in the array used for these studies was 2.3 μm in diameter, 7.2 μm in height, and had 6 μm center-to-center spacing.

Live-Cell Imaging

A phase contrast video was taken in the optical plane at the tips of the microposts to track the movement of a post during twitch contractions, and a fluorescent image was taken at a plane where the base of the posts was in focus to establish the reference position for each post (Figure 8A). A Hamamatsu ORCA-Flash2.8 Scientific CMOS camera fitted on a Nikon Eclipse Ti upright microscope was used to acquire these images at 60× magnification using a water immersion objective. Additionally, a live cell chamber was used to maintain the cells at 37 °C throughout the imaging process.

Contractility Analysis

Approximately one week following cell seeding onto the microposts, individual hiPSC-CM muscle twitches were recorded using high-speed video microscopy. To determine micropost deflections over time, a custom-written MATLAB code was used to locate and track the centroid of each micropost, using grayscale and binary imaging tools (Figure 8B). The position of a micropost in each image frame was compared to the position of its centroid in the reference plane (Figure 8C). The difference in the position of these centroids is the deflection of the micropost at that instance in time. Figure 8D shows the position of these centroids for an individual micropost during a twitch event; where a red dot indicates the position of the bottom of the micropost, and a blue dot represents the position of the tip of the micropost. This deflection of a micropost over time can then be plotted with the same MATLAB code, and the twitch force at that micropost at a given time can be calculated by multiplying its deflection by the bending stiffness of the micropost (Figure 8E):

$$F_i = k\delta_i \tag{2}$$

where F_i is the force at a single micropost at time i, k is the bending stiffness of the post (27.83 nN/μm), and δ_i is its deflection at time i. Assuming that each micropost can be modeled as a cantilever beam that is fixed at one end, and undergoes small deflections at the other, the stiffness can be calculated using beam bending theory [288]:

$$k = \frac{3\pi E D^4}{64 L^3} \tag{3}$$

where D is the diameter (2.3 μm), E is the Young's Modulus (2.9 MPa), and L is the length (7.2 μm) of a micropost. However, if the height-to-diameter ratio of the posts is low, the spring constant used for these force calculations needs to be adjusted to account for rotation at the base of the microposts [289]. Using the same MATLAB code, the velocity of a micropost at a given time point is calculated from (Figure 8F):

$$V = \frac{\delta_{i+1} - \delta_{i-1}}{t_{i+1} - t_{i-1}} \tag{4}$$

where the subscript *i* designates the frame of the video, and *t* represents the time elapsed from the start of the video. In turn, twitch force and twitch velocity at a given time point can by multiplied together to obtain the twitch power for an individual micropost beneath the cell (Fig. 1G):

$$P = F\,V \tag{5}$$

From this data, the total force produced by a single cell was determined by summing the absolute magnitudes of the force measured at each post beneath the cell. Twitch force is calculated as the difference between the passive force, i.e. the resting tension, and the average peak force measured during each twitch event. Force per area is the twitch force divided by the spread area of the cell. The values reported for the maximum twitch velocities were determined by comparing the maximum contraction and relaxation velocities measured at each post beneath a cell, and then averaging these values across multiple beats. Values of contraction and relaxation twitch power were calculated at each time point by multiplying the force and velocity of each micropost for an image frame and summing these values for all posts beneath the cell.

Structural Analysis

After live experiments, the cells were fixed and stained in order to image their myofibril structure while still on the posts. Prior to fixing, a Triton extraction protocol was used to permeabilize the samples [127, 268]. Briefly, samples were submerged for ten seconds in a buffer containing 10 mM PIPES (J.T.Baker), 50 mM NaCl (BDH), 150 mM sucrose (J.T.Baker), 2 mM PMSF (Electron Microscopy Sciences), 3 mM MgCl (BDH), 20 μg/ml aprotinin (G-Biosciences), 1 μg/ml leupeptin (G-Biosciences), and 1 μg/ml pepstatin (G-Biosciences) with a pH of 6.5. The samples were then placed in the same buffer for two minutes, with the addition of 0.5% Triton X-100. Following Triton extraction, the samples were fixed in 4% paraformaldehyde (EMD Chemicals) in PBS. Cell nuclei were stained with Hoechst 33342 (Life Technologies) and sarcomeric α-actinin was treated with monoclonal mouse anti-α-actinin (Sigma Aldrich) and stained with goat anti-mouse AlexaFluor 488 (Life Technologies).

Once fluorescent images were taken, NIS Elements software was used to manually measure sarcomere lengths and Z-band widths, as well as cell circularity and spread area. For Z-band width analysis, at least five Z-bands were selected at random from the α-actinin stained image of the cell, and their lengths were measured using the NIS Elements 2 Points Length tool. These values were averaged to get an overall average Z-band length for each cell. Using the same tool, the average sarcomere length for each cell was determined by measuring the horizontal distance between the midpoints of two parallel Z-bands. At least two measurements of sarcomere length were measured per cell. Circularity, which is a measure of how round an object is, was calculated as follows:

$$C = \frac{4\,\pi\,A}{p^2} \tag{6}$$

where A is the area of the cell, and p is the length of its perimeter. The values for area and perimeter used in this calculation were determined by manually tracing around the image of the cell with the NIS Elements Polygon Area tool. Alternatively, cell area measurements used in the force per area calculations were taken from a screenshot of the recorded phase contrast videos (Figure 8B) to ensure proper matching between cell area and force production. Only the areas of cells with measurable beating forces were used for the overall average spread area calculation.

2.1.3 Results

Live Cell Imaging

The camera and microscopy set-up is able to record phase light images at frame rates over 100 frames per second, depending on the selected area of the region of interest (ROI). And, due to the open chamber design, micropost deflections can be imaged using either an upright or inverted microscope.

Contractility Analysis

Each twitch contraction of a hiPSC-CM has two distinct phases: a contraction phase and a relaxation phase. These phases can be seen in representative curves of the force (Figure 8E). I observed that, similar to previous studies utilizing microposts as a means to measure cell traction force, the largest forces appear at the cell's edges, and the majority of the force vectors point towards the center of the cell.

These phases are also seen in representative traces of twitch velocity (Figure 8F). From the start of the contraction phase, the contraction velocity speeds up, reaches a maximum value, and then decreases back down to zero when the maximum twitch force is reached. Here, this maximum value in the velocity is identified as the contraction velocity. Similarly, during relaxation, the cell contraction speed starts at zero, decreases to some negative maximal value, and then returns to zero until the next twitch contraction. The greatest negative velocity reached during this phase is referred to as the relaxation velocity.

Twitch power, which is the product of the twitch force and twitch velocity at each time point of the video, has a similar temporal trend as twitch velocity. Initially, the power is near zero and is

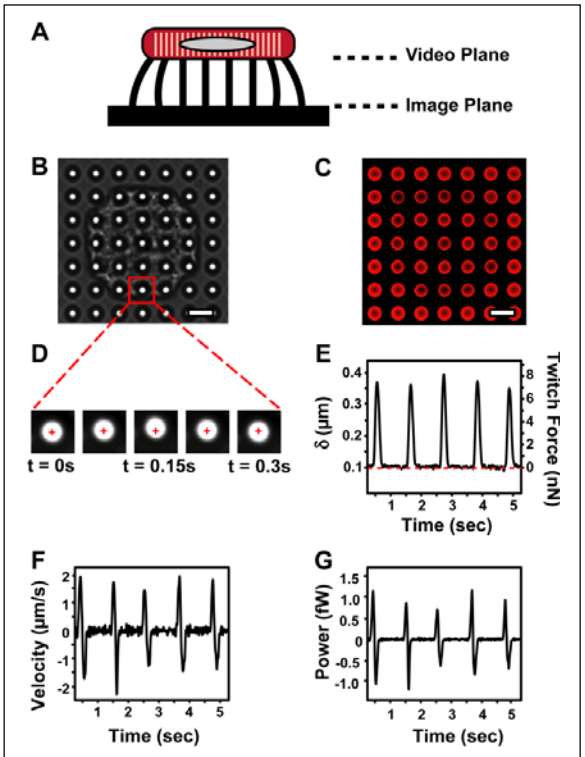

Figure 8 Live cell imaging and analysis of hSC-CM contractility. Reproduced from: Rodriguez, M.L., et al. (2014) *J Biomech Engr*. 136(5), 051005; with permission from ASME.

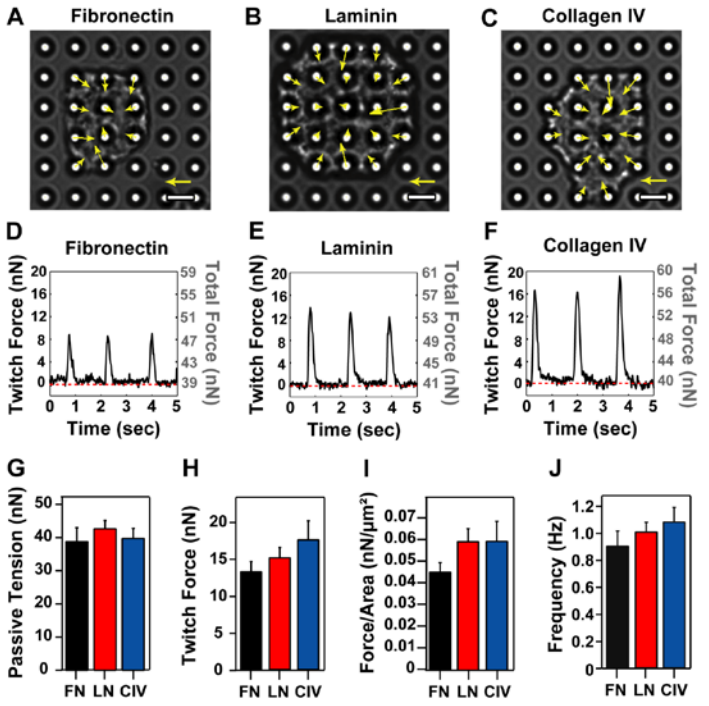

Figure 9 Force analysis of hiPSC-CMs on different ECM proteins. Reproduced from: Rodriguez, M.L., et al. (2014) *J Biomech Engr*. 136(5), 051005; with permission from ASME.

then followed by a contraction phase that reaches a maximum and reduces back down to zero. A relaxation phase follows next, where the twitch power reaches a minimum (negative) power and rises back up to zero (Figure 8G). I noted that maximum contraction power is reached after maximum contraction velocity, but prior to maximum force. Similarly, I observed that maximum relaxation power is reached before maximum relaxation velocity, but after maximum force.

Human iPSC-CMs were seeded onto micropost arrays that had been microcontact printed with fibronectin, laminin, or collagen IV. The total forces produced at each post underneath a cell were analyzed from video microscopy (Figure 9A-2C) to determine the passive tension, twitch force, force per area, and frequency of these cells. Upon investigating the passive tension i.e. baseline total force produced by cells from each of the three conditions (Figure 9D-F), I found no statistical differences between any of the ECM groups (Figure 9G). Additionally, I observed that the total force produced by hiPSC-CMs was lowest on fibronectin-stamped posts (13.34 nN), followed by laminin (15.23 nN) and then collagen IV (17.64 nN) (Figure 9H), although there were no significant differences in these values. Similarly, the force per area measured for cells on the three different ECMs were not statistically different from one another (Figure 9I). Moreover, there were no

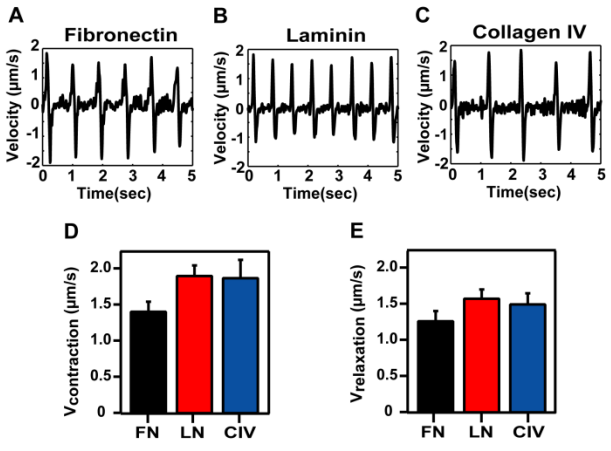

Figure 10 Twitch velocities for hiPSC-CMs on different ECM proteins. Reproduced from: Rodriguez, M.L., et al. (2014) *J Biomech Engr*. 136(5), 051005; with permission from ASME.

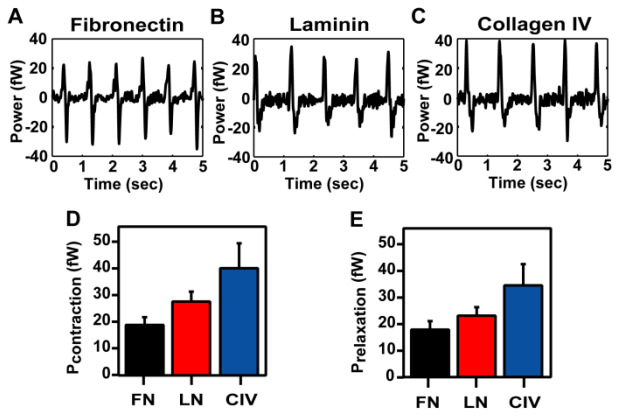

Figure 11 Power produced by hiPSC-CMs on different ECMs. Reproduced from: Rodriguez, M.L., et al. (2014) *J Biomech Engr*. 136(5), 051005; with permission from ASME.

significant differences in the spontaneous beating frequency of the cells on all three ECM proteins, although cells on laminin or collagen IV tended to have higher beating frequencies (Figure 9J).

The maximum twitch velocities for hiPSC-CMS on laminin, fibronectin, and Collagen IV stamped microposts averaged between 1.4 to 2 μm/sec for contraction and 1.2 to 1.6 μm/sec for relaxation across multiple experiments, with no significant differences in either parameter seen for ECM protein type (Figure 10D-E). Although the velocities obtained for cells on collagen IV were larger on average, the variation precluded statistical significance. Similarly, upon quantifying data obtained from power curves for cells on each of the all three ECM proteins, I found no significant differences in contraction power (averaging 19-41 fW) or relaxation power (averaging 18-35 fW). Similar to velocity, cells on collagen IV tended to produce the most power, but larger variance precluded statistical significance (Figure 11D-E).

Attachment & Structural Analysis

Upon fixing and staining hiPSC-CMs, I found that this technique is capable of resolving the sarcomeric structure of these cells on top of microposts by staining for α-actinin. Additionally, cell nucleation on top of the posts can be assessed by staining for cell nuclei.

Previously, researchers have found that early stage stem cell-derived cardiomyocytes exhibit an unspread, spherical shape when re-plated onto tissue culture surfaces, which subsequently results in a low degree of cell attachment. The effectiveness of the micropost platform is dependent on how many cells attach and spread on top of the microposts. Therefore, in order for this system to effectively yield the contractile properties of stem cell-derived cardiomyocytes, the microposts need to allow for a high degree of cell attachment and cell spreading. To determine whether the stamped protein had any effect on these properties, cell counts were taken from substrates stamped with fibronectin, laminin, and collagen IV, and the spread areas of these attached cells were

measured. On average, there were 13-20 microposts per cell (Figure 12A-C). While hiPSC-CMs attached to all three of the ECM proteins, a significantly higher percentage of cells adhered onto microposts stamped with laminin than to those stamped with fibronectin or collagen IV (Figure 12D). This same trend also held for cell spread area (Figure 12E).

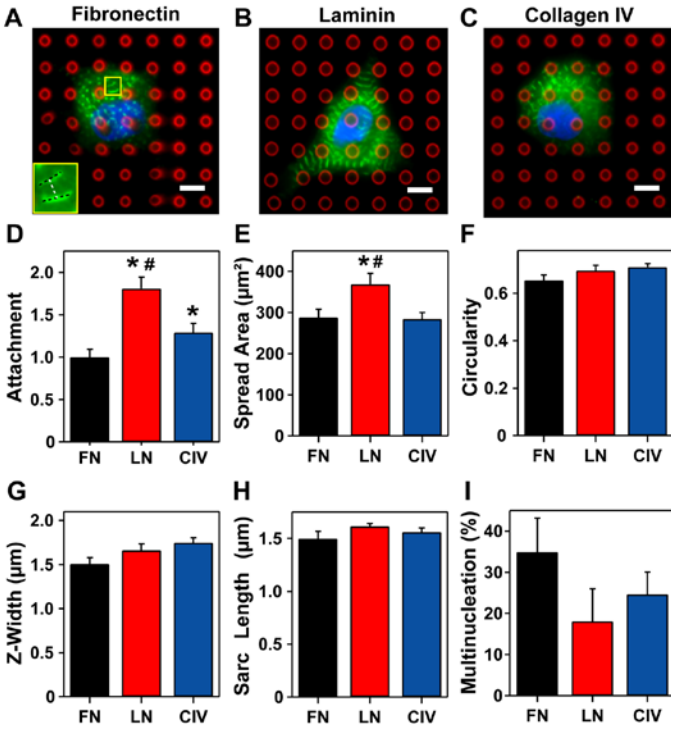

Figure 12 Attachment and structural maturation of hiPSC-CMs on different ECMs. Reproduced from: Rodriguez, M.L., et al. (2014) *J Biomech Engr*. 136(5), 051005; with permission from ASME.

As a cardiomyocyte matures, its cross-sectional area transitions from a circular to a rectangular shape. Along with this shape change, the cell's sarcomeres grow in length, becoming perpendicularly aligned to the long axis of the cell, and the spacing between parallel Z-bands increases. These structural changes lead to increases in the ability of cells to produce contractile force in accordance with the Frank-Starling mechanism [282]. Upon analyzing immunofluorescent images of cells on all three ECM proteins (Figure 12A-C), I found no significant differences in circularity (Figure 12F), Z-band width, sarcomere length (Figure 12H), or multinucleation (Figure 12I).

2.1.4 Discussion

Here, I reported the development of a platform technology for the assessment of hPSC-CM contractility. I demonstrated that micropost arrays can be used to analyze the passive tension, as well as the twitch force, velocity, and power of single hiPSC-derived cardiomyocytes; furthermore, I demonstrated that all of the posts under a cell can be analyzed with sufficient temporal resolution to determine the maxima in force, velocity, and power. Additionally, I established that this technique is compatible with immunofluorescent staining, which enables the visualization of cytoskeletal organization and maturation as well as measurements of cell hypertrophy and nucleation. Therefore, this technology could be used to determine quantifiable differences in

contractility between populations of hPSC-CMs that are from: i) cultures of different developmental states, ii) patients with heart disease, iii) different differentiation or culture protocols, iv) virally or chemically treated cultures, or v) cultures exposed to different external stimuli. Thus, this technique has the potential to serve as a very powerful tool within the field of heart mechanics. However, it is not without its limitations.

I observed that the cell area and elongation of hiPSC-CMs on microposts are reduced when compared to those on flat culture surfaces. Additionally, in its current configuration, this system does not allow for electrical stimulation which is essential to heart maturation and maintenance in vivo. Finally, because this technique relies upon optical means to track the location of posts over time, the temporal resolution of the measurements is limited by the speed of the camera used to acquire them.

When hiPSC-CMs were seeded onto microposts stamped with laminin, fibronectin, or collagen IV, I found that those cells which had been seeded onto laminin, demonstrated significantly higher attachment and spread area as well as higher contraction and relaxation velocities than those seeded onto fibronectin or collagen IV. These findings indicate that the laminin coating resulted in better adherence between the hiPSC-CMs and the microposts and may have led to enhanced contractile maturation.

Previous studies have found that cells can attach to a variety of different substrates and coatings, but only a handful of these have the right macromolecule surface to elicit long-term cell attachment and spreading [255, 284-286]. Specifically, neonatal cardiomyocytes were found to attach to collagens I through IV, fibronectin, and laminin, whereas adult cardiomyocytes preferentially adhere to laminin and collagen IV [255, 284-286]. Furthermore, adult cardiomyocytes were unable to attach to collagen I, II, III, or V, and had very low attachment on fibronectin [255, 284, 285]. Therefore, our finding that hiPSC-CMs attach and spread to a greater degree on laminin, than on fibronectin or collagen IV, support the notion that these cells exhibit some of their “adult-like” characteristics with regard to their recognition of ECM components.

Recognition, attachment, and survival of cells on surfaces coated with different matrix proteins is governed by integrins, which initiate intracellular signaling cascades and serve as physical links between the ECM and a cell’s cytoskeleton [282, 290, 291]. Integrins are heterodimeric receptors

composed of α and β subunits [292], and the pairing of these subunits results in a specificity towards different ECM proteins [291]. Cardiomyocytes primarily express β_1-specific integrins that bind to the fibronectin ($\alpha_3\beta_1$, $\alpha_5\beta_1$, $\alpha_v\beta_1$, and $\alpha_9\beta_1$), laminin ($\alpha_1\beta_1$, $\alpha_3\beta_1$, $\alpha_6\beta_1$, and $\alpha_7\beta_1$), and collagen IV ($\alpha_1\beta_1$, $\alpha_3\beta_1$, and $\alpha_{10}\beta_1$), as well as β_3 and β_5 subunits, whose specificity for these ECM proteins is largely unknown [283, 284, 290-292]. Neonatal cardiomyocytes express α_1, α_3, α_5, α_6, and α_7 chains, whereas adult myocytes have no expression of α_1, low expression of α_3 and α_6, and high expression of α_7 [284, 290, 292, 293]. Alternatively, human embryonic stem cell-derived cardiomyocytes were found to express the α_3, α_5, α_6, α_7, α_v and β_1 integrin subunits, while the α_1, α_2, α_4, and α_{10} subunits were absent [294]. Although the presence of other alpha chains in neonate and adult cardiomyocytes and the integrin expression for hiPSC-CMs have not been previously investigated, these studies indicate that integrin expression within cardiomyocytes changes during development, and suggest there are similarities in integrin expression between adult myocytes and stem cell-derived cardiomyocytes. Similar findings were discovered in the present study. However, in order to better understand the relationship between hiPSC-CMs and their underlying ECM protein, these cells should be stained for specific integrin subunits.

I found that hiPSC-CMs produced an average total twitch force of 13.3 nN to 17.6 nN, which falls within the range of values previously seen for hESC-CMs and hiPSC-CMs [125, 232-235]. Using micropost arrays, Taylor et al. found an average twitch force of around 50 nN for cells on 27 μm-diameter posts [234]. However, it is unclear whether or not these values came from single cells or groups of cells. In general, groups of cells beat with more force than single cells, so this could account for the discrepancy in values obtained by the Pruitt group and our own [233]. Nevertheless, all of these values are substantially lower than those measured for adult rat cardiomyocytes [145, 146, 167, 168]. Therefore, the contractile properties of these cells are still very immature in nature, and require further maturation to replace, or to serve as a model for, adult cardiomyocytes. Additionally, there was not a statistical difference in the forces measured for hiPSC-CMs on posts coated with different ECM proteins, neither on a basis of a twitch force nor force per area. Similarly, upon investigating the passive force produced by individual hiPSC-CMs on different ECMs, I found an average force of 40.7 nN, with no statistical differences between the three conditions. Passive force (or tension) is an important factor in cardiac muscle because it determines the extent to which the heart fills – which dictates the stroke volume – and has been shown to have an effect on cardiomyocyte shortening velocity [161]. This tension is primarily governed by the

sarcomeric protein titin, which acts like a mechanical spring, and has been found to have an altered isoform in ischemic heart disease [295, 296]. Therefore, passive tension, assessed via arrays of microposts, could be used as a means to distinguish between wild type and disease cell lines.

Using our micropost technique, I found that the average contraction twitch velocity of early-stage hiPSC-derived cardiomyocytes fell within the range of 1.4 to 2.0 μm/s, while the relaxation velocity averaged values between 1.2 to 1.6 μm/s. These values are similar to those previously found for hESC and hiPSC derived cardiomyocytes, but in general, are much lower than those found for adult cardiomyocytes [145]. I measured the average maximum contraction twitch power of early to mid-stage hiPSC-CMs to fall within the range of 19 to 41 fW, and relaxation power to be between 18 to 35 fW. I are unaware of any previous studies which have measured the power-producing capabilities of hPSC-CMs, however the maximum twitch power of neonate rat cardiomyocytes has been found to fluctuate between 75 and 200 fW [127], while adult cardiomyocytes can generate around 25 pW of power [240]. Therefore, these results further substantiate that the contractile properties of these cells are still fairly immature in comparison to adult cardiomyocytes. Furthermore, I found that the average beat frequency of hiPSC-CMs on microposts coated with all three ECM proteins was approximately equal, and only varied from 0.9 to 1.1 Hz. These findings agree with previous measurements of the spontaneous beating rate for early stage iPSC-derived cardiomyocytes, but these values are slightly higher than the spontaneous beating rate for adult cells [233, 235, 236]. However, these results should be confirmed with paced cells, to assess the effect of pacing on cytoskeletal organization and maturation, as well as on the contractile properties of these cells.

Upon measuring the spread area of hiPSC-CMs on microposts, I found that the average spread area for cells on fibronectin-coated posts was 287.62 ± 20.12 μm^2, 368.56 ± 26.34 μm^2 for cells on laminin coatings, and 284.53 ± 15.50 μm^2 for cells on collagen IV coatings. Previous studies employing micropost arrays have found that, on average, non-muscle cells spread to a similar degree on microposts as they do on flat surfaces [270]. These results demonstrate that laminin-coated posts yield cell spread areas that most closely replicate those found for early stage stem cell-derived cardiomyocytes on flat surfaces; however, these values are still much smaller than that of an adult cardiomyocyte [283]. Additionally, I found average circularities within the range 0.65 to 0.71, which are higher than values previously found for early stage stem cell derived

cardiomyocytes [115, 116], and much higher than those that you would expect for adult cardiomyocytes. This discrepancy in cell geometry could be due partially to the lower degree of spreading on microposts arrays for hiPSC-CMs and to the limited adhesive geometry of the micropost arrays. Overall, these results suggest that strategies for improving the spread area and alignment of hiPSC-CMs on arrays of microposts should be included in future research efforts in order to further enhance the structural maturation of these cells.

In our studies, I found that the average Z-band width for hiPSC-CMs was 1.51 ± 0.07 μm for cells on fibronectin posts, 1.66 ± 0.07 μm for those on laminin posts, and 1.75 ± 0.06 μm for cells on collagen IV posts. I were unable to find references to Z-band width for stem cell-derived cardiomyocytes, but the average Z-band width of a neonate cardiomyocyte has been found to vary from 2.35 – 3.84 μm, and adult Z-band widths can be even larger [127, 281]. Additionally, I found sarcomere lengths ranging from 1.5 μm to 1.6 μm, which are slightly shorter than those measured for an adult cardiomyocyte [145, 146, 167-169]. These shorter sarcomere lengths and z-band widths likely contribute to the overall lower force seen in hiPSC-CM cells, when compared to adult cardiomyocytes.

Lastly, previous work has found that the multinucleation percentage of early-stage stem cell-derived cardiomyocytes is around 4.2% [73]. We found multinucleation percentages of 35 6 8% for fibronectin, 18 6 8% for laminin, and 25 6 5% for collagen IV. In the human heart, the percentage of multinucleated cells increases from the neonatal stage to comprise approximately 26% of the cardiomyocytes in the adult human heart, while the other 74% of these cells remain mononucleated [77]. Therefore, collagen IV stamped posts yielded multinucleation percentages that most closely mimic those seen in the adult heart, while laminin coatings resulted in fewer multinucleated cells, and fibronectin coatings resulted in extra multinucleated cells. However, all of these values are much larger than those previously seen for early-stage stem cell-derived cardiomyocytes.

Overall, the results of this study suggest that future micropost experiments with this cell line should be stamped with laminin to enable the highest degree of cell attachment and spreading. If another hPSC-CM line is used, it is possible that a different protein will optimize cell attachment and spreading. Though, based on these studies, other hPSC-CM cell lines will likely attach to all three proteins, and have similar contractile properties.

2. Development of a Pro-Maturation Tissue Culture Environment for hPSC-CMs

2.1 Background

Previous studies with immature cardiomyocytes have shown that a number of different methods are able to enhance their maturation (Figure 13). Prolonged cell culture is perhaps one of the most basic techniques, as this process simply involves allowing the cells grow in culture for an extended period of time [115, 118, 236]. Alternatively, cell mechanotransduction pathways can be activated via cues such as cell alignment [114, 133, 135, 297, 298], cell-cell contact [233], substrate stiffness [126, 245, 246], applied strain [299-304] or electrical stimulation [305]. As well as a number of different pharmacological and viral biochemical agents which have also been found to enhance the maturation of immature cardiomyocytes [306-308]. These results are summarized in Table 6. However, it is important to note that some of these results are inconsistent from study to study or cell line to cell line. Therefore, the effects of some of these stimuli are still not well established, and further experiments would be beneficial to help clarify their impact on hPSC-CM maturation.

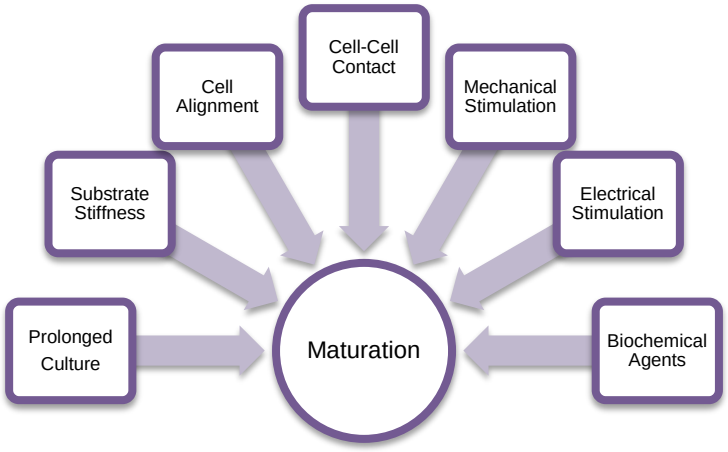

Figure 13 Techniques for enhancing hSC-CM maturation.

A small number of studies have also investigated the effect of simultaneously applying two or more of these stimuli to cells in a bioreactor type system [309-311]. These studies have discovered that combining these culture stimuli has a beneficial effect on cardiomyocyte maturation (Appendix B, Table 13). Based on these results, it is hypothesized that the proper combination of many of these techniques could be used to quickly advance hPSC-CM maturation to a more adult-like phenotype. However, the majority of current systems that are attempting to achieve this, are custom-made by individual labs, and are inaccessible to other researchers. Therefore, a single culture environment that is capable of promoting hPSC-CM maturation, and that only requires basic laboratory technologies to build, could catalyze the progress of research within the field as a

whole. The following paragraphs go over the stimuli that I chose to include in my dissertation work, the techniques that I used to achieve them, and my reasoning for these choices.

Table 6 Effect of pro-maturation stimuli on cardiomyocytes.

	Aging	Stiffness	Alignment	Cell-Cell	E-Stim
Cell Area	++	^ + ^ x	- x ^	+	+ x
Cell Aspect Ratio	+	x + x	+		+ x
Cell Alignment		x	+ +		+ x
Binucleation	+		+		
Sarcomere Length	+	+ x	x		
Sarcomere Content		^ +	^ x		
Z-Band Width		+	^ x		
Beating Frequency	-	x - x x	x x x	x -	
Passive Tension		x +			
Force/Stress	+	+ + + ^	+ ^ x	+	+
Velocity	+ +	- -	-	+	
Power		+ + x	x		
Intensity	x +	^ -	+ -		+ + -
Time to Peak	-	- x	- x -		-
Time to 50% Relaxation	-		x	+	
Time to 90% Relaxation	-	-	+ x	+	-

NOTE: + = increase, - = decrease, x = no relationship, ^ = Intermediate peak, and red = hESC-CM, blue = hiPSC-CM, and black = non-human neonate cardiomyocytes.

Prolonged Cell Culture

In the human body, it takes approximately 18 years for cardiomyocytes to reach their fully mature state. Keeping this in mind, one might expect that it would take even longer for cells grown upon a standard tissue culture dish to reach this level of maturation, due to the lack of developmental stimuli within the culture environment. Or whether it is even possible for hPSC-CMs to fully mature without these stimuli. Although there is some discrepancy from lab to lab, most differentiation protocols take around 20-30 days, from the induction of differentiation, to produce a population of beating cardiomyocytes. Researchers have found that certain properties of these cells are able to significantly mature after only an additional 30-40 days of growth [115, 236]. However, these cells are still very immature when compared to adult cardiomyocytes, which suggest that long term culture is not a clinically feasible means of achieving mature hPSC-CMs, because no one really knows how long it would take to produce these cells via this method.

Stiffness

A large range of different materials have previously been used as substrates for cell culture. However, only a handful of these are biocompatible over long periods of time, are non-degradable, are transparent, can be chemically functionalized, can be made to have a range of different

stiffnesses, can be molded into various shapes, and can be activated to interact with various different chemical groups. Two materials that meet all of these requirements are polyacrylamide (PA) gels, and polydimethylsiloxane (PDMS).

PA gels are essentially polymer networks that are swollen with water, and are made by mixing together acrylamide monomer and bisacrylamide cross-linker in a buffer solution. Polymerization of this solution is typically initiated with ammonium persulfate and tetramethylethylenediamine (TEMED), though photoactivated initiators have also been used [312]. Polyacrylamide is biologically inert and must be chemically modified to support cell attachment [313]. This functionalization is generally achieved by using UV light to initiate an additional crosslinker on the surface of the hydrogel, which covalently links proteins to its surface [314]. Following this process, protein can be attached to the surface of the hydrogel. The mechanical properties of PA gels, including the stiffness, can be tuned based on monomer concentration and crosslink density.

Although PA gels have proven a very useful culture environment for various different cell lines, they have a number of undesirable properties. Namely, for very soft substrates, cross-linking can happen very quickly, which makes it very difficult to produce a homogenous gel. And due to the complexity of the process, is also difficult to achieve identical gels with uniform protein coatings across multiple experiments. Also, most labs that work with PA gels have their own particular method for producing them, which could lead to slightly different results when comparing their work with that from another lab. Lastly, PA gels swell in cell culture media, which changes their mechanical properties, and distorts any topology or patterning applied to the gel surface [315]. Due to these reasons, PA was eliminated as a potential culture surface for my dissertation work.

PDMS is a silicone elastomer that is commercially available from Dow Corning (Sylgard 184). Like PA gels, PDMS surfaces are made by first mixing together a base (vinyl terminated polydimethylsiloxane), and cross-linker (methylhydrosiloxane-dimethylsiloxane copolymer). In order to yield a polymer that is fully cross-linked, and does not contain any extra cross-linker, it is recommended that these two components are mixed together in a 1:10 ratio (1 gram of cross-linker for every 10 grams of base). After mixing and degassing, this liquid blend will cure on its own, but is more often placed in an oven to speed up this process.

Compared to PA gel fabrication, this process is very simple, cost-effective, and generally yields identical substrates with uniform material properties. Also, Because PDMS is permeable to gas and small molecules, but not water, it does not swell upon submersion into media. Much like PA gels, PDMS surfaces of different stiffnesses can be made by altering the base to curing agent mixing ratio [134, 140, 316]. That is, more curing agent results in stiffer substrates, and less results in softer ones. However, to yield substrates with physiological stiffnesses (10-20 kPa), very little curing agent can be used. This results in a large amount of uncured oligomers in the mixture, which can leach out and be toxic to cells. However, recently researchers have shown that PDMS substrates with physiological stiffnesses (5 kPa and higher) can be made by mixing together two commercial forms of PDMS: the commonly-used Sylgard 184, and the silica-free PDMS Sylgard 527 gel [317].

Alignment

In vitro, cellular alignment can be induced by patterning the cell culture surface, or by applying an external force to the culture environment (Figure 14). Cells can be patterned by chemically limiting the adhesive area that the cells are able to spread upon or by culturing the cells on top of surfaces with topologies that induce alignment. Compressive, tensile, shear, and electrical forces have also been previously used to achieve cell alignment [318].

With regard to cardiomyocytes, both electrical [141] and tensile [319] forces have been shown to elicit cardiomyocyte alignment. However, only a portion of experiments employing electrical stimulation have found it capable of inducing cell alignment, and in these cases, the degree of alignment induced by electrical stimulation was very slight when compared to that which was achieved with the substrate pattern [320]. And, in order to expose cardiomyocytes to tensile forces, one must either attach their distal ends to support structures that are under tension, or expose the cells to applied

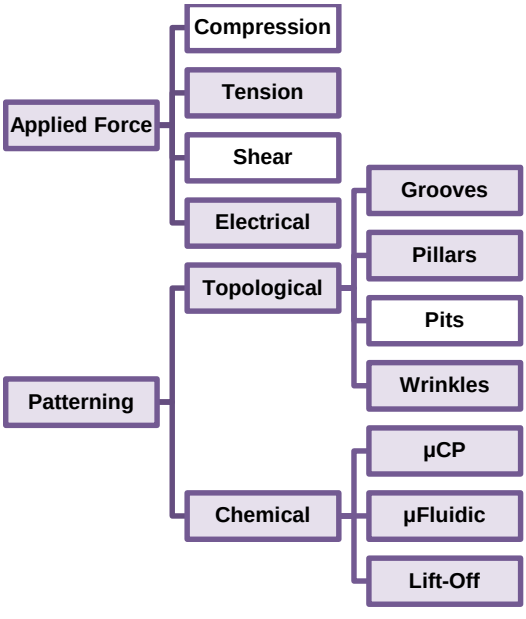

Figure 14 Methods to align cells.

strain. The former is relatively easily achieved when using three-dimensional tissue engineered constructs [321, 322], but these systems are not widely available. Similarly, because systems that expose cells to strain are expensive, many labs have opted to build their own customized systems, which are not available to other labs.

Alternatively, the adhesive area that a cardiomyocyte sees is governed by the ECM environment, which has been patterned onto flat or topological surfaces via microcontact printing [133, 135, 138, 298, 323], microfluidic techniques [311, 324], or by using a stencil [140]. And topologically, cardiomyocyte alignment has been induced by seeding cells on anisotropic surfaces with micro or nanoscale dimension grooves [136], abrasions [207, 320], pillars [234], or wrinkles [204]. Both types of surfaces are generally fabricated via photolithography, hot embossing, e-beam lithography, reactive ion etching, abrasion, laser writing, electrospinning, or a combination of these processes [141, 318, 320, 325, 326]. These processes are available at most large universities, but even so, customized “master” wafers can be ordered from various different outlets at a reasonable price, and then used for thousands of identical substrate castings.

Due to their pattern customizability, cost effectiveness, ease of use, and repeatable fabrication, grooved topological surfaces and microcontact printing are the two techniques most commonly used to pattern cardiomyocytes. Topographical elicit cell orientation by confining cytoskeletal attachment between focal adhesions in a particular orientation [327, 328]. That is, cellular orientation is achieved by confining focal adhesion molecules within the ridges of the microgrooves, since the adhesion clusters and the ridges are on the same order of magnitude (1-2 um). Previous have found that subcellular topographical patterns with dimensions around 800 nm in width are most efficient at eliciting enhanced cellular alignment and maturation towards the adult phenotype [117, 136]. Past a pattern width of approximately 10 μm, cardiomyocytes will migrate down into the pattern band, rather than sitting on top of it [320, 326], and will align in patterns with widths up to 80 μm. Additionally, surfaces with deep features result in more alignment than those with shallow ones [320, 325, 326].

Alternatively, in microcontact printing, If this technique is used as a means to induce cell alignment, it has been observed that this patterned area must be given an aspect ratio of at least 3:1, in order to yield cells with anisotropic sarcomere alignment [133, 135]. Furthermore, if the pattern width is larger than 17 μm, multiple cells can reside within the pattern, side by side [137,

323]; and if the pattern is less than 10 μm wide, cells tend to budge out from the pattern, do not attach, cannot form cell-cell connections at their intercalated disks, or undergo apoptosis [137, 140].

Although both methods have proven effective in alignment cardiomyocytes, for my dissertation work, microcontact printing was chosen over surface topography. This choice was made for a number of reasons. First, some researchers have found it difficult to enzymatically dissociate cardiomyocytes from nanotopological surfaces. Often, the only ways to remove a cell from these surfaces are to use a cell scraper or remove the cell membrane. However, one of the goals of this dissertation work was to create a culture environment in which the cells can be easily removed from these surfaces, intact, and used for regenerative therapies. Second, in order for topological surfaces to retain their patterned surface, they are often made out of relatively stiff materials. However, one of my aims is to test the effect of substrate stiffness on cell maturation, so having the ability to use substrates with tissue-like stiffnesses is preferred. Some researchers have proven the ability to fabricate grooved surfaces out of softer gel materials, however these surfaces do not retain their patterned topology over time, and are feature-size limited [139, 325]. And lastly, topological surfaces alone do not have the ability to highly control cell-cell contact area. Therefore, for my dissertation work, I chose to use microcontact printing to elicit hPSC-CM alignment, since it does not have any of these limitations.

Cell-Cell Contact

Through patterning techniques, cell-cell contact can be controlled to yield two-dimensional interactions of various different hierarchal complexities, such as cell pairs, cell lines, and cell monolayers. Alternatively, a higher degree of cell-cell contact can be achieved by seeding cells within a three-dimensional tissue. While these tissues provide a culture environment that is more representative of the physiological environment within the heart, as briefly discussed in Aim 1.1, they also have a number of disadvantages. Briefly, unless built from layers of organized cardiomyocytes, it is nearly impossible to control cell organization within a cardiac tissue. Furthermore, in multicellular tissues, one cannot separate the effect of the resident cells from that of the extracellular matrix, the presence of unique subpopulations of cardiomyocytes is obscured, one cannot control the amount of cell-cell contact, cells toward the surface of the tissue are structurally distinct from those toward the center of the tissue, as well as those closer to the support

structures are distinct from those in the middle of the tissue [305, 329]. For these reasons, I chose to use a two-dimensional technique for my studies.

The lowest hierarchy of two-dimensional cell-cell contact is a cell pair. These interactions are most often achieved by microcontact printing [330, 331] or microwells [332], and offer the advantages of providing very repeatable cell interactions, allow for the close scrutiny of cellular structure, and allow for simplified calculations when determining functional properties on a per cell basis. However, in this format, cell throughput is very low, the pro-maturation benefit of cell-cell contact is likely to be limited, and this interaction does a poor job at accurately representing cardiomyocyte organization within the heart.

Cardiomyocytes within the human heart are structurally and functionally connected to neighboring cardiomyocytes at their intercalated disks, forming chain-like strands of contractile tissue. This structure allows for the shearing of adjacent myocytes chains, which is thought to be necessary for efficient systolic contraction [333]. To enable homogenous beating throughout the entire tissue, there is a small degree of branching between adjacent strands, but this branching is limited. Therefore, in order to more closely replicate the in vivo culture environment of the heart, it would seem that hPSC-CMs should be cultured in strands or lines rather than in compact monolayers. Previous work has found that, if there are multiple cells within the same pattern region, cells toward the outside of the pattern align with the pattern direction, while those in the center do not [323]. Therefore, these strands should be one cell wide, to reduce this effect, and to promote cell-cell contact along the distal ends of these cells. Furthermore, when compared to monolayers, lines of cells have higher action potential conduction velocities, better calcium handling properties, more aligned myofibrils, are thicker, produce higher systolic stress, and preferentially express cell-cell proteins along their intercalated disks [114]. Additionally, in monolayers, cell width cannot be controlled, and neither can the amount of cell-cell contact between adjacent cells. For these reasons, I chose to study cell-cell contact by culturing the hPSC-CMs in strands, rather than in monolayers.

Electrical Stimulation

Electrical stimulation can be applied to cultures of cells by point or field stimulation. In point stimulation, the electrical signal originates at a single electrode, and induces cardiomyocyte depolarization by delivering a radiating electrical signal across the culture environment [207].

Alternatively, field stimulation delivers a directed electrical signal between two parallel electrodes [309]. Both techniques have proven capable of stimulating cardiomyocytes, but field stimulation is the more commonly used technique, due to advantages it has over point stimulation. Namely, the ability to direct the applied stimulus using field stimulation, allows for a higher degree of control over the path that the induced current takes. Furthermore, when only one electrode is used, ions tend to build up in areas surrounding the electrode, which can be cytotoxic to the cells. For these reasons, field stimulation was chosen as the preferred means of electrical simulation for my studies. Furthermore, it has previously been demonstrated that cardiomyocytes are more excitable and have better action potential properties if stimulation is applied parallel to cell alignment, rather than perpendicular [141, 334]. Therefore, for my own experiments, patterned substrates were aligned such that the electrical signal traveled parallel to the direction of cellular alignment.

With regard to electrode material, previous studies have used electrodes made from carbon [122, 132, 139, 154, 203, 329, 335], platinum [138, 207], stainless steel [329, 336], and titanium [329]. However, when compared to these other materials, carbon electrodes have been found to be superior, due to their high capacitance, high resistance to corrosion, and lower excitation thresholds requirement [329]. As such, carbon electrodes were chosen for these studies.

Electrical stimulation can be delivered to electrodes by means of commercial [122] or custom-made [305, 309, 335, 337] stimulation systems. In-house systems have the advantage of being custom designed to fit the needs of a particular study. However, any results obtained from their use cannot be confirmed by other labs, and user error tends to play a larger role in these systems. Alternatively, commercial waveform stimulators offer the advantages of being robust, user-friendly, widely available, and having the ability to deliver repeatable waveforms over long periods of time and across multiple experiments. Because of these advantages, a commercial waveform stimulator, the C-Pace EP bulk cell stimulator from IonOptix, was selected for my stimulation regimens. In combination with the C-Dish 6-well plate, this system delivers field stimulation, via parallel carbon electrodes, to cells seeded within 6-well tissue culture plates. Therefore, it has the capability to deliver the same stimulation regimen to six different culture conditions.

Lastly, the field properties i.e. pulse phase and duration, voltage, and frequency, were chosen based on those that have previously been found to be capable of eliciting cardiomyocyte maturation. With regard to pulse phase, there are two options, monophasic and biphasic. In monophasic

stimulation, the impulse is delivered from one electrode to the other, and this directionality does not change throughout the entire stimulation protocol. Alternatively, in biphasic experiments, the directionality of the field is reversed in between alternating pulses. Biphasic stimulation is thought to be more beneficial for cardiomyocytes, as it has been shown to require a decreased amount of current for excitation, it is more efficient at eliciting excitation, it is less likely to lead to defibrillation, it results in better connexin 43 expression, and it reduces electron buildup [203, 338-341]. Therefore, biphasic pulses were chosen for electrical stimulation experiments.

Table 7 Reported electrical stimulation parameters for cardiomyocytes.

Author	Year	Cells	Format	Direction	Voltage (V/cm)	Pulse (ms)	Freq. (Hz)	Duration (days)
Lieu, D.K.	2013	hESCs	Single	NR	2.5	5	1	14 days
Heidi Au, H.T.	2009	NRVM	Monolayer	Bi	1.15	1	1	7 days
Kujala, K.	2012	NRVM	Monolayer	Mono/Bi	5-5.3	2	1	2 - 3 days
Heidi, Au, H.T.	2007	NRVM	Monolayer	Mono	2.3-4.6	1-2	1	3 days
Chiu, L.L.Y	2011	NRVM	Monolayer	Bi	2.5	1	1	6 days
Barash, Y.	2010	NRVM	Tissue	Bi	5	2	1	4 days
Tandon, N.	2011	NRVM	Tissue	Mono	3	2	3	8 days
Chan, Y.C.	2013	hESCs	Single	Bi	6.6	2	1	4 days
Chiu, L.L.Y	2011	NRVM	Monolayer	Mono/Bi	2.5 - 5	1 - 2	1	5 days
Hirt, M.N	2014	NRVM hiPSCs	Tissue	Bi	2	2	0.5 0.5 - 2	16 - 18 days 14 days
Nunes, S.S.	2013	hESCs	Tissue	Bi	3 - 4	1	1 - 6	7 days
Radisic, M.	2004	NRVM	Tissue	Mono	5	2	1	5 days
Sathaye, A.	2006	NRVM	Monolayer	NR	2.5	4	2	4 - 8 days

Previously, field voltages in the range of 1.15 to 10 V/cm, pulse widths from 1 to 5 ms, and frequencies from 0.5 to 6 have all shown the ability to enhance cardiomyocyte maturation (Table 7). However, it has also been found that cells do not contract uniformly at field strengths under 5 V/cm [337]. As such, for my experiments, a voltage of 10 V/cm was chosen. Recently, multiple labs have shown that gradual increases in the stimulation rate leads to more robust increases in cardiomyocyte structure and function [204, 305, 309]. However, in some experiments, using pacing frequencies above 5 Hz has been found to have adverse effects on cardiomyocytes [114, 305]. As such, for my experiments, the stimulation frequency was increased by 0.5 Hz every other day for six days (to match with other experiments), starting at 0.5 Hz, and ending at 2 Hz. And lastly, I arbitrarily chose a pulse width of 5 ms, because it has shown promise in studies performed

by collaborators. However, to further improve upon this system, in future experiments I plan to optimize these electrical stimulation parameters for lines of hPSC-CMs on substrates of soft PDMS.

2.2 Methods

Cell Culture

Undifferentiated GCaMP3-expressing RUES2 hESCs [21] were cultured with mouse embryonic fibroblast conditioned media supplemented with basic fibroblast growth factor (R&D Systems). Cardiac differentiation of the cells was based on a previously published directed differentiation protocol [342]. Briefly, after plating in a monolayer, the cultures were switched to RPMI media (Gibco) supplemented with B-27 minus insulin (Gibco), activin A (R&D Systems), and Matrigel (BD Corning). This was followed by subsequent feedings supplemented with BMP4 (R&D Systems) and CHIR 99021 (Cayman Chemical), followed by Xav 939 (Tocris). After 20 days of directed differentiation, cells were treated with a "pro-survival cocktail" previously shown to increase survival [45] and cryopreserved [210]. Dissociated cells were seeded at a density of approximately 250,000 cells per 25 mm diameter substrate (500,000 cells for cell-cell studies) in RPMI medium supplemented with 10% FBS. The following day, the media was removed and replaced with serum-free RPMI medium, which was exchanged every other day.

Stamp Fabrication

Layout Editor© software was used to design a multi-patterned line stamp with 12 µm, 18 µm and 24 um wide lines, as well as stamp masters with only 18 µm and only 24 µm lines. To prevent cell bridging across pattern gaps, the spacing between adjacent lines for all stamp masters was designed to be 20 µm. SU-8 versions of these patterned stamps were fabricated at the University of Washington Nanofabrication Facility via photolithography processes, as previously described [288]. The resulting line stamp master was subsequently used to make 1:20 (base to

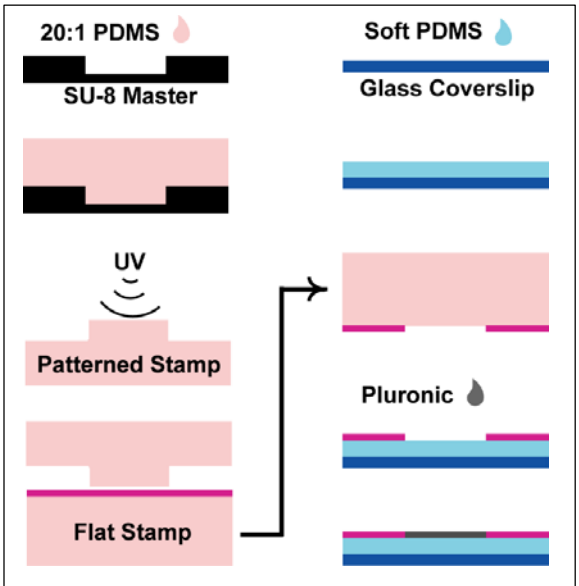

Figure 15 Substrate preparation and stamp-off technique.

curing agent) negative copies of the stamp pattern out of PDMS (Dow Corning) (Figure 15). Flat stamps were made by casting 1:30 PDMS off of a clean, pattern-free silicon wafer.

Fabrication of Soft PDMS Surfaces

I created PDMS surfaces with effective shear moduli ranging between 5-100 kPa, which spans the physiological range from normal to pathophysiological for cardiac tissue [126, 130, 245, 246]. These substrates were made by combining two commercially-available blends of PDMS together at different mass ratios [317]. This first involved independently mixing Sylgard 184 (Dow Corning) at its standard 1:10 ratio, and Sylgard 527 (Dow Corning) at its manufacturer recommended ratio of 1:1. Then, these two blends were combined to yield PDMS mixtures of 0%, 5%, 10%, 15%, and 20% Sylgard 184, by weight. Following mixing, the PDMS mixtures were poured onto oxygen plasma (SPI Supplies) treated glass slides (VWR), and baked in an oven at 65ºC for 20-24 hours. Following baking, substrates were UV-treated (Jelight Company Inc.) and stamped with 50 μg/ml of mouse laminin (Life Technologies), as described in aim 1.1. To create surfaces with laminin line patterns, the well-established stamp-off technique was used [343], which is depicted in Figure 15. Briefly, a patterned stamp was UV activated and used to selectively remove laminin absorbed to the surface of a flat stamp, which was subsequently transferred to the soft PDMS substrates.

Mechanical Testing of Soft PDMS Surfaces

The young's modulus of each Soft PDMS mixture was experimentally determined by compression tests using an Instron 5585H Universal Testing System. Compression samples were cylindrical, 25 mm in diameter, and 15-20 mm in height. During testing, a constant strain of 1 mm/s was applied to all samples, and the corresponding stress was evaluated using Bluehill 3 Testing Software. Young's moduli were then calculated from the stress-strain curves, and averaged across three replicate experiments.

Immunofluorescence

Following live experiments, the substrates were fixed and stained to assess their morphological and structural maturation. A Triton extraction protocol was employed prior to fixing, in order to permeabilize the samples [1, 127, 268]. Fixing was achieved with a solution of 4% paraformaldehyde (EMD Chemicals) in PBS. Cell nuclei were stained with Hoechst 33342 (Life

Technologies), sarcomeric α-actinin was treated with monoclonal mouse anti-α-actinin (Sigma Aldrich) and stained with goat anti-mouse AlexaFluor 488 (Life Technologies). Additionally, patterned regions of laminin on top of the soft PDMS were treated with rabbit anti-laminin (Sigma Aldrich) and stained with a goat anti-rabbit AlexaFluor 647 (Life Technologies).

Electrical Stimulation

Electrically-stimulated substrates were fixed to the bottom of a 6-well plate using a 30:1 (base to curing agent) mixture of PDMS, which was allowed to cure overnight. Following seeding, cells were given three days to recover from cell detachment and form permanent connections with their new culture surfaces, preceding to the initiation of the stimulation protocol. This choice was also based on previous observations that initiating stimulation at an earlier time leads to poor contractile behavior [154]. Just prior to the application of stimulation, all substrates were oriented to ensure parallel electrical field stimulation. For all electrical stimulation experiments, a biphasic field with pulse width of 5ms, and voltage of 10 V/cm for 6 days. The frequency of this field was sequentially increased in a step-wise manner from 1 Hz on day 1, to 1.5 Hz on day 3, to 2 Hz on day 5. This protocol was applied using a C-Dish 6-well plate (IonOptix) in conjunction with a C-Pace EP bulk cell stimulator (IonOptix). All C-Dish plates were autoclaved prior to use to ensure the electrodes were clean and sterile.

Structural Analysis

Cell and nuclear alignment were assessed using NIH ImageJ software. This was accomplished by binarizing the fluorescence laminin image, and determining the angle of the ECM pattern with respect to the horizontal axis. The orientation of the corresponding cell and nuclei were determined by thresholding the images, and using the measure function to determine their long-axis angle orientation. Cell and nuclei alignment were then calculated based on the difference between their orientation, and that of the laminin pattern.

Statistics

The majority of data was found to be non-parametric, as such statistical differences between pairs of data were determined by a Mann-Whitney Rank Sum Test, while differences between more than two conditions were determined with a Kruskal–Wallis ANOVA on Ranks. To compare multiple treatments, a Mann–Whitney post hoc test with a Bonferroni correction was performed. Due to the

binary nature of the multinucleation data, multiple treatments were compared with a chi-squared test, and individual groups were compared with a two proportion test. Normality of the data distributions was determined by the Ryan Joiner test. Statistical significance was assessed at $p < 0.05$, and is denoted by horizontal lines. Error bars in graphs represent standard error of the mean.

2.3 Results

Mechanical Characterization of Soft PDMS Surfaces

The stress and strain data obtained from the instron compression test was used to determine the compressive moduli of the 0%, 5%, 10%, 15%, and 20% Sylgard 184 compression samples. Moduli were then calculated from the linear portion of the stress-strain curves, and averaged across three replicate experiments. The resulting moduli were calculated to be 5 kPa, 17 kPa, 21 kPa, 59 kPa, 101 kPa (Figure 16).

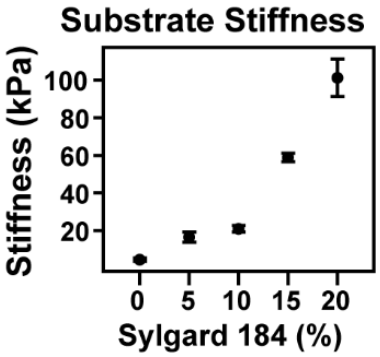

Figure 16 Stiffness of soft PDMS substrates.

Microcontact Printing

The ability of the stamp-off and microcontact printing techniques in transferring lines of patterned laminin onto soft PDMS surfaces was assessed by immunofluorescently staining the line patterns on all five soft PDMS mixtures (Figure 17A). Furthermore, upon comparing the fluorescence intensities of the three different pattern widths on the 10% Sylgard PDMS substrates, no significant difference was found (Figure 17B). This implies that, the concentration of the transferred protein was not dependent on the substrate stiffness or pattern width.

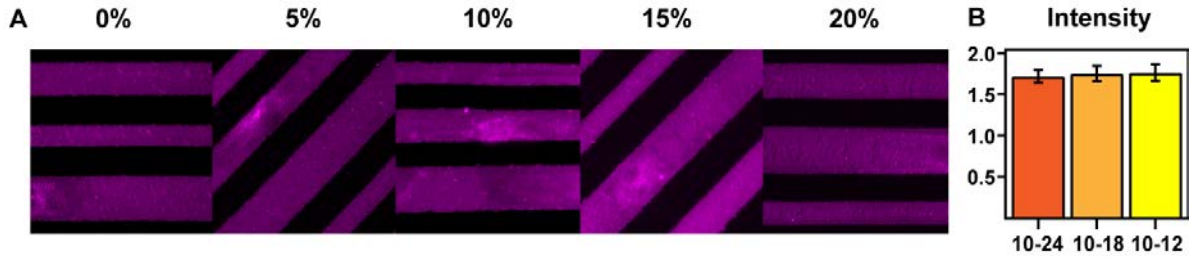

Figure 17 Patterned laminin lines on soft PDMS substrates of different stiffnesses. Normalized intensity of laminin lines on different pattern widths.

Alignment

To assess the effectiveness of the transferred line patterns in achieving cell alignment, hPSC-CMs were seeded onto the stamped substrates. Following a week of culture, hPSC-CM cell and nuclei alignment were assessed using ImageJ software. This assessment was performed on unpatterned cells, aligned cells, those in cell-cell contact, and those undergoing electrical stimulation, to determine the effect of each stimulus on cell alignment. Not surprisingly, we found no effect of substrate stiffness on cell or nuclear alignment (Figure 18A and E). With the addition of alignment, there was a significant increase in cell alignment (reduction in angle deviation) and a moderate increase in nuclear alignment, both of which increased with decreasing pattern width (Figure 18B and F). This high degree of cellular alignment was maintained when cells were placed in cell-cell contact and/or under electrical stimulation (Figure 18C & D), however, there was a slight decrease in nuclear alignment under both conditions (Figure 18G & H).

Cell-Cell Contact

Upon plating cells at a high seeding density onto line-patterned soft PDMS surfaces, the majority of cells were observed to form cell-cell contacts along their distal ends. However, in some cases, cells formed side by side in the widest 24 µm pattern. Additionally, cell contact was observed to be less frequent within the 12 µm line pattern. Occasionally, cells were seen to bridge the gap between adjacent patterns, but in general, this was not prevalent throughout the culture substrate.

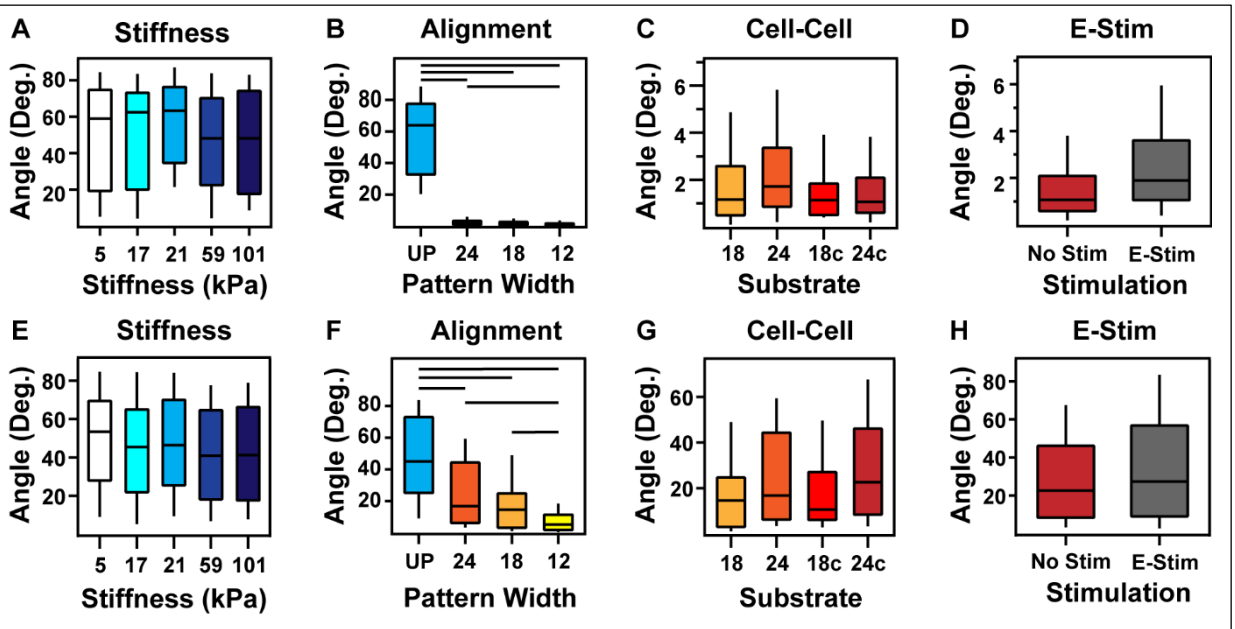

Figure 18 Alignment of cell (A-D) and nuclei (E-H) under various different stimuli.

Electrical Stimulation

Upon electrically-stimulating hPSC-CMs, we found that the cells were able to follow the applied pacing. Additionally, throughout the stimulation regime, we did not observe any changes in medium color nor bubble formation, which are signs of pH imbalance. However, we did observe that electrical stimulation appeared to result in increased cell detachment. This detachment was not quantified.

2.4 Discussion

In this study, I successfully created a culture environment with tunable stiffness, alignment, and cell-cell contact, which could also be exposed to directed electrical stimulation. The purpose of this culture environment is to expedite the, otherwise slow, maturation of cardiomyocytes derived from human pluripotent stem cells; for uses in developmental, drug screening, disease modeling, and regenerative studies.

The ability of soft PDMS to be used as a culture substrate for hPSC-CMs was assessed by combining the commonly-used commercial Sylgard 184 PDMS, with a purer (silica particle-free) formula of PDMS from the same commercial source i.e. Sylgard 527. Because the 527 formulation has the same chemical structure as 184, it stands to reason that mixtures of the two would retain the same chemical properties as either individually. This has been confirmed by earlier work, which also found that these mixtures have more uniform culture surfaces than 184 alone [317]. Likely, due to the fact that the Sylgard 527, unlike Sylgard 184, does not contain silica particles. Upon mixing these two forms of PDMS together, and performing mechanical testing on these samples, we found that we were able to make substrates with stiffnesses as low as 5 kPa, which is the stiffness of Sylgard 527. Therefore, soft PDMS, as we call it, retains the chemical properties of standard PDMS, with the added benefits of more uniform culture surfaces, and stiffnesses in the physiological range of heart tissue.

Next, we determined whether soft PDMS is compatible with micro-contact printing, a technique commonly used to pattern cells onto standard PDMS surfaces. To do this, we created a line stamp master, and used the stamp-off technique to create flat stamps with patterned lines of laminin. After stamping this pattern onto the soft PDMS surfaces of various stiffnesses, the patterns were immunofluorescently stained to assess the effectiveness of the stamping procedure. Upon

examining this structure, we found that the patterned lines were successfully transferred to each of the substrates, and that the amount of protein transferred was neither dependent on the substrate stiffness, nor the pattern width.

To assess the ability of these transferred proteins in aligning hPSC-CMs, I seeded these cells onto the line-stamped substrates, fixed them, and immunofluorescently stained for the cytoskeletal proteins actin and α-actinin, as well as for cell nuclei. Cellular and nuclei alignment were then determined using ImageJ software and compared to the orientation of the underlying laminin pattern, to determine the difference between the two. Upon performing this analysis, I found that, not surprisingly, cell and nuclear alignment were not dependent on substrate stiffness when these substrates were stamped with unpatterned laminin. This has been previously observed in other studies assessing the effect of stiffness on the alignment of immature hPSC-CMs [116]. However, cells and nuclei aligned very well to the patterned surfaces, and maintained this alignment when seeded at a high densities, as well as under electrical stimulation.

Next, we assessed how well the chosen pattern widths were able to restrict cell-cell attachment to the distal ends of adjacent hPSC-CMs. This was achieved by seeding hPSC-CMs at a high density onto line-stamped substrates, and then fixing and staining for cellular proteins and cell nuclei, as previously described. Upon examining cells seeded at high densities, I observed that cell-cell contact was not as prevalent along 12 μm lines, and that, rarely, cells formed side by side within the 24 μm lines. Furthermore, despite the fact that the spacing between patterns was 20 μm, a few individual cells were seen to bridge across adjacent line patterns. To completely remove this effect, a new stamp master with even larger gaps could be fabricated, but since this was not prevalent throughout the entire culture surface, we deemed a small degree of cell bridging acceptable for our studies.

Lastly, to determine the ability of cells on these substrates to follow stimulation applied by the IonOptix commercial waveform stimulator, line-stamped soft PDMS substrates were affixed to the bottom of 6-well tissue culture dishes, aligned to the direction of applied stimulation, seeded with hPSC-CMs, and then stimulated with a 10 V/cm, 5ms, biphasic signal for 6 days. The frequency of this stimulation was increased by 0.5 Hz every other day, starting at 1.0 Hz, and ending at 2 Hz. During this stimulation routine, cell beating was observed to follow pacing, and there were no apparent signs of pH imbalance. However, we did notice that cells undergoing this

stimulation routine appeared to be detaching from the substrate at a faster rate than those left in stagnant culture. Based on previous studies, it is unclear whether electrical stimulation leads to increased cell death. Some studies have found that there is no difference in cell viability, as indicated by live/dead stains, when comparing stimulated and non-stimulated cells [203, 320, 337]. Others have found that electrical stimulation leads to higher degree of cell death on unpatterned surfaces, but not on patterned surfaces [141, 337]. And some have even found that electrical stimulation reduces the incidence of cell death [344]. In future studies, cell death will be quantified by a live/dead stain to determine the actual contribution of electrical stimulation to cell death, but even with this increased detachment, there were still plenty of analyzable cells left on the substrate for analysis.

Based on the results of this study, I believe that soft PDMS is a valuable material for tissue culture, and could prove beneficial in assessing the effect of physiological substrate stiffnesses on various other cell types. Furthermore, I showed that, within this physiological range of stiffnesses, these substrates are compatible with micro-contact printing, which is able to prompt cell and nuclear alignment. When cell were seeded at a high density onto patterned substrates, I found that hPSC-CMs patterned onto 18 and 24 μm wide lines primarily form their cell-cell contacts along their distal ends, and that cell bridging between these patterns is limited. Lastly, I observed that aligned cells on these substrates could be electrically stimulated along the pattern direction by affixing the substrates to tissue culture dishes with PDMS. Therefore, this combined culture environment, which only requires the use of commercially-available equipment, and standard cell culture techniques, is capable of applying stiffness, alignment, cell-cell contact, and electrical stimulation to a culture of hPSC-CMs. The effectiveness of this environment in promoting hPSC-CM maturation is discussed in further detain in Aim 2 of this work.

AIM 2: STUDIES ON THE EFFECT OF BIOMECHANICAL MANIPULATIONS ON hPSC-CM MATURATION

2.1 Prolonged Cell Culture

2.1.1 Background

Cardiomyocytes derived from human stem cells are round, poorly spread, have highly unorganized cytoskeletons, and produce weak, unaligned contractile forces [53, 55, 119]. In contrast, adult cardiomyocytes are elongated, brick-shaped cells, which have a high level of cytoskeletal organization and produce strong, unidirectional contractile forces [145, 146, 287]. This discrepency between adult cardiomyocytes and stem cell derived cardiomyocytes is somewhat expected, since hPSC-CMs are at an earlier stage in the differentiation process and have not had the time needed to mature into adult cardiomyocytes. As a cardiomyocyte matures *in vivo*, the spacing between Z-discs in its sarcomeres increases, its shape transitions from a circular to a rectangular profile, and its overall volume increases [113, 114, 282]. These structural and morphological changes lead to increases in the ability of cells to produce strong contractile forces. Therefore, cardiomyocytes derived from hPSC-CMs cells would serve as a more effective model of adult cardiomyocytes if they were first matured to a more adult-like state.

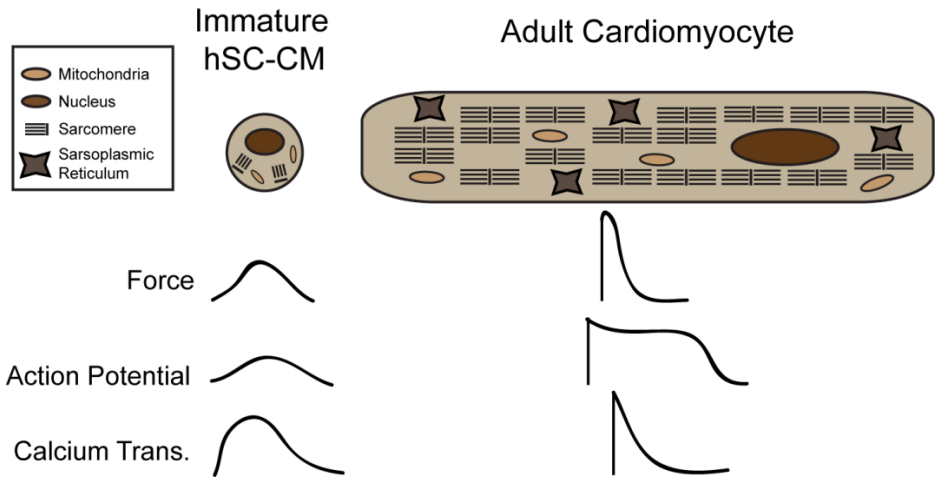

Figure 19 Structural and functional differences between immature hSC-CMs and adult cardiomyocytes.

It has previously been shown that prolonged culture can lead to increases in the structural [115, 118, 119] and functional [188, 236] properties of hPSC-CMs. However, the effect of prolonged culture on human induced pluripotent stem cell derived cardiomyocyte (hiPSC-CM) structure, twitch force, and twitch power has not been quantified.

2.1.2 Methods

The cells used in these studies were analyzed for the same structural and functional properties as those listed in Aim. 1.1. Specifically, the cells were analyzed for twitch force, velocity, power, and spontaneous beating frequency as well as average z-band width, sarcomere length, circularity, and spread area.

Cell Culture

The cell culture protocols performed in this work were executed in accordance with our previous publication [1], and the procedure outlined in aim 1.1.2. Briefly, human iMR90 induced pluripotent stem cells were differentiated into cardiomyocytes and cultured on Matrigel-coated plates. At 20, 70, and 100 days post-differentiation, the hiPSC-CMs were dissociated from their culture surfaces and seeded onto micropost arrays at a density of approximately 500,000 cells per array. These cells were then cultured in RPMI 1640 medium, which was exchanged every other day for a week. Prior to imaging, the micropost coverslips were transferred into Attoflour® viewing chambers (Life Technologies) and the cell media was replaced with HEPES RPMI medium (Gibco).

2.1.3 Results

Contractility

The contractile force, velocity, and power of 20, 70, and 100 day old human iPSC-CMs were measured using arrays of microposts. The contractile properties of these cells were analyzed from video microscopy using a custom MATLAB code. This analysis revealed that there was a decrease in the spontaneous beating frequency of the cells that correlated with cell age, but there were no significant differences between any of the cell groups (Figure 20A). Overall, the average spontaneous beating frequency was measured to be 1 Hz (60 bpm) for all three age groups. Additionally, I found that the total twitch force produced by hiPSC-CMs were significantly higher in the day 70 group than the day 20 groups ((Figure 20B). Similarly, both the contraction

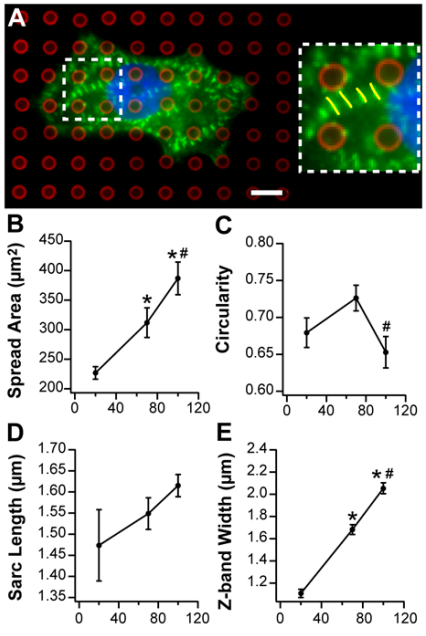

Figure 20 Structural maturation of aged hiPSC-CMs.

and relaxation twitch velocities were significantly higher for cells in the day 70 group than they were for cells in the day 20 group ((Figure 20C). Moreover, twitch power was observed to correlate with the days in culture (Figure 20D). These results indicate that longer culture times result in cells with enhanced contractile maturation.

Structure

Upon analyzing fluorescent images of cells in the 20, 70, and 100 day groups (Figure 20), I observed a significant correlation in the average cell spread area (Figure 20B) and Z-band width (Figure 20E) with cell age. Additionally, I found a significant decrease in the cell circularity between cells in day 70 and day 100 groups, but there was not a significant difference in the circularity between cells in day 20 and day 70 groups (Figure 20C). While the average sarcomere length appeared to correlate with cell age, there were not significant differences between the three groups measured (Figure 20D).

2.1.4 Discussion

In this work, I reported on the structural and functional maturation of hiPSC-CMs that have undergone prolonged culture. Upon analyzing the contractile and structural properties of 20, 70, and 100 day old hiPSC-CMs, I found that older cells demonstrated enhanced contractile function and improved sarcomeric organization when compared to younger cells (Table 8). If, one were to compare our results with those previously reported for adult cardiomyocytes, they would find that, even after 100 days of growth in culture, the hiPSC-CMs are significantly less mature than their adult counterparts [143-146, 167, 240, 244, 280, 345-348] .

If I assume that the increase in the structure and contractile function of hiPSC-CMs that I found follows a simple linear trend over time, then I can make estimations on how long it would take these properties to reach values reported for adult cardiomyocytes in the literature. Our results indicate that it would take at least 300 days for the hiPSC-CMs to achieve cell areas, z-band widths, and sarcomere lengths that match those found in an adult cardiomyocytes. Additionally, it would take approximately 20 years for these cells to achieve twitch velocities on the order of adult cells, 100 years to achieve equivalent twitch forces, and 135 years to attain similar levels of twitch power. However, it's possible that culturing hiPSC-CMs for these extended periods of time would not yield cells with contractile properties equivalent to those measured in adult cardiomyocytes,

would be extremely expensive, and would likely result in massive cell death. Therefore, these results suggest that prolonged culture is not a practical means to achieve mature hiPSC-CMs, and that additional culture stimuli are required in order to accelerate this process.

Table 8 Contractile and structural properties of aged hiPSC-CMs.

Cell Age (Days)	Twitch Force (nN)	Twitch Velocity (μm/s)	Twitch Velocity (μm/s)	Twitch Power (fW)	Freq. (Hz)	Area (μm^2)	Sarc. Length (μm)	Z-Width (μm)	Circularity
20	11.5±1.2	1.35±0.14	1.05±0.07	12.9±1.8	1.11±0.09	227±11	1.47±0.08	1.11±0.04	0.68±0.02
70	18.6±2.1	2.26±0.21	1.97±0.19	36.3±6.1	0.92±0.07	312±25	1.55±0.04	1.68±0.04	0.73±0.02
100	19.9±2.2	2.19±0.19	1.89±0.15	53.3±8.7	0.97±0.10	387±28	1.62±0.03	2.05±0.05	0.65±0.02

Past studies with cardiomyocytes have shown that exposing them to mechanical cues such as substrate stiffness [126, 245, 246], applied strain [299-304], cell alignment [114, 133, 135, 297, 298], and cell-cell contact [233] can lead to improvements in their maturation and contractile performance. Therefore, it is likely that the same mechanotransduction pathways may also enhance hiPSC-CM maturation and contractility.

In contrast to the other structural characteristics investigated in this work, I observed that the circularity of hiPSC-CMs did not appear to increase with culture time. These findings are in contrast with those found for prolonged cultures of hESC-CMS [115]. This inconsistency could be due to the difference in the cell line being used, but is more likely caused by the limited adhesive area seen by the cells on an array of microposts as compared to a flat surface in a culture dish [349]. Therefore, these results suggest that a means to encourage cell alignment on top of the microposts should be investigated for future studies employing microposts to assess the development of hPSC-CMs.

2.2 Stiffness

2.2.1 Background

The cardiac tissue within the heart stiffens during development, as well as during each cardiac cycle, but tends to fall within the range of 10-30 kPa in its healthy adult state [116, 246, 282, 350]. Stiffening of the heart past a value of approximately 50 kPa will inhibit contraction, and is a hallmark of cardiovascular disease and fibrosis [351, 352]. It is well accepted that mechanical interactions between the extracellular matrix and cell surface receptors play an important role in regulating cellular hypertrophy and maturation [353, 354]. The ECM imparts a passive force to the cells, which is an artifact of the ECM's elasticity. Thus, the elasticity of the ECM environment

surrounding a cell can directly affect the propagation of these mechanical signals to intercellular structures. Therefore, in order to produce populations of cardiomyocytes with a high degree of cell maturation, the optimal ECM environmental stiffness on which to culture them, must first be determined.

Previous studies have shown that substrate stiffness can affect the twitch force, velocity, and power produced by individual immature cardiomyocytes, as well as their average spread area, sarcomere length, Z-band width, aspect ratio, calcium transients, and expression of cardiac-specific markers [116, 126, 127, 147, 245, 246, 355, 356]. In some cases, researchers have found that these properties have a maximum value within a narrow range of stiffnesses close to that of native heart tissue (10-25 kPa), while others properties have been shown to increase in proportion to substrate stiffness. Conversely, other studies have found that some of these same properties are not stiffness-dependent [126, 316], or have a different response to changes in stiffness, even when using the same cell line. To determine which of these relationships is the case for hPSC-CMs, I presented hPSC-CMs with a physiological range of extracellular stiffnesses that cardiomyocytes experience *in vivo* [127], and assessed their calcium transients, myofibril structure, and hypertrophy to identify the stiffness or range of stiffnesses that result in the highest degree of cell maturation.

2.2.2 Methods

With the exception of the techniques used below, the same methods used in Aim 1.2 were used for these studies, with the addition of the following procedures.

Calcium Imaging

For live calcium transient imaging, cell media was replaced with Krebs-Henseleit buffer equilibrated at 95% O_2 and 5% CO_2 a week following cell seeding. Calcium transients in beating hESC-CMs were then recorded using a Hamamatsu ORCA-Flash2.8 Scientific CMOS camera fitted on a Nikon Eclipse Ti upright microscope. All videos were taken at 40x magnification using a water immersion objective. Additionally, a live cell chamber was used to maintain the cells at 37 °C throughout the imaging process.

Structural Assessment

Differences in nuclear and cellular spread area, aspect ratio, and alignment, along with multinucleation percentage, volume percentage of nuclei, sarcomere lengths, and Z-band widths

were assessed using ImageJ for all fixed and stained cells. For spread area, aspect ratio, and alignment measurements, actin and nuclei images were thresholded to define the object outline, and the measure tool was used to determine the area (spread area), shape descriptors (aspect ratio), and fit ellipse (angle with respect to x-axis) of the cell or nuclei. For binucleated cells, these values were averaged between the two. For sarcomere length measurements, the Plot Profile function was used to determine the average sarcomere length across at least 5 parallel Z-bands, at 3 different locations throughout the cell. These values were then averaged together to yield the average sarcomere length for each cell. For Z-band width measurements, we used the Fast Filter, Despeckle, Remove Outliers, and Binary functions, in order to define the borders of individual Z-bands. Then, to avoid connected or eroded Z-bands, groups of at least 5 parallel Z-bands, at 3 different locations throughout the cell were analyzed using the Analyze Particles function to find the major axis of each Z-band. These values were then summed together to determine the average Z-band width value for each cell. For these experiments, alignment is defined as the difference, in degrees, between the longitudinal axis of the cell, and that of the underlying ECM pattern.

Calcium Transient Analysis

Whole-cell calcium transients were analyzed using a custom-written Matlab code. This code was first used to convert collected videos of live GCaMP calcium transients into TIFF stacks. Each image within this stack was then thresholded to define the cell boundary. The whole-cell calcium signal within this boundary was then averaged over the entire cell area to determine the average calcium signal intensity within each TIFF image. These intensities were then normalized to background and baseline levels of intensity using the following equation:

$$\frac{F}{F_0} = \frac{F_{Max} - F_{Background}}{F_{Baseline} - F_{Background}}$$

To determine differences in calcium transient properties between different cell groups, normalized baseline intensity (F), normalized max intensity (F_0), normalized intensity (F/F_0), time to peak intensity (T_{Peak}), time to 50% calcium reuptake (T_{50}), time to 90% calcium reuptake (T_{90}), and the rates of calcium release (R_{Peak}), 50% reuptake (R_{50}), and 90% reuptake (R_{90}) were analyzed. Where:

$$R_{Peak} = \frac{F/F_0}{T_{Peak}}$$

$$R_{50} = \frac{0.5\ F/F_0}{T_{50} - T_{Peak}}$$

$$R_{90} = \frac{0.9\ F/F_0}{T_{90} - T_{Peak}}$$

2.2.3 Results

Cell Structure

Upon analyzing fixed and stained images of unpatterned hESC-CMs on soft PDMS substrates of different stiffnesses (Figure 21), I found that cell aspect ratio, Z-band width, and sarcomere length are not effected by substrate stiffness. Alternatively, cell area, multinucleation, and the nuclear volume fraction all showed significant trends based on substrate stiffnesses. More specifically,

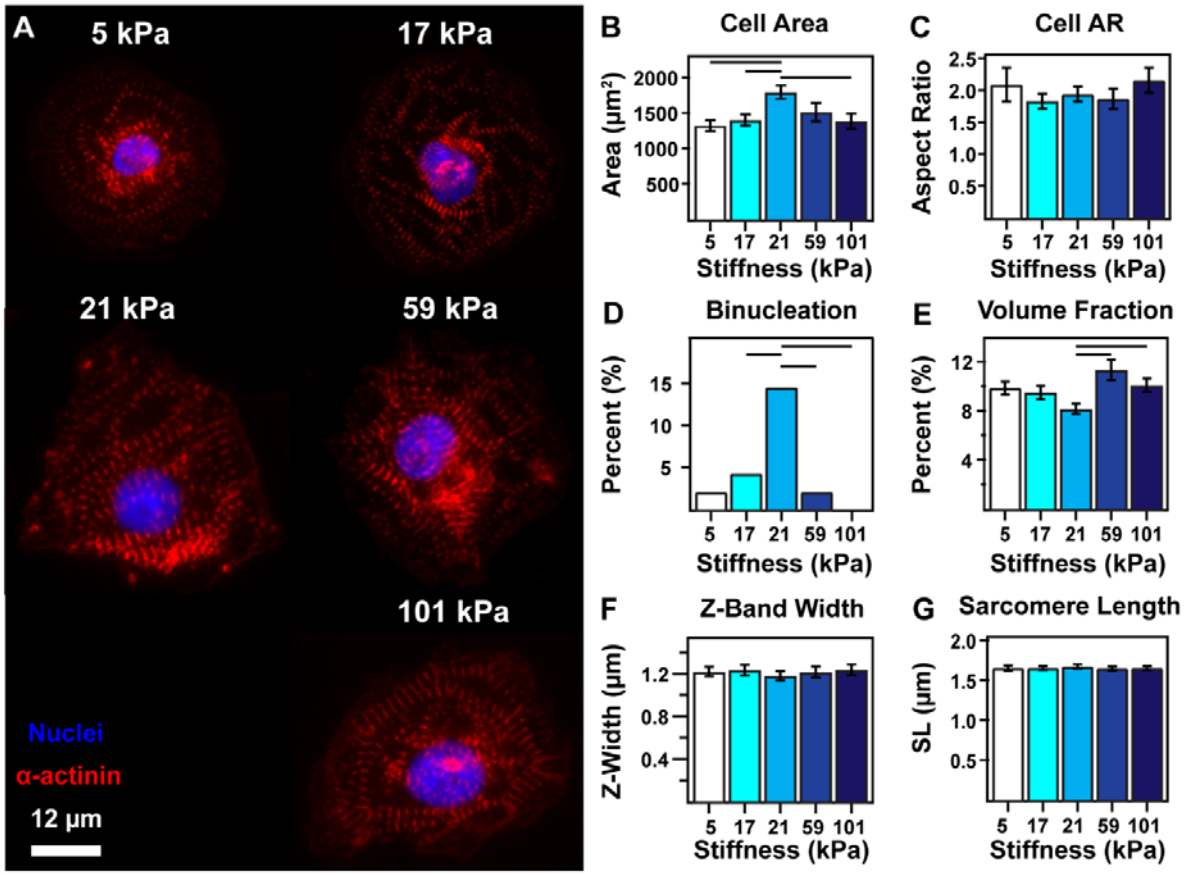

Figure 21 The effect of stiffness on hSC-CM structure.

cell area was highest on the 21 kPa (10% Sylgard 184) substrate, and decreased with increasing or decreasing stiffness. This same substrate was also found to have the highest degree of cell binucleation, as well as the lowest nuclei to cellular volume ratio. These results suggest that the the 21 kPa substrate served as the best culture subsstrate for promoting the structural maturation of hESC-CMs.

Cell Function

Calcium transient analysis for cells on the 5 kPa, 21 kPa, and 101 kPa substrates revealed that there was little to no difference in the kinetic properties (T_{Peak}, T_{50}, T_{90}) of the calcium transients for these cells (Figure 22). Likewise, there was no difference in the rates of whole cell calcium release or 50% reuptake, but the 90% reuptake rate was almost two times faster in the low and high stiffness substrates. Furthermore, the normalized baseline and maximal calcium signals were significantly stronger in cells cultured on the 21 kPa substrates, as compared to the low and high stiffness substrates.

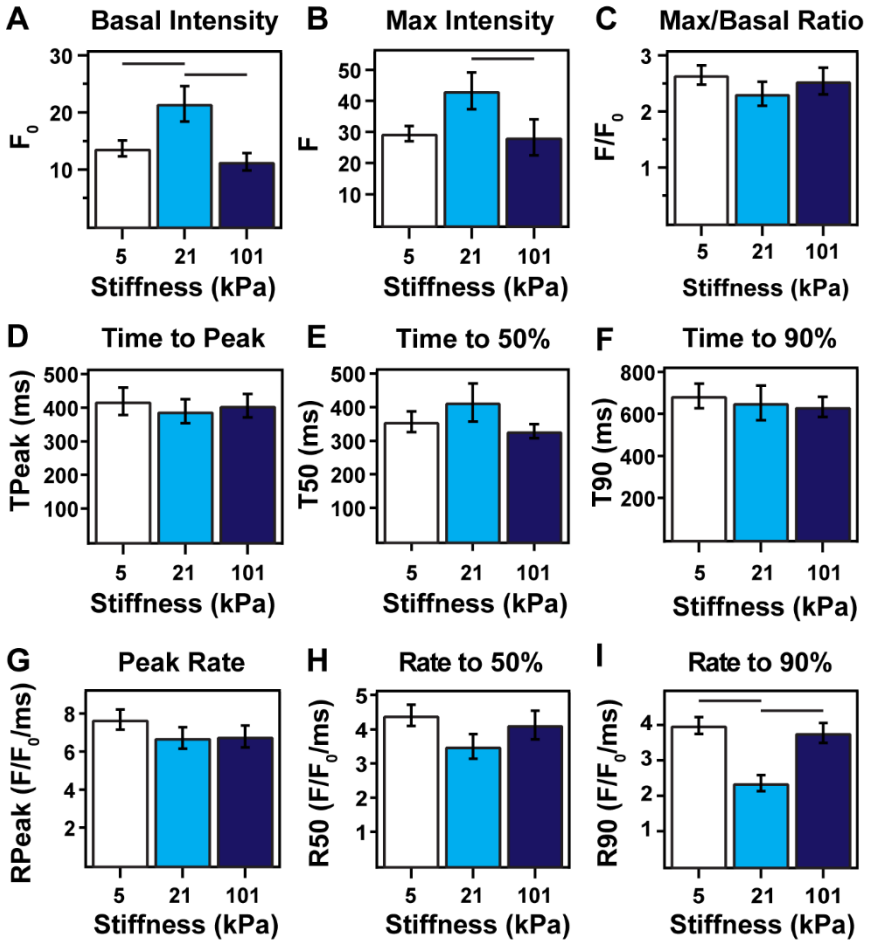

Figure 22 The effect of substrate stiffness on hPSC-CM calcium transients.

2.2.4 Discussion

Heart tissue samples of different ages reveal that the stagnant embryonic elastic modulus of murine heart tissue is around 12 kPa, healthy adult tissue falls within the range of 20-30 kPa, and infarcted tissue ranges from 50-70 kPa [246]. Alternatively, the modulus of healthy rat heart tissue has been

discovered to fall within the range of 10-15 kPa, and that of infarcted tissue was measured to be 50 kPa [351]. To the best of my knowledge, there have not been any studies which have assessed the stiffness of healthy human heart tissue, so based on animal studies, it has been approximated to fall within the range of 10-30 kPa.

Previous studies which have assessed the effect of substrate stiffness on cardiomyocytes have found that cells within this range of stiffnesses tend to exhibit a more mature structural appearance, and better contractile properties. However, there is conflicting data that suggests some of these relationships do not hold, or are cell-line dependent (Appendix B, Table 10). Therefore, it is unclear what environmental stiffness serves as the best culture substrate for immature hPSC-CMs. To determine the substrate stiffness best suited for immature RUES2 hESC-CMs, these cells were cultured on soft PDMS-coated glass coverslips for a week, after which their structural and calcium transient properties were analyzed. The substrates used in this study had stiffnesses spanning the physiological range of 5 kPa to 101 kPa.

Upon investigating the structural properties of these cells, cell aspect ratio, Z-band width, and sarcomere length were not found to be affected by substrate stiffness (Figure 21). However, measured values of cell spread area were significantly higher on the 21 kPa (10% Sylgard 184) substrate, and decreased with increasing or decreasing stiffness. This same substrate was also found to have the highest degree of cell binucleation, as well as the lowest nuclei to cellular volume ratio. These results agree with earlier studies examining the effect of substrate stiffness on the structural maturation of cardiomyocytes.

Morphologically, cell aspect ratio and cell area have both been found to increase with increasing substrate stiffness over a large range of stiffnesses from 0.1 kPa to 3 GPa in NRVMs [356]. Alternatively, other studies using NRVMs have found that cell aspect ratio [126, 130] is highest at an intermediate stiffness somewhere within the range of 10 – 50 kPa. Other studies with more immature cell lines have found that hiPSC-CM spread area is highest on substrates with a stiffness around 50 kPa [116], while embryonic myocytes preferentially spread more on substrates with stiffnesses close to 11 kPa [147]. Therefore, the dependence of cell spread area and aspect ratio on substrate stiffness appears to be cell line dependent. In these studies, we found that hESC-CMs had equivalent aspect ratios on substrates ranging from 5 kPa to 101 kPa, and exhibited higher spread areas on the intermediate 21 kPa substrates. To the best of our knowledge, no other studies

have examined the effect of substrate stiffness on the spread area and aspect ratio of single hESC-CMs. However, the relationships that we observed between these variables agree with at least one or more other previously-reported experiments.

In the mature adult heart, approximately 74% of cardiomyocytes have a single nucleus, which occupies about 5% of the cellular volume [153, 154]. The remaining 26% of the cells are binucleated, which is significantly higher than the 4.2% found for human stem cell derived cardiomyocytes [73]. Interestingly, we found that cell multinucleation was significantly higher on the 21 kPa substrate, as compared to all other substrates, with the exception of the 5 kPa slide. As far as I am aware, no other studies have investigated the effect of substrate stiffness on cell multinucleation. However, our other results suggest that multinucleation might be linked to cell hypertrophy, as cell spread area was also significantly higher on this culture stiffness.

It has previously been observed that, culture substrates that are too stiff or too soft can result in cardiomyocytes with poor sarcomeric organization [126, 202, 355, 356]. Considering that sarcomere formation is contractility-dependent, this relationship makes sense. That is, if myosin formation is inhibited via a very stiff culture surface, and a cell is not able to contract, sarcomeres look scattered and punctate, and have misaligned z-bands [357]. Similarly, if the environmental stiffness acting on a cell is very low, cell contraction is also low, and sarcomere development is inhibited. In these studies, no dependence on sarcomere length or z-band width were found for cells on substrates from 5 kPa to 101 kPa. This implies that the substrates used in this study were neither too soft, nor too stiff to impede sarcomere formation. These results have also been observed in NRVMs [358].

In addition to these structural endpoints, we also analyzed the calcium transient properties of the RUES2 GCaMP3 cells via live fluorescence microscopy. These transients were analyzed using a custom Matlab code. It is important to note here that there are two primary differences between our analysis, and that which has been previously done to analyze calcium transients within cardiomyocytes. First, the majority of other studies employ a line-scanning technique. That is, a line is drawn along the long axis of each cell, and the calcium signal is averaged along that line. As such, the resulting calcium transient data is highly dependent upon how this line is selected, especially when it is user-defined. Additionally, line-scanning techniques do not account for the

area, or rather the width, of the analyzed cell. This was our motivation for developing a code that could analyze whole-cell transients.

The other difference being that, we used the genetic calcium indicator GCaMP3, rather than a ratiometric Fluo calcium indicator. Therefore, we cannot definitively state what the actual amount of calcium within each cell is, but rather, can only make inferences based on changes in this calcium signal. Another well-known limitation of genetically encoded calcium indicator proteins is their prolonged response time due to the slow kinetics of calcium binding. Although, ratiometric calcium dyes, such as Fluo-4, Fluo-3, and Fura-2 have a relatively high affinity for calcium, which can also artificially prolong calcium transients [359]. Consequently, both dyes can underestimate calcium kinetics, but Fluo dyes offer the ability to determine the actual amount of calcium within the cell, and genetic calcium indicators allow for imaging over days and weeks, which is advantageous when assessing changes in the functional maturation of immature cardiomyocytes. In future experiments, we plan to treat the same RUES2 cell line with a ratiometric Fluo dye, to determine actual amounts of calcium within these cells, and to compare calcium kinetics between the two indicators.

Previous studies have found that, in NRVMs, the time to 90% relaxation decreases with increasing substrate stiffness [127], and the intensity ratio is highest at a midrange stiffness of around 10 kPa [126]. To my knowledge, no other studies have examined the effect of substrate stiffness on the calcium transient properties of hESC-CMs. In our studies, we found no changes in the calcium kinetics, other than a reduced rate to 90% calcium reuptake. However, we also found that cells seeded onto substrates with an intermediate stiffness of 21 kPa had the highest normalized baseline and maximal calcium intensities (no change in the ratio of max to basal). This suggests that cells on this substrate stiffness were able to store more calcium than those on softer or stiffer substrates. Which perhaps explains why the calcium reuptake rate was longer i.e. simply because there was more calcium to reuptake.

Overall, the results of this study imply that the substrate stiffness of 21 kPa was best able to elicit individual RUES2 hESC-CMs with enhanced structural and functional properties. Therefore, this substrate stiffness will be used in all following experiments.

2.3 Alignment

2.4.1 Background

Within the heart, adult human cardiomyocytes are elongated and aligned parallel to one another. This organization facilitates electrical signal propagation and efficient force production. However, in disease states, alternations in cytoskeletal and cellular alignment, as well as cell aspect ratio, coincide with a reduction in contractile function, and can ultimately result in heart failure. Therefore, the functional properties of a cardiomyocyte are directly related to the orientation and organization of its contractile proteins. Additionally, the ECM environment within the heart is composed of layers of aligned protein fibers, arranged in a well-organized pattern. This high degree of organization suggests that these proteins may help to guide myocardial alignment during development and tissue remodeling via nanoscale topographical cues.

The two most common techniques used to elicit cardiomyocyte alignment are topological surfaces, and microcontact printing. Studies employing these surfaces have found that sarcomere alignment, actin alignment, cell area, cell perimeter, junctional protein expression and localization, action potential propagation, force directionality, calcium handling properties, and conduction velocity are enhanced by the forced alignment of single neonatal rat ventricular cardiomyocytes [133, 135, 136, 138, 141, 191, 192, 298, 320, 325, 326]. Similarly, previous work with hESC-CMs has found that aligned monolayers of these cells have higher levels of sarcomere organization, contraction, and cytoskeletal alignment [230, 323]. However, other studies have found that sarcomere length, z-band width, cell spread area, calcium properties, and contractile force are unaffected by cell alignment [133, 135, 138, 140, 142, 323, 360].

To determine the effect of cell alignment on the structural and functional maturation of hESC-CMs, the stamp-off technique was used to pattern lines of laminin onto soft PDMS surfaces. Three different pattern widths, 12 μm, 18 μm, and 24 μm, were chosen in accordance with previous studies on cell alignment, as outlined in Aim 1.2. Additionally, these substrates were made to have the same stiffness found to promote cell maturation in Aim 2.2. Following a week of culture on these substrates, aligned and non-aligned cells on the same substrate were compared, to determine whether alignment affects the structural and calcium transient properties of these cells.

2.4.2 Methods

The same methods employed in Aims 1.2 (cell culture, stamp fabrication, fabrication of soft PDMS, immunofluorescence, and statistics) and 2.2 (calcium imaging, structural assessment, and calcium transient analysis) were used for these studies, with the addition of the following procedures.

2.4.3 Results

Cell Structure

A number of significant changes in cell organization and morphology were found upon forcing hESC-CMs to adopt an elongated cell morphology via microcontact printing (Figure 23). Cell area was found to significantly decrease with decreasing pattern width, while the opposite relationship held for cell aspect ratio (Figure 23A & B). Upon investigating nuclei within pattern cells, I found that binucleation was not significantly different among cells on different pattern widths (Figure

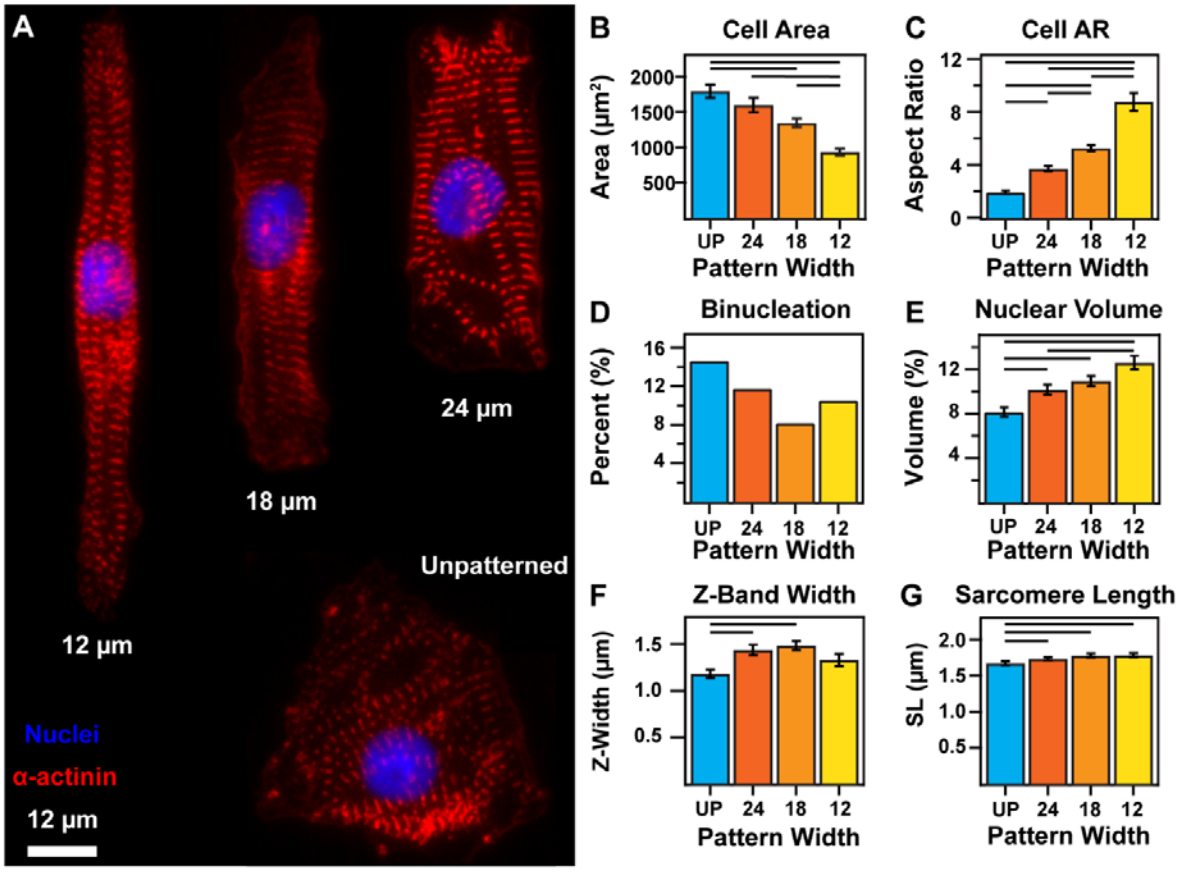

Figure 23 Effect of alignment on hSC-CM structure.

23D), but the percentage of the cell volume occupied by these nuclei significantly increased with decreasing pattern width (Figure 23E). Lastly, Z-band widths were highest on the 18 and 24 μm width patterns (Figure 23F), and sarcomere length was found to increase with decreasing pattern width (Figure 23G).

Cell Function

Due to the poor structure of cells on the 12 μm pattern width i.e. nuclei bulging out of cells and very large aspect ratios, calcium transients were only examined for unpatterned cells, and those on the 18 and 24 μm patterns. Analysis of these transients revealed that aligning hESC-CMs on micropatterned lines of laminin led to a significantly higher maximum to basal calcium intensity ratio (Figure 24C), with no change in basal or maximum intensity (Figure 24A & B). Alternatively, there were no significant differences in the time to peak, time to 50% signal decay, or time to 90% decay (Figure 24D-F). And, while there were no changes in the rate of calcium release (Figure 24G), alignment did lead to significant increases in the rates of 50% and 90% signal decay (Figure 24H & I).

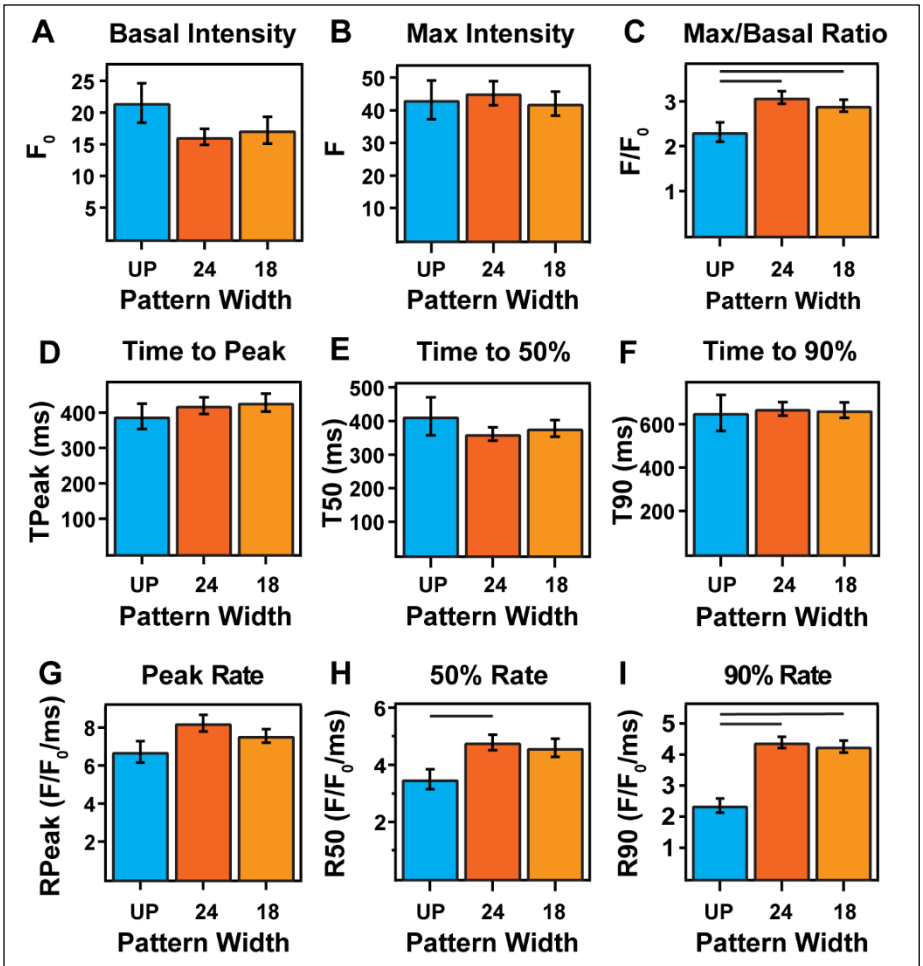

Figure 24 Calcium transient properties of hSC-CMs on different pattern widths.

2.4.4. Discussion

A particular degree of cell elongation and alignment within the heart is paramount in maintaining normal heart function. Adult healthy human cardiomyocytes are estimated to be 10-30 in

width, 100-130 in length, and have an aspect ratio of 6 to 8 [137, 150, 282, 283]. Alterations in cell size and aspect ratio have been found to coincide with disease states, and are coupled with reductions in cellular function. The aspect ratio of cardiomyocytes within patients experiencing pathological hypertrophy has been seen to get as high as 11 [361, 362]. Without any external cues, human pluripotent stem cell derived cardiomyocytes in culture adopt a spherical morphology, and have aspect ratios around 2. Such that these cells more closely mimic the morphology of adult cardiomyocytes, various different techniques have been employed to force their elongation in culture. Similar to the influence of substrate stiffness, previous work assessing the effect of cell alignment on the structural and functional maturation of cardiomyocytes has yielded conflicting results (Appendix B, Table 11). However, overall, cell alignment appears to be beneficial in enhancing these properties.

In these studies, for reasons outlined in Aim 1.2, microcontact printing was used to encourage hESC-CM elongation on soft PDMS substrates. Following a week of culture, the structure and morphology of these cells were assesssed via immunofloursescence staining and live calcium transient analysis. Unpatterned cells were directly compared to cells on 12 μm (structure only), 18 μm, and 24 μm wide patterns of laminin to determine the effect of pattern width on these endpoints.

Structurally, I found that hESC-CM alignment led to significant increases in cell aspect ratio, nuclear volume ratio, and sarcomere length. Additionally, Z-band width was significantly higher on the 18 and 24 pattern widths, as compared to the unpatterned cells. These alternations coincided with a significant decrease in cell area, and no change in the percentage of binucleated cells. I am unaware of any other studies which have investigated the effect of cell alignment on nuclear volume ratio, however other studies have also found that alignment of NRVMs leads to significant increases in cell aspect ratio [136-138, 325] and decreases in cell area [138, 325].

Furthermore, patterned NRVMs with aspect ratios close to 7 have been seen to have larger Z-band widths [142]. Alternatively, we saw the highest Z-band widths on pattern widths that yielded aspect ratios from 3 to 6. However, we did not directly compare aspect ratio to Z-band width, so it is possible that individual cells with aspect ratios around 7, indeed had the highest aspect ratios. Previous results have also shown that there is no significant effect of cell aspect ratio on sarcomere length [133, 358], however, we found that increases in cell aspect ratio coincided with increases

in sarcomere length. Although these changes were small, it makes sense that, if a cell containing same amount of sarcomeric content elongates, that one would expect the sarcomere spacing to increase. We did not directly assess the sarcomeric content of these cells, but plan to do so in future experiments.

From previous studies, assessing the effect of cell alignment on cardiomyocyte function, it has been found that the contractile properties of NRVMs are enhanced within the aspect ratio range of 1:6 – 1:8 [114, 142, 191]. Alternatively, a conflicting study demonstrated no effect of cell shape on twitch force [140]. Similarly, only a handful of studies have examined the effect of cell alignment on the calcium transient properties of cardiomyocytes, and the majority of these studies have been performed on NRVMs, and have used a line-scanning technique. One such study found that cell alignment leads to increased rates of diastolic calcium rise, and elevated diastolic and systolic levels of calcium [192]. Another group found that alignment leads to an increased maximal intensity to basal intensity ratio, decreased time to peak fluorescence, and increased time to 50% reuptake [114]. Conversely, a third study found that an increase in aspect ratio led to an increased time to peak fluorescence and an increased time to 90% calcium reuptake [191]. Therefore, the effect of cell alignment on the calcium transients of cardiomyocytes is unclear. Especially in immature hPSC-CMs.

In these studies, aligned hESC-CMs were found to have significantly higher maximal to basal calcium signal intensity, which agrees with previous results using NRVMs. Aligned cells also had significantly faster rates of calcium reuptake, which somewhat agrees with the findings of others. However, the majority of these previous studies employed a line-scanning technique, rather than the area-scanning technique employed in our studies. And, as discussed earlier, line-scanning techniques do not account for the width of the analyzed cell. So one could argue that the two cannot be directly compared. However, if the rate of calcium reuptake is higher over the whole cell area, then one would expect that it would also be higher along the central axis of the cell. Furthermore, all previously-discussed studies employed NRVMs, so we do not have any data from hPSC-CMs to directly compare to.

In future experiments, in addition to using Fluo dyes, we plan to assess calcium transients using both the line and area scanning methods, in order to directly compare to other line-scanning studies. Additionally, it would also be of interest to investigate the relationships between cell

aspect ratio (rather than pattern width) and calcium transient properties, as well as spatial trends in calcium transients, do determine whether cell alignment results in more uniform calcium waveforms. Furthermore, confocal images of these cells could reveal the effect of cell alignment on changes in overall cell volume, which contributes to a cardiomyocyte's ability to create contractile forces.

Overall, these studies demonstrated that cell alignment led to significant enhancements in a number of morphological and functional characteristics of hESC-CMs, which suggest that forced alignment of these cells resulted in the maturation of these cells. However, cells on the 12 μm substrate were found to have reduced cell areas and aspect ratios indicative of pathological hypertrophy, increased nuclear to cellular volume, and these nuclei appeared to bulge out from the cell pattern. Therefore, succeeding experiments will only use the 18 μm and 24 μm line patterns.

2.4 Cell-Cell Contact

2.4.1 Background

In the heart, cell-cell coupling is important for maintaining the normal function and development of the heart, serves to direct cell maturation, and plays a role in regulating cell survival [363, 364]. In fact, it has been observed that isolated cardiomyocytes cannot survive in culture for long periods of time [363, 365]. However, other research has found that two cells do not have to be in direct contact to "communicate." If seeded on a flat deformable surface, an individual cardiomyocytes has been found to activate neighboring quiescent cells to contract, if they are spaced less than 10 μm apart from on another [366]. Therefore, single cardiomyocytes are only likely to survive in culture for longer periods of time if they are in direct contact with other cardiomyocytes, or have close neighbors.

Studies assessing the effect of cell-cell contact on cardiomyocytes in culture have found that direct contact between cardiomyocytes is necessary for maintaining ion channel expression, coordinating cell polarization, and directing cell migration [356, 367]. Furthermore, when immature cardiomyocytes are grown in an environment which enables cell-cell contact, these cells tend to have enhanced cell-cell protein expression, organization, and localization, calcium dynamics, contractile forces, and survival [140, 363, 365, 368, 369]. Similar improvements in structural and functional properties are found for cells grown in contact with mature cardiomyocytes [336].

To determine whether or not cell-cell contact enhances the maturation of hPSC-CMs, hESC-CMs were seeded at a high density onto 18 and 24 μm patterned lines of laminin, to form a one-dimensional strip of cardiomyocytes. Following a week of culture on these substrates, the same properties described in preceding studies were assessed, on a single-cell basis, to determine the effect of cell-cell contact on the structural and functional maturation of these cells.

2.4.2 Methods

The same methods used in Aim 2.3 (described in detail in Aims 1.2 and 2.2) were used here, with a seeding density of 500,000 cells per substrate.

2.4.3 Results

Cell Structure

Analysis of immunofluorescently stained lines of hESC-CMs (Figure 25A) revealed that cell-cell contact within 24 μm width patterns led to significant increases in cell spread area when compared

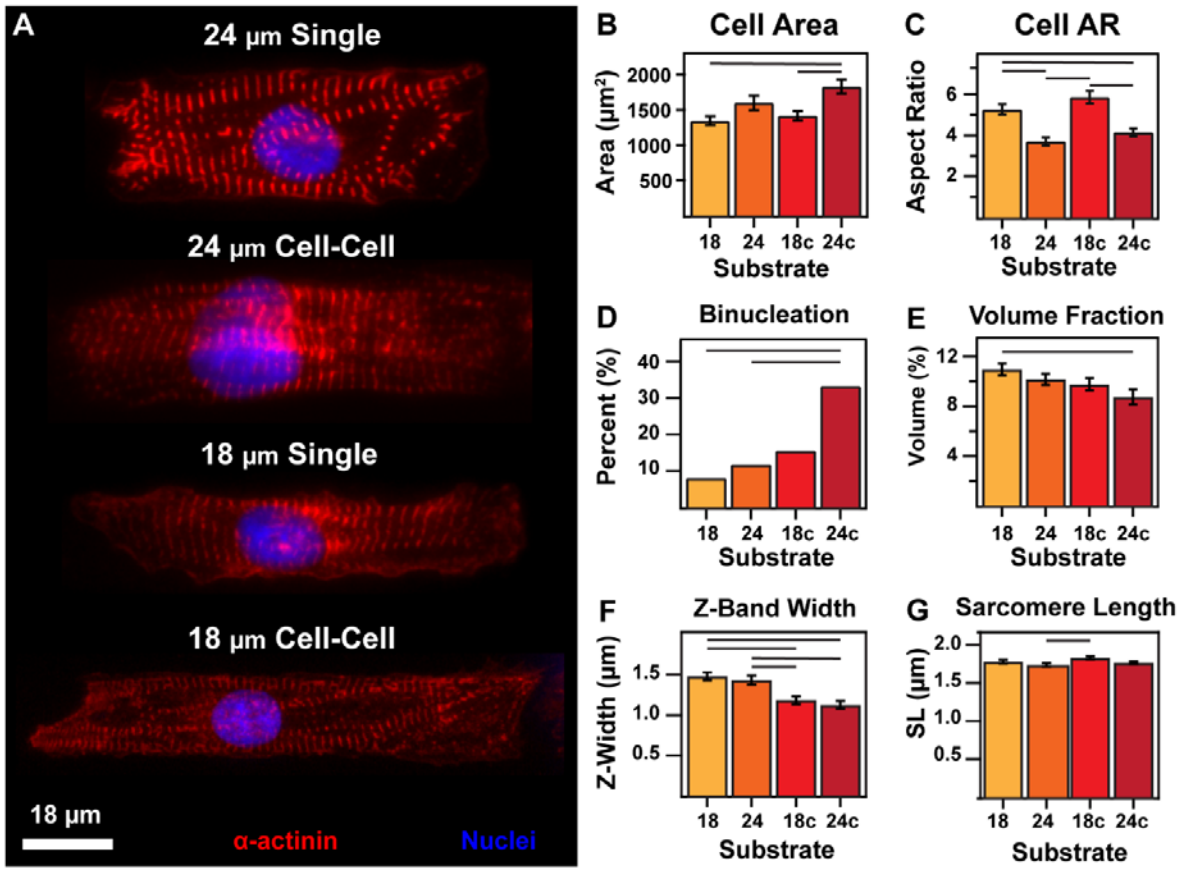

Figure 25 Effect of cell-cell contact on hSC-CM structure.

to single cells or lines of cells on the 18 µm pattern width (Figure 25B). Alternatively, cell-cell contact resulted in no changes to the aspect ratio for both pattern widths, but was significantly higher on the 18 µm pattern in both single cell and cell-cell conditions (Figure 25C). Interestingly, cell-cell contact resulted in significant increases in the percentage of binucleated cells on the 24 µm width pattern, as well as decreases in the nuclear volume ratio for both pattern widths (Figure 25E). Upon investigating the cytoskeletal structure of these cells, Z-band width was found to decrease with cell-cell contact on both pattern widths (Figure 25F), and sarcomere length significantly increased on the 18 µm pattern width under cell-cell contact when compared to single cells on the 24 µm pattern width (Figure 25G).

Cell Function

Calcium transient analysis of single isolated cells and cells in contact with neighboring cardiomyocytes revealed that cell-cell contact resulted in slight increases in normalized basal calcium intensity (Figure 26A), increases in average maximal calcium intensity (Figure 26B), and significant decreases in the maximal to basal intensity ratio (Figure 26C). Perhaps the most striking changes in calcium transients coinciding with cell-cell contact were significant decreases in time to peak intensity, time to 50% calcium reuptake, and time to 90% calcium reuptake on both pattern widths (Figure 26E-G). Additionally, in both single cell and cell-cell groups, cells on the 24 µm width

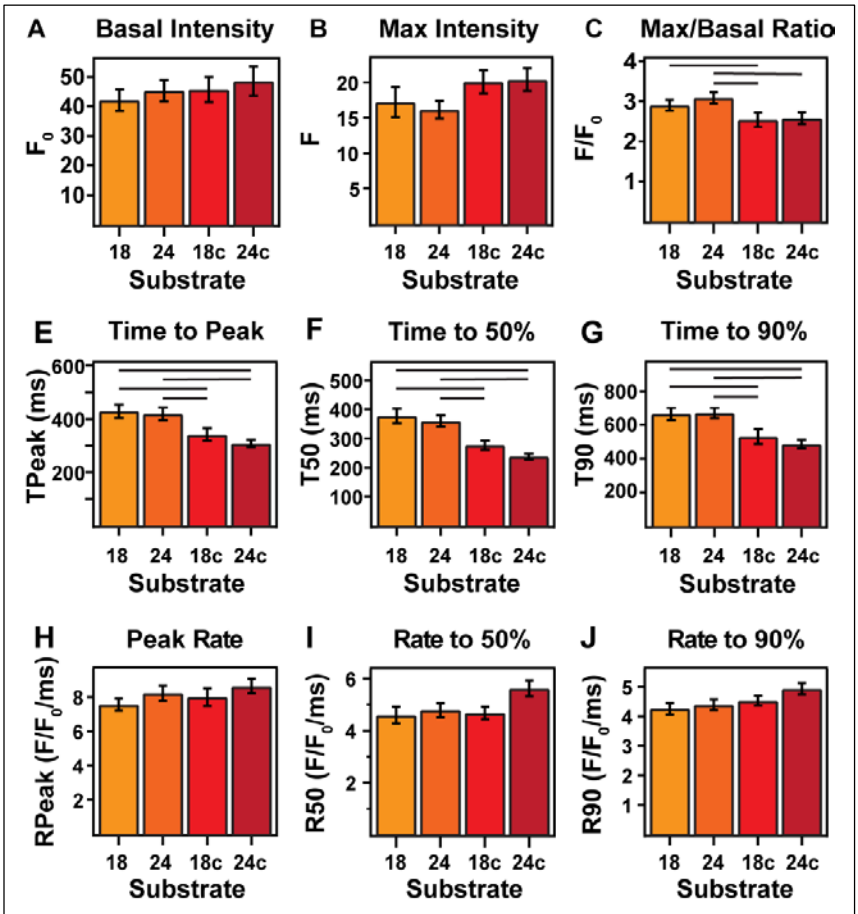

Figure 26 Calcium handing properties of hSC-CMs in cell-cell contact.

pattern had shorter transient times. I also found increases in the peak rate of calcium release, rate of 50% calcium reuptake, and rate of 90% reuptake (Figure 26H-J) for cells on both pattern widths in cell-cell contact. Furthermore, these rates were found to be highest on the 24 μm pattern width. However, these changes were not found to be significant.

2.4.4. Discussion

Cardiac myocytes are mechanically and electrically coupled via intercalated disks, which are principally composed of desmosomes, gap junctions, and adherens junctions [370]. Desmosomes are highly adhesive junctions that connect the intermediate filaments of neighboring myocytes, resist mechanical stresses caused by contraction, and may also act as signaling centers, thereby participating in fundamental processes such as cell proliferation, differentiation and morphogenesis [371]. Gap junctions allow for small molecule exchange between myocytes as well as the passage of microRNAs between adjacent cells [372]. The primary functional gap junctional protein in cardiomyocytes is connexin 43. In adult cardiomyocyte tissue these proteins are localized to the intercalated disks between two myocytes [373]. Adherens junctions are the physical link between the intercalated disk and the actin cytoskeleton. In cardiomyocytes, the primary adheren junction is the transmembrane glycoprotein N-cadherin (N-cad). N-cadherins provide mechanical connections between cells, which allow for myofibril alignment across the plasma membrane. N-cads mediate this organization by anchoring myofibrils to the intercalated disks via catenins, which are mechanosensory i.e. α-catenin (link between N-cad and the actin cytoskeleton) localizes to areas of high stress [357].

The development and maintenance of these structures are linked to cell-matrix interface. When a cardiomyocyte encounters a new surface, they lose their cell polarity, spread out, and form new cell-cell contacts. During this process, the intercalated disk is dismantled, new focal adhesions form throughout the cell, and eventually, the intercalated disk is reassembled at sites of new cell-cell adhesion. Cytoskeletal reassembly is then initiated by the recruitment of N-cadherin to these new intercalated disks. Once N-cad proteins have established mechanical stabilization of the intercalated disk, desmosomal proteins, cx 43, and potassium channels are able to form. [373-376], and the cytoskeleton begins to reorganize.

Proper function of these structures is highly important in maintaining normal heart function. Cardiovascular diseases, such as HCM and DCM often eventually result in structural adaptations

to the junctional proteins, and increased localization of these proteins to the lateral edges of the cell, which can result in arrhythmias [356, 374]. Upon deleting or inhibiting individual cell-cell proteins, multiple different structural and functional abnormalities have been found to result [370]. Specifically, in N-cad null cells, myofibril organization and alignment are disrupted, as well as catenin and Cx43 expression [377, 378]. Further investigation into this effect revealed that N-cad is not necessary for Cx43 formation, but it enables a higher degree of formation [369]. Alternatively, blocking gap junctions results in electrical abnormalities, and inhibits cell pacing [154]. And mutations in desmosomal protein genes have been found to contribute to arrhythmogenic cardiomyopathy [379].

In immature isolated cells, the expression of N-cadherin and cx43 tend to be very low, and diffuse throughout the cell. However, more junctional N-cad and cx43 is found in cells that have a larger cell-cell contact area [368]. Furthermore, studies examining the effect of cell-cell contact on hPSC-CMs have found that, on average, the force produced by an individual cardiomyocyte within an aggregate of cells is larger than that measured for an isolated cardiomyocyte [140, 233]. Additionally, when combined with alignment, previous studies with NRVMs in contact have seen increases in cell-cell protein expression at the intercalated disk, enhanced calcium dynamics, and increased cell contractility [138, 140, 326, 380]. However, to my knowledge, none of these studies have examined the direct effect of cell-cell contact on the structural and calcium transient properties investigated in this Aim.

Upon plating hESC-CMs at high and low densities onto 18 and 24 μm lanes of laminin, immunofluorescently staining for cell nuclei and α-actinin, and analyzing morphological properties of these cells, I found that cell-cell contact within 24 μm width patterns led to significant increases in cell spread area when compared to single cells or lines of cells on the 18 μm pattern width. Alternatively, cell-cell contact resulted in no changes to the aspect ratio for both pattern widths, but was significantly higher on the 18 μm pattern in both single cell and cell-cell conditions. An increase in cell area, coupled with no change in cell aspect ratio, implies that cell-cell contact within the 24 μm pattern width led to cell widening and elongation in equal proportions. However, as mentioned in earlier aims, since we did not directly compared cell area to cell aspect ratio, but rather quantified overall changes in these properties, so we cannot be sure that this is the case. Although, these results suggest that cells which were perhaps unable to

completely fill the width of the 24 μm pattern, are able to do so in the presence of cell-cell contact. Therefore, if these cells can be stimulated to elongate even further, this pattern could yield cells that have lengths and widths on the order to adult ventricular cardiomyocytes.

I also found that cell-cell contact resulted in increases to the percentage of binucleated cells on both pattern widths, as well as decreases in the nuclear volume ratio on both. These decreases in nuclear volume ratio suggest that, cell area is increasing, nuclear area is decreasing, or a combination of the two is happing at the same time. However, we already saw that cell area increases, and analysis of nuclear area for these cells demonstrated that the nuclei of hESC-CMs in cell-cell contact were not significantly larger than those in isolated cells (data not shown). Perhaps more remarkable, although cell-cell contact stimulated binucleation on both pattern widths, cells on the 24 μm width reached levels equivalent to those seen in the adult myocardium. To my knowledge, no other study has found equivalent levels of binucleation in early-stage hPSC-CMs. These results imply that nuclear division in cardiomyocytes is catalyzed by cell-cell contact, and that a higher degree of contact i.e. larger cell-cell interface, leads to higher rates of binucleation. At this point, it is unclear whether this is due to the additional mechanical stress imposed on one cell by the other, due to chemical communication between the cells, or a combination of the two. However, to reveal which factor plays a larger role in cardiomyocyte binucleation in immature hPSC-CMs, one could selectively inhibit various different junctional proteins between these cells, and then assess the effect on cell binucleation.

Upon quantifying sarcomere lengths and Z-band widths across patterned single hESC-CMs and those in cell-cell contact, Z-band width was found to decrease with cell-cell contact on both pattern widths. It is possible that, since these cells are still growing, and have only been in contact for a week, the stress from adjacent cells pulls Z-bands out of register. However, it is possible that, given longer culture times, or with the addition of additional pro-maturation stimuli, this effect will diminish. Alternatively, sarcomere length significantly increased on the 18 μm pattern width under cell-cell contact when compared to single cells on the 24 μm pattern width. This increased spacing is likely an effect of the increased external stress on these cells, and one would expect that the addition of additional stimuli could result in even further improvements.

Cell-cell contact was also found to stimulate slight increases in both normalized basal and maximal calcium intensity, and significant decreases in the maximal to basal intensity ratio. This result is

somewhat unexpected in that, the average maximal intensity appeared to increase to a higher degree than the basal intensity. However, since these properties were averaged over many cells, it is possible that outliers in the data skewed the averages in one direction or the other. At this point, the physiological implications of this data are unclear, but perhaps future experiments with Fluo dyes will reveal further information regarding the total amount and amount of utilized calcium within these cells.

The effect of cell-cell contact on time to peak intensity, time to 50% calcium reuptake, and time to 90% calcium reuptake was much more robust. Quantification of these values showed that all three endpoints significantly decreased on both pattern widths with the addition of cell-cell contact. Therefore, cell-cell contact appears to result in faster calcium transient times. Based on previous studies which have investigated the expression and localization of gap junction proteins in cardiomyocytes in cell-cell contact, it is not unreasonable to credit these increases in calcium transients with the localization of Cx43 to the intercalated disk; as directed calcium transients (such as those under electrical stimulation) tend to be faster than non-directional transients. Additionally, in both single cell and cell-cell groups, cells on the 24 μm width pattern had shorter transient times, which implies that this relationship is improved by a large cell-cell contact area i.e. more junctional Cx43 leads to faster calcium transients. As previously discussed, staining for cell-cell junctions in future experiments will yield additional information regarding the origin of these improvements in calcium transients.

Lastly, the rates of peak calcium release, 50% calcium reuptake, and 90% reuptake for cells on both pattern widths in cell-cell contact were seen to increase, albeit not significantly. These results suggest that, not only are calcium transient times faster for hESC-CMs in cell-cell contact, but the rates at which these signals travel throughout the entire cell area also increase. Like calcium transients, these rates were also found to be higher on the 24 μm pattern width. Implying that, not only do increases in cell-cell contact area result in faster calcium transients, but also faster rates of calcium release and reuptake. In future work, it would be interesting to see if these properties plateau or even decrease past a particular pattern width.

Overall, this study demonstrated that cell-cell contact led to modifications in the structural and functional properties of hESC-CMs patterned onto laminin lanes, and that the majority of these changes can be linked to positive alterations in cell maturation. Furthermore, a number of these

properties seemed to improve with cell-cell contact area, and cells on the wider 24 µm pattern were capable of completely filling the pattern width. Therefore, I decided to use this pattern for the preliminary electrical stimulation experiments described in Appendix A1. In future experiments, it would be beneficial to stain for the junctional proteins N-cadherin and Cx43 to compare the enhancements in structural and functional maturation seen in this study, to the expression and organization of these proteins.

AIM 3 STUDIES ON THE EFFECT OF BIOCHEMICAL MANIPULATIONS ON hPSC-CM MATURATION

3.1 Thyroid Hormone Supplementation

3.1.1 Background

Triiodothyronine serves various different roles during the progression of heart development. In the perinatal stages, T3 has been found to regulate the switching of myosin heavy chain (MHC) and titin from their fetal to their adult isoforms [381, 382]. Additionally, during the neonatal stages of development, T3 has been observed to prevent the expression of fetal genes, and enhance cardiac maturation [382, 383]. And in adult cardiomyocytes, T3 has been found to regulate cardiac physiology and hypertrophy.

T3 treatment in vivo has previously been found to result in increased cardiac differentiation, the upregulation of cardiac maturation markers in immature cells, the induction of adult-like action potentials and calcium transients, an increase cardiomyocyte hypertrophy, increased binucleation, and the suppression of proliferation [188, 308, 384]. All of which are markers of cardiomyocyte maturation. Additionally, in a recent study, T3 treatment was found to modulate the gene expression profile of hiPSC-CMs to a more adult-like phenotype [188]. Based on these results, I hypothesized that T3 treatment would result functional improvements to hiPSC-CM maturation. Here, the contractile function of hiPSC-CMs with or without T3 treatment was assessed using the micropost bioreactor system described in aim1 of this work.

3.1.2 Methods

Cell Culture

The same hiPSC cell line and cell culture protocols as described in Aim 1.1. were used here to produce hiPSC-CMs. After 20 days of *in vitro* differentiation, the cells were dispersed using 0.05%

trypsin-EDTA and replated. Cultures were fed every other day thereafter with serum-free RPMI-B27 plus L-glutamine. Only cell preparations containing greater than 80% cardiac troponin T-positive cardiomyocytes (by flow cytometry) were used for experiments. Cells were treated with 20 ng/ml T3 between days 20 and 27 after induction, and media were changed every other day prior to contractile function assessment.

Micropost Fabrication

The microposts used in this study were fabricated as described in the background sections of this work. Each micropost in the arrays used for these studies was 6.45 μm in height and 2.3 μm in diameter, and the center-to-center spacing between adjacent microposts is 6 μm. The stiffness of each micropost was 38.39 nN/μm. Twenty days following differentiation, hiPSC-derived cardiomyocytes were seeded onto the arrays at a density of 250,000/cm^2.

Live Cell Imaging

One week after T3 treatment, individual cardiomyocyte twitch forces were recorded under phase light using high-speed video microscopy, as described in Aim1.1.

Statistical Analysis

Data are expressed as mean ± SEM. Differences were compared by ANOVA with Student–Newman–Keuls post hoc testing. P b 0.05 was considered significantly different.

3.1.3 Results

Contractile force analyses were performed on individual cardiomyocytes using arrays of microposts. In this study, individual cardiomyocytes were allowed to adhere and spread out on elastomeric microposts (Figure 29A). Figure 29B shows representative traces of the total force generated by individual cardiomyocytes from the control and T3-treated groups. Control hiPSC-CMs exhibited a twitch force of 6.4 ± 0.4 nN/cell (Figure 29C). T3-treated hiPSC-CMs exhibited a significantly higher twitch force of 10.4 ± 0.7 nN/cell ($P < 0.001$). Contractile time analysis revealed that T3-treated hiPSC-CMs displayed shorter time to peak contraction time (0.15 ± 0.01 sec versus 0.25 ± 0.02 sec in control cells, as shown in Figure 29D). T3 also significantly decreased time to 90% relaxation (Figure 29E) and total twitch time (Figure 29F).

In addition to an almost twofold increase in contractile force, the hiPSC-CMs treated with T3 had increased spread area, anisotropy, and sarcomere length. T3 treatment was also associated with reduced cell cycle activity, indicated by reduced DNA synthesis, as well as improved calcium handling properties. Specifically, there were increases in rates of calcium release and reuptake, along with a significant increase in sarcoendoplasmic reticulum ATPase expression. Additionally, there was a significant increase in the maximal mitochondrial respiratory capacity and respiratory reserve capability after T3 treatment. However, there was a decrease in β-MHC expression, which is the opposite of what one would expect to see in mature cardiomyocytes.

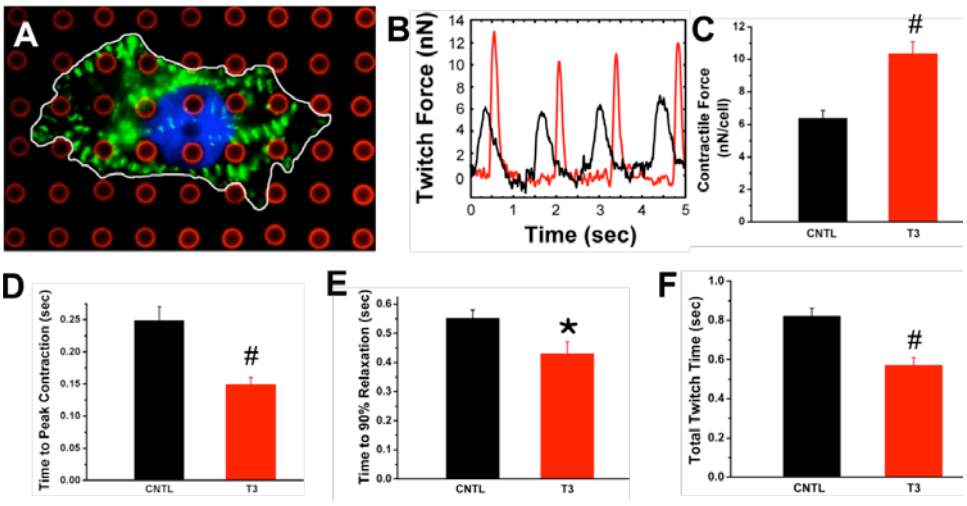

Figure 27 Contractile properties of T3-treated hiPSC-CMs. Reproduced from: Yang, X., Rodriguez, M.L., et al. (2014) *J Mol Cell Cardiol*. 72:296-304; with permission from Elsevier.

3.1.4 Discussion

Here, the effect of T3 on hiPSC-CM maturation was assessed by multiple different endpoints. This was achieved by treating the cells with T3 for a week, and then analyzing the cells for changes in size, anisotropy, sarcomere length, DNA synthesis, contractile force, calcium-handling properties, and mitochondrial function. Upon analyzing these cell properties, I found that T3-treatment not only results in morphological and molecular changes indicative of maturation, but that functionally relevant parameters such as contraction are also positively-regulated. Based on the results of this study, I concluded that T3 enhances hiPSC-CM maturation, and could enhance the utility of hiPSC-CMs for therapeutic, disease modeling, or drug/toxicity screens. However, these results also hint at the limitations of using a single factor to induce complete cardiomyocyte maturation, and suggest that future studies should determine the concurrent effect of T3 treatment and other maturation techniques on hiPSC-CM development.

3.2 AMPK Activation

3.2.1 Background

As previously discussed, a number of different approaches have been investigated as a means to mature human pluripotent stem cell derived cardiomyocytes in culture. An area that has not been intensely studied is the metabolic aspects of hPSC-CM maturation. It is known that the immature cardiomyocytes rely heavily on glucose as their primary source of energy [385], while adult cardiomyocytes get the vast majority of their energy from fatty acid oxidation. Approaches for enhancing the fatty acid oxidation capabilities of hPSC-CMs have not been well investigated, and it is currently unclear whether hPSC-CMs are capable of oxidizing fatty acids at all.

AMPK is a ubiquitously expressed heterotrimeric kinase that is viewed as a "cellular fuel gauge" and "super metabolic regulator" [386]. It is a Serine-Theorine kinase that is allosterically activated by increases in the ratio of [AMP] or [ADP] to [ATP]. Its activation also requires phosphorylation of the α subunit, which can occur via liver kinase B1 (LKB1) or calcium/calmodulin-dependent protein kinase kinase 2 (CAMKKβ), although the LKB1 pathway is thought to predominate in cardiomyocytes [386]. Shortly after birth, upon suckling, cardiac AMPK protein and activity levels increase in association with the conversion from glucose metabolism to fatty acid oxidation [387]. AMPK directly regulates pathways involved in fatty acid and glucose transport into the cell, increases glycolytic flux, and enhances mitochondrial entry of fatty acyl carnitine [387]. Additionally, AMPK regulates transcription via the estrogen-related receptor-α (ERR-α) [388], peroxisome proliferator-activated receptor coactivator 1-α (PGC-1α) [389], and nuclear regulatory factor-1 (NRF-1) [390]. Through these pathways, AMPK contributes to control of mitochondrial biogenesis and other gene regulatory networks. We therefore hypothesized that AMPK agonist treatment leads to cardiac metabolic maturation.

AICAR (5-amino-4-imidazolecarboxamide riboside-1-β-D-ribofuranoside) has been widely used to induce AMPK activation in cardiomyocytes [391, 392]. AICAR is taken up by adenosine transporters and subsequently phosphorylated by adenosine kinase to ZMP (5-aminoimidazole-4-carboxamide-1-β-D-furanosyl 5′-monophosphate), which in turn mimics AMP to activate AMPK.

3.2.2 Methods

Cell Culture

Cells from the IMR90 human induced pluripotent stem cell line were differentiated as previously outlined in Aim 1.1. For these studies, only cell preparations containing >80% cardiac troponin T-positive cardiomyocytes (by flow cytometry) were used.

Contractile Analysis

Contractile forces were assessed using the micropost assay developed in Aim 1.1 of this work. The microposts used in this study (6.45 μm in height, 2.3 μm in diameter, 6 μm center-to-center post spacing, and 44.54 nN/μm bending stiffness) were cast onto 25mm diameter round # 1 glass coverslips (VWR). To enable cell attachment, the tips of the microposts were stamped with 50 μg/ml of mouse laminin (Life Technologies) via microcontact printing, while the remaining surfaces of the micropost array were fluorescently stained with BSA conjugates with Alexa Fluor 594 and blocked with 0.2% Pluronic F-127 (in PBS) [288]. Twenty days following differentiation, hiPSC-derived cardiomyocytes were seeded onto the micropost arrays in Attoflour chambers at a density of approximately 500,000 cells per chamber (~100,000 cells/cm^2), in RPMI media supplemented with 5% fetal bovine serum. After 24 hours, the media was replaced with serum-free RPMI-B27 plus L-glutamine, which was exchanged every other day. Beginning two days after seeding, half of the substrates were treated with 1 mM AICAR for one week. Prior to live imaging, the media was exchanged to Tyrode's buffer. Individual cardiomyocyte twitch forces were recorded under phase light using high-speed video microscopy in a live cell chamber at 37°C, as previously described [393]. Only the contractile forces of single cardiomyocytes (no junctions with adjacent cells) with obvious beating activity were assessed. Cell forces were analyzed using the same custom-written MATLAB code described in Aim 1.1. For these studies, passive tension, total twitch force, average twitch force per post, and beating frequency were used to compare the independent biological replicates (N = 2, with 16 to 38 cells per independent biological replicate).

Statistical Analysis

Data are expressed as mean ± SEM. Differences were compared by ANOVA with Student-Newman-Keuls post hoc testing. $P < 0.05$ was considered significantly different.

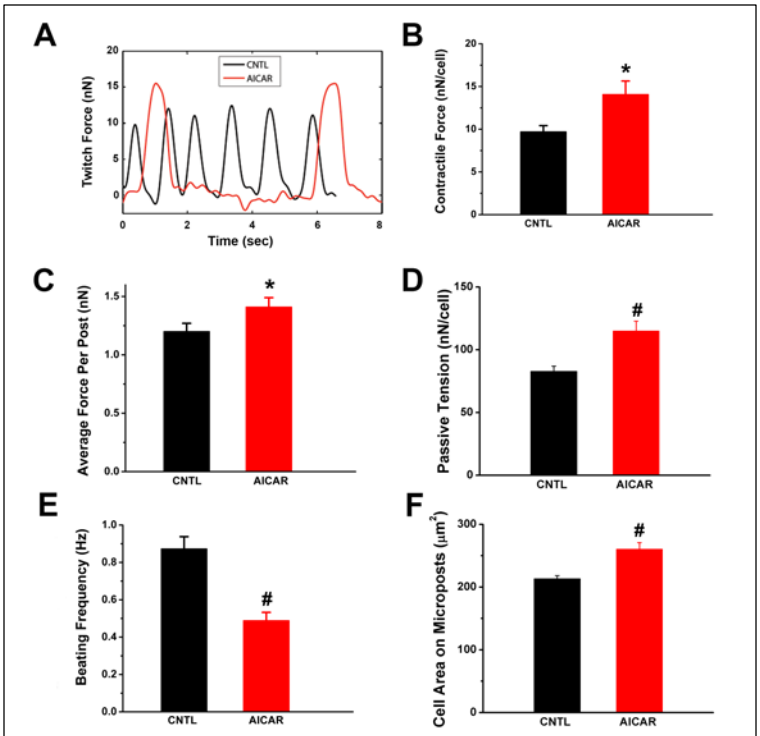

Figure 28 Effect of AICAR treatment on hiPSC-CM contractility.

3.2.3 Results

To characterize force production on a per-cell basis we used micropost arrays [127, 394]. Figure 30 shows representative traces of the total twitch force generated by individual cardiomyocytes from the control and AICAR-treated groups. Control hiPSC-CMs exhibited a twitch force of 9.71 ± 0.72 nN/cell (Figure 30B). AICAR-treated hiPSC-CMs exhibited a significantly higher twitch force of 14.07 ± 1.57 nN/cell (P=0.014). Similarly, the average force per post analysis revealed that after AICAR treatment, there was a significant increase in the local force generated at each post (Figure 30C). In addition to the active twitch force, the passive tension generated by the AICAR-treated hiPSC-CMs was significantly higher than the controls (Figure 30D). The observed increase in passive tension could be attributed to a significantly higher titin N2B expression level in the AICAR-treated hiPSC-CMs. The beating frequency analysis also showed that AICAR-treated cells beat significantly slower (Figure 30E). Lastly, in agreement with the morphological changes after AICAR treatment, the hiPSC-CMs on microposts also displayed a larger cellular size (Figure 30F) (213.09±5.27 vs 260.07±10.93, P<0.001).

In addition to these changes in contraction, upon examining the metabolic properties of AICAR-treated cells, my co-author found that the OCR-induced by palmitate-albumin went up by ~2.32-fold. Additionally, there were increased expression levels of transcripts involved in fatty acid oxidation, including FA binding protein (FABP), carnitine palmitoyltransferase-1B (CPT1B), and pyruvate dehydrogenase kinase-4 (PDK4). Furthermore, AMPK activation led to enhanced mitochondrial maximal respiratory capacity and increased mitochondrial biogenesis as shown by mtDNA to nDNA ratio.

Structurally, she found that AICAR treatment led to a significant increase in cell size (cell area) and sarcomere length, and a significant decrease in cell circularity. Quantitative RT-PCR revealed that AICAR led to up-regulation of α-myosin heavy chain (α-MHC) (2.64 ± 0.51-fold vs. control, P=0.03), phospholamban (PLN) (1.44 ± 0.11-fold, P=0.017) KCNJ2 (1.71±0.17-fold vs. control, P=0.04), titin N2B, ssTnI, and cTnI.

3.2.4 Discussion

Metabolically hPSC-CMs rely heavily upon glucose as their primary energy source, while adult cardiomyocytes obtain the majority of the energy from fatty acid oxidation. Therefore, we hypothesized that encouraging the immature hPSC-CMs to undergo a switch from glucose consumption to fatty acid oxidation might promote cell maturation. Specifically, the goal of this study was to promote hPSC-CM metabolic maturation by activating the "super metabolic regulator" AMPK.

Our micropost assay demonstrated that AICAR treatment increased spontaneous total twitch force generation from ~9.7 nN/cell to ~14.1 nN/cell. Since the AICAR-treated cardiomyocytes were significantly larger than the controls, we also compared the average twitch force per post to account for the role of hypertrophy in the total increased contractile force. The average twitch force per post was also significantly higher in the AICAR-treated cardiomyocytes (~1.4 nN/post) compared to the controls (~1.2 nN/post). Therefore, some factors besides increased cell size must also contribute to the increased force. One possible mechanism is through phosphorylating cardiac Troponin I at Ser 150, as it has been shown that AMPK phosphorylation at this site leads to increased myocyte contraction by increasing myofilament calcium sensitivity [395, 396]. In addition, the decreased beating frequency of the AICAR-treated hiPSC-CMs on microposts is another maturation parameter. One characteristic property of an immature cardiomyocytes is automaticity, which diminishes during cardiac development. The decreased beating rate agrees with the detected lower expression level of the Kir channel subunit KCNJ2, important in setting resting membrane potential.

In addition to these changes in contractility, my co-author found that AMPK activation by AICAR dramatically enhances the fatty acid oxidation capacity of hPSC-CMs by phosphorylating acetyl CoA carboxylase (ACC), leads to enhanced mitochondrial biogenesis, increased cell size, a decrease circularity index, and improved cardiac gene expression.

All of these positive outcomes suggest that AMPK is a promising treatment for the maturation of hPSC-CMs in culture. However, despite these structural and functional improvements, these values did not reach the levels seen in adult cardiomyocytes. Therefore, we believe that future studies will benefit from combinatorial approaches that utilize AMPK with other factors such as T3[394], glucocorticoids[397], IGF-1[398, 399], electrical stimulation[122, 154, 400, 401], microRNA[402-404], and/or altering the mechanical properties of the environment that these cells are cultured in[405]. Such an approach will likely be the best way to rapidly mature these cells.

3.3 Let-7 Overexpression

3.3.1 Background

Similar to hiPSC-CMs, hESC-CMs are immature following differentiation to the cardiac lineage, making them a poor model for adult cardiomyocytes. Among the list of viral techniques previously investigated to improve the maturation of stem cell derived cardiomyocytes are microRNAs (miRNAs). MicroRNAs are short, single-stranded, non-coding RNA molecules, which can regulate gene expression within a cell by inhibiting mRNA translation [406]. Previous research has found that certain miRNAs are important during in vitro cardiomyocyte differentiation [402, 407, 408], as well as some are able to control levels of cardiac gene expression [409]. Therefore, it is likely that there is a group of miRNAs that could be used to enhance the maturation of stem cell derived cardiomyocytes.

In initial experiments for this study, two different protocols were used to mature H7 derived cardiomyocytes in vivo. One technique involved culturing the cardiomyocytes in a static stress environment for two weeks in a collagen type I three-dimensional human cardiac tissue construct (cEHT) [405]. Cardiomyocyte maturation was also achieved by subjecting the cells to a prolonged culture time of one year. Following cardiomyocyte maturation, the illumina high throughput miRNA sequencing platform was used to elucidate miRNAs that were highly expressed in these two populations of cells. Out of the approximately 600 miRNAs that were identified from these two data sets ~80 miRNAs were found to be significantly regulated in both 1yr old and cEHTs. A heat map analysis of these miRNAs revealed four different groups miRNAs: 1) those that were up regulated in both data sets, 2) those that were down regulated in both the data sets, 3) those that were up regulated in cEHTs but not in 1 year old cardiomyocytes, and 4) those that were up regulated in 1yr old cardiomyocytes but not in cEHTs. This grouping revealed that the let-7 family

of miRNAs were consistently and significantly upregulated in 1 year old cells and cETH cells. This family of miRNAs was also found to have a large number of the targets among the down regulated transcripts in mature cardiomyocytes. Therefore, it is possible that the let-7 family of miRNAs may enhance stem cell derived cardiomyocyte maturation.

3.3.2 Methods

Lentiviral Transduction

For lenti-let7 OE constructs, Pri-miR-let7i and pri-miR-let7g sequence was amplified from H7 genomic DNA using forward primer for let7i- TCCGCGTGGTCCCGT; reverse primer for let7i- ATTGTCCTCCGCGGCGC and forward primer for let7g- AGAGTTCCTCCAGCGCTCC; reverse primer for let7g- CCCCACTTGGCAGCTGGC, resulting in 153bp and 154bp products, respectively. The amplicons were cloned between AgeI and EcoRI sites of pLKO.1 TRC vector (Open Biosystems) under human U6 promoter. 293FT cells were plated one day before transfection and pLKO.1-pri-mir-let7 was co-transfected with packaging vectors (pMK-VSVG, pMDL-G/P-RRE and pRSV-REV) in the presence of 2.5M CaCl2. Medium was changed 24 hours later and the lentiviruses were harvested 48 hours after transfection. Viral transduction of cardiomyocytes was performed by a spin infection technique. In brief diluted virus in the presence of hexadimethrine bromide (Polybrene, 4µg/ml)) was added to the beating cardiomyocytes at day 12 of the directed differentiation protocol. These were then subjected to centrifugation at 3000 RPM for 1 hour followed by overnight incubation with the virus.

Cell Culture

Undifferentiated human embryonic stem cell line RUES2 (NIHhESC-09-0013) were expanded using mouse embryonic fibroblast-conditioned medium with 5ng/ml basic fibroblast growth factor. These cells were then differentiated into cardiomyocytes as described in methods section 1.1.2, with the exception that at day 12 of the directed differentiation protocol the cells were either transduced with a virus carrying the pLKO-let-7 or empty vector control pLKO plasmid. After overnight transduction the virus was removed, cells were rinsed with PBS and new media added. After 20 days of in vitro differentiation, the cells were trypsinized and replated. The cells were then analyzed 10 days following replating. Only those cell preparations that had at least 70% cardiac troponin T- positive cardiomyocytes (as observed by flow cytometry) were analyzed.

Micropost Fabrication

The microposts used for these studies were fabricated as described in methods section 1.1.2. Each micropost within the arrays used for these studies was 6.45 μm in height, 2.3 μm in diameter, and the center to center spacing between adjacent posts was 6 μm. Prior to cell seeding, the tips of these microposts were stamped with 50 μg/ml of mouse laminin (Life Technologies). Cardiomyocytes that were 20 days post-differentiation and 1 week post pLKO-let7OE or EV lentiviral transfection, were seeded onto these arrays at a density of around 800,000 cells per substrate.

Contractility Assessment

One week following cell seeding, muscle twitches from individual hESCs-CMs were recorded and analyzed in a manner consistent with methods section 1.1.2. These cells were analyzed for twitch force and spontaneous beating frequency.

3.3.3 Results

Representative traces of total twitch force generation by single cardiomyocytes from the control and let7 OE groups are represented in Figure 31. Empty vector control hESC-CMs exhibited a twitch force of 7.77 ± 0.7 nN/cell (Figure 31). Let-7i and let-7g OE CMs exhibited significantly higher twitch forces of 9.28 ± 0.7 and 11.32 ± 0.86 (nN/cell; $P<0.001$), respectively. Additionally, let-7OE CMs (let-7i OE: 1.05 ± 0.1 Hz; let-7g OE: 0.92 ± 0.094 Hz) exhibited lower spontaneous beating frequency when compared to cells with the EV control (1.57 ± 0.1 Hz). This study also found that let7 overexpression resulted in increased cell size, perimeter, sarcomere length, and respiratory capacity.

3.3.4 Discussion

Cardiomyocytes derived from human embryonic stem cells exhibit spontaneous beating, cardiac related action potential, calcium transients and have the ability to engraft to form gap junction with the host myocardium [410] . In spite of their functional and physiological similarity to the cardiomyocytes in the developing heart, several lines of evidence suggest that the hESC derived cardiomyocytes are at a fetal state [149] with respect to their ion channel expression [411], electrophysiological signals [412] and physical properties [172] and thus serve as poor models for studying adult related heart disease and therapeutic screening.

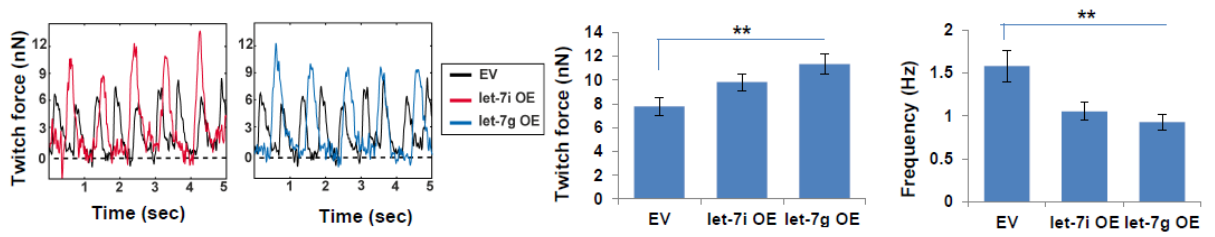

Figure 29 Contractile properties of let-7 treated hESC-CMs. Reproduced from: Kuppusamy, K.T., et al. (2015) Proc Natl Acad Sci 112(21): E2785-E2794; with permission from PNAS.

In this study, a large scale miRNA sequencing strategy was used to identify of let-7 family of miRNAs to be integral in promoting the maturation of hESC derived cardiomyocytes. Additionally, miRNA-mRNA targeting analysis using datasets from mature cardiomyocytes indicated that the let-7 family of miRNAs targets key cardiomyocyte pathways including PI3/AKT/Insulin pathway during maturation. These data demonstrate that let-7OE not only results in morphological and molecular changes indicative of maturation, but that functionally relevant parameters, such as contraction and beat frequency are also correctly regulated.

In conclusion, in order to recapitulate the features of in vivo maturation process more closely and to achieve a broader effect on cardiac function and physiology, future studies should use let-7 overexpression in combination with other promising approaches in order to induce the highest degree of cardiac maturation.

CONCLUSIONS

The current and potential applications for hPSC-CMs in cardiovascular medicine are vast. Investigators have used human cardiomyocytes derived from pluripotent stem cells (hPSC-CMs) as a model system to study the developmental and pathological states of the heart at the cellular level [9-13], to screen new pharmacological treatments for heart disease [9, 10, 14], and to partially restore heart function by supplanting dead or diseased tissue. [13, 15-20]. However, upon differentiation into cardiomyocytes, these cells are distinctly immature. Therefore, in order for these cells to serve as a valid replacement or model for more developed cardiomyocytes, their structural and functional maturation must be assessed and enhanced.

The primary function of a cardiomyocyte is to produce contractile forces. Therefore, having the ability to quantify this contraction would provide a powerful assessment tool for determining the

maturational state of hPSC-CMs. In Aim 1.1 of this work, a novel micropost technique was developed in order to allow for real-time measurements of hPSC-CM contractility. I demonstrated that this method can be used to analyze the passive tension, twitch force, velocity, and power produced by single hPSC-derived cardiomyocytes with high enough temporal resolution to resolve changes in kinetic properties i.e. time to peak, time to 50% relaxation, time to 90% relaxation. In an initial assessment of this system, I found that cells attached and spread to a higher degree on laminin-coated posts, suggesting that future experiments utilizing this system should also use laminin coatings. In Aims 2.1 and 3, I found that this system can be used to assess differences in the contractile properties of hPSC-CMs undergoing long term culture, as well as to resolve contractile changes due to various different biochemical treatments.

With regard to the maturation of hPSC-CMs, previous studies have shown that a number of different stimuli are capable of enhancing the functional and structural maturation of these cells. However, any one of these stimuli on their own, is incapable of achieving maturation levels consistent with mature ventricular cardiomyocytes. For Aims 2.2 – 2.4 of this work, significant improvements in hPSC-CM maturation were achieved after only a week of culture by combining substrate stiffness, cell alignment, and cell-cell contact into a single culture environment.

Through these studies, I found that the micropost assay is capable of accessing the contractile state of immature human cardiomyocytes, which makes it a powerful tool for developmental studies, pharmacological screening, and disease modeling applications. Furthermore, the pro-maturation environment that I developed was able to elicit cardiomyocyte maturation in the absence of any biochemical cues. Ultimately, I believe that these novel culture and analysis techniques will provide future researchers with a means to culture and assess large populations of rapidly matured stem cell-derived cardiomyocytes, for developmental, pharmacological, and therapeutic studies, which could lead to the discovery of novel treatments for heart disease.

FUTURE WORK

In the future, there are a number of improvements that can be made to the engineered systems described in Aim 1 of this work, as well as additional experiments which would strengthen the results obtained in Aims 2 and 3. With regard to the micropost system described in Aim 1.1, we and others have observed that the spread area and elongation of hPSC-CMs on microposts are

reduced when compared to those on flat culture surfaces. This spherical morphology results in out of plane contractile forces, which cannot be accurately measured by the microposts. We hypothesize that these morphologies are caused by the limited amount of attachment area presented to the cells by the microposts. Preliminary experiments using closely-packed posts with smaller diameters have demonstrated that these surfaces not only allow for a higher degree of cell spreading, but a higher resolution of subcellular force measurements. Therefore, future experiments would benefit from using these smaller "nanoposts." Additionally, we and other labs would benefit from our converting the Matlab code used for micropost analysis, into a user-friendly open source ImageJ or Java based code, so that scientists with little to no experience with coding could use it without extensive instruction or assistance.

In addition to adding biochemical treatments described in Aim 3 to the pro-maturation environment developed in Aim 1.2, this system could be adapted to allow for real-time measurements of contractile force by incorporating fluorescent beads into the soft PDMS, and using them as fiduciary markers for traction force microscopy. Based on previous studies employing polyacrylamide gels as a culture substrate for TFM, I believe that the soft PDMS substrates described in this work are sufficiently soft to allow for measurable bead deformations, and that these measurements would be compatible with all the other maturation stimuli described in Aims 2 and 3. Additionally, having the ability to measure live calcium transients and live contractile forces would allow for comparisons between the two, and would add important information regarding the functional maturation of these cells.

With regard to the studies described in Aim 2, all of these studies would benefit from the addition of parallel Fluo experiments, assessments of calcium transient conduction velocity, further investigation into the spatiotemporal trends in calcium transients, comparisons between area and line-scanning calcium techniques, immunofluorescent staining of connexin-43 and N-cadherin, assessments of sarcomere content, as well as further investigation into the reasons behind the observed structural and functional improvements in cell maturation. Specifically, the cell alignment experiments would also benefit from confocal imaging, to determine the effect of cell alignment on cell volume, and cross-sectional area, as these properties would influence a cell's ability to contract. Additionally, since cell length was not strictly controlled in these experiments, direct comparisons between cell aspect ratio and the measured endpoints would give further insight

into the indirect effect of alignment on alterations in cell maturation. Additionally, cell-cell contact experiments would benefit from a closer examination into the effect of the number of connected cells on the assessed structural and functional properties. As well as calcium transients along strips of cells would yield information regarding signal transduction from one cell to another, which is an important function of mature cardiomyocytes. I believe that future experiments would greatly benefit from all of these additions.

APPENDIX A: IN PROGRESS STUDIES

The following sections contain information regarding studies that are still in their early stages of progress, or have been passed onto other students.

A1 Electrical Stimulation

A1.1 Background

In the human heart, synchronized fluctuations in ionic currents result in sinusoidal oscillations in calcium transients, which stimulate the whole-heart contractions responsible for maintaining regular blood flow throughout the entire body. Therefore, regular maintenance of these signals is highly important for maintaining normal heart function, as well as the function of the body as a whole. Furthermore, electrical signals are also known to play an important role during normal fetal development. In-vivo, these fields are involved in embryonic development and disturbances can result in abnormal embryonic development [413]. Similarly, interruption in the electrical signals of the fully mature heart, such as those caused by fibrosis or necrotic tissue, can results in heart arrhythmias, and even death.

As discussed in the introductory sections of this dissertation work, immature cardiomyocytes in culture spontaneously beat, while adult cardiomyocytes are quiescent, and require electrical signaling to beat [414]. This discrepancy has been attributed to the fact that stem cell derived cardiomyocytes lack fully mature calcium stores and channels, so calcium transients are thought to originate from ion diffusion across the cell membrane, rather than from adjacent cells. As such, individual cells, or groups of cells within populations of hPSC-CMs contract somewhat irregularly, and at various different frequencies. However, electrical stimulation can be used to trigger regular membrane depolarizations, and pace the entire cell population at the same beating rate.

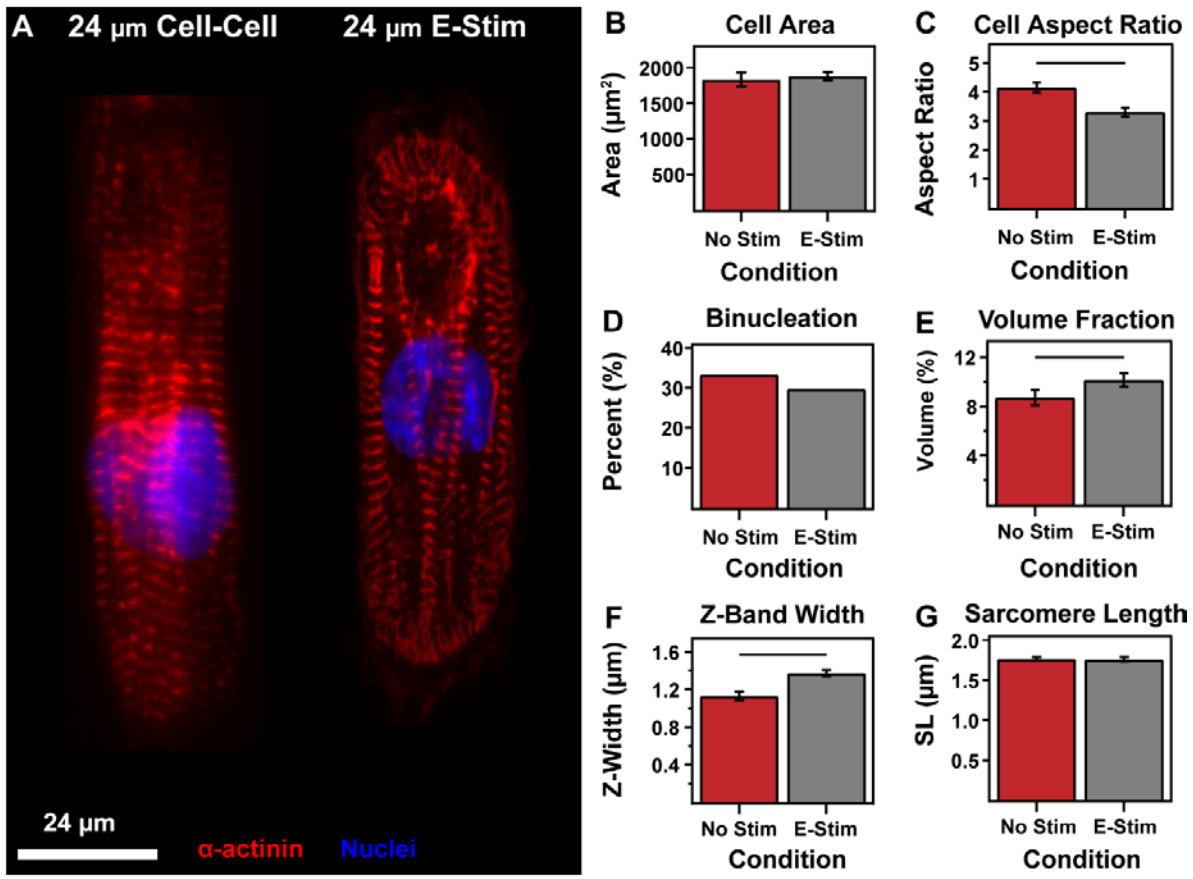

Figure 30 Effect of electrical stimulation on hSC-CM structure.

Previous research has found that electrical stimulation can lead to improvements in sarcomeric maturation and organization, calcium transient properties, action potentials, gene expression, and contractile force [189, 305, 309, 320]. However, much like the other stimuli investigated in this work, some of these responses appear to be cell line dependent, and in this case, they are also stimulation parameter-dependent (Appendix B, Table 12). Therefore, electrical stimulation parameters must be optimized for the cell line of interest.

To determine the effect of electrical stimulation on patterned strips of hESC-CMs on soft PDMS surfaces, a commercial waveform system was used to apply electrical stimulation (biphasic, 0.5-2 Hz, 5ms, 10 V/cm) to the cultured cells over a period of 6 days. These parameters were selected based on the results of other stimulation studies with cardiomyocytes. Following this protocol, to determine the effect of this protocol on the cells, live calcium transients and immunofluorescent images of these cells were analyzed as described in earlier Aims.

A1.2 Methods

The methods outlined in Aims 1.2 and 2.2-2.4 were used here, to apply electrical stimulation to high densities of hESC-CMs seeded onto patterned substrates of soft PDMS.

A1.3 Preliminary Results

Cell Structure

Structurally, the beneficial effect of electrical-stimulation on hESC-CMs was unclear (Figure 27A). I found that there were no significant differences in cell spread area, binucleation or sarcomere length (Figure 27B, D, and G) for unpaced versus paced cells. However, cell aspect ratio significantly decreased (Figure 27C), nuclear volume fraction significantly increased (Figure 27E), and Z-band width was also seen to significantly increase (Figure 27F), upon application of electrical stimulation.

Cell Function

Similarly, calcium transient properties of electrically-stimulated cells were also not distinctly different from non-electrically stimulated cells. In fact, there were no significant differences in any of the measured quantities, with the exception of a significant increase in basal calcium intensity (Figure 28A) for electrically stimulated cells. Additionally, upon examining the other measured properties, it

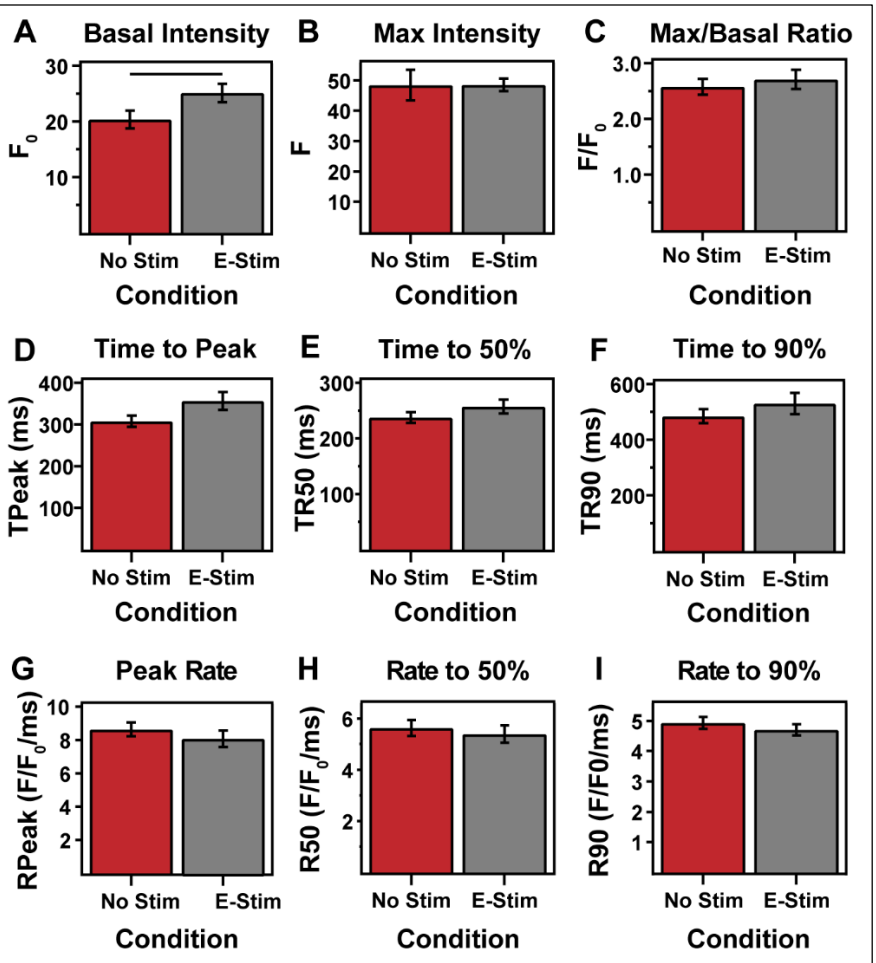

Figure 31 Calcium handling properties of electrically-stimulated hPSC-CMs.

appears that, overall, most of the changes induced by electrical stimulation are indicative of a reduction in cell maturation, rather than an enhancement.

A1.4 Future Work

Based on the non-beneficial effect of electrical stimulation found in these preliminary experiments, for my future work on this aim, I will be optimizing the electrical stimulation parameters for this particular cell line, seeded in one cell wide strands, on top of soft PDMS surfaces. Additionally, it is also possible that the cells require more time to stabilize prior to the initiation of electrical stimulation. Other studies have waited 7 days prior to the initiation of stimulations [309], so a longer pre-stimulation culture period could be another alteration incorporated into these future experiments. Upon completing this work, I will be the first author on the resulting publication.

A2 Fatty Acid Supplementation

A2.1 Background

As discussed in Aim 3.2, glucose is the primary energy source for immature cardiomyocytes [385], while adult cardiomyocytes obtain the majority of their energy from fatty acid oxidation. From our results in Aim 3.2, we now know that hPSC-CMs have the ability to oxidize fatty acids, therefore, it is possible that simply providing them with a source of fatty acids could prompt these cells to become more metabolically mature. In these studies, hiPSC-CMs were grown in media supplemented with fatty acids, to determine their effect on the structural and functional maturation of these cells. My contribution to this work was to assess the effect of fatty acid supplementation on the contractile properties of the cells, using the micropost assay described in Aim 1.1.

A2.2 Methods

The cell culture and substrate preparation methods employed for this study are the same as those used for our AMKP study described in Aim 3.2, with the exception that the media was supplemented with 52.5 µM of Palmitic acid, 40.5 µM of Oleic acid (Sigma Aldrich), and 22.5 µM of Linoleic acid (Sigma Aldrich), rather than AICAR.

A2.3 Preliminary Results

Upon analyzing the contractile properties of hiPSC-CMs cultured on top of arrays of microposts in fatty acid doped medium for a week, I found that fatty acid treatment resulted in a significant increase in the total twitch force produced by the treated cells versus control cells of the same age (Figure 32). This data was obtained from three replicate experiments, with at least 40 cells per condition.

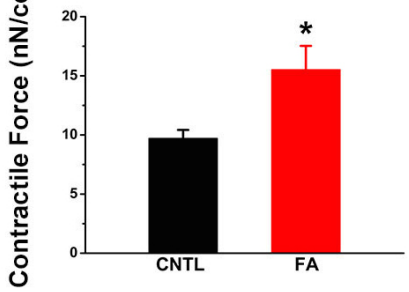

Figure 32 Effect of fatty acid supplementation on hiPSC-CM contraction.

A2.4 Future Work

In completing this study, I will be analyzing the time to peak, time to 50% relaxation, time to 90% relaxation, upstroke velocity, and decay velocity, from the same cells, to determine the effect of fatty acid supplementation on the kinetic properties of hiPSC-CMs. For this work, I will be the second author on the resulting publication.

A3 Wild-Type versus Patient-Derived hiPSC-CMs

A3.1 Background

Cardiomyocyte contractile function is primarily regulated by the sarcomere, which consists of approximately 20 proteins. There are approximately the same number of proteins that connect the sarcomere to the external ECM environmental, and serve to transmit mechanical signals from the ECM to the cell, or vice versa. Therefore, if one of these proteins is impaired, cardiomyocyte function could be greatly impaired. Thus far, over 400 mutations in 13 sarcomeric proteins have been associated with cardiomyopathies, as well as a number of mutations associated with cell-cell and cell-ECM coupling [8]. Previous research has also found that mutations in the same gene can result in different phenotypes, and that external environmental factors can influence the presentation of said phenotype[8]. Therefore, classification of these cardiomyopathies is not straightforward.

Of the currently classified inherited cardiomyopathies, HCM is the most prevalent. It is approximated that one out of every 500 people has HCM, and it is currently the leading cause of sudden cardiac death among people under the age of [415, 416]. HCM is linked to all 13 of the identified sarcomeric mutations associated with cardiomyopathies, and can result in a number of

different clinical outcomes. Namely, HCM is marked by increases in heart mass and asymmetric interventricular septal thickening, and on the cardiomyocyte scale, by cell hypertrophy and myofibrillar disarray [415, 417, 418]. Ultimately, these traits can result in ventricular wall thinning chamber dilation, which lead to decreases in cardiac output, and eventually heart failure [8].

In a recent publication, patient-specific hiPSC-CMs were derived from a ten-member family with a hereditary HCM missense mutation (Arg663His) in the MYH7 gene [419]. These cells were found to recapitulate various different characteristics of the HCM phenotype including cellular enlargement, contractile arrhythmia, hypercontractility, and a dysregulation of Ca^{2+} cycling, at the single-cell level. Therefore, I would also expect to see some of these same properties for HCM patient-derived hiPSC-CMs on top of microposts.

A3.2 Methods

The micropost fabrication and contractile analysis employed in these studies are the same as those previously described in Aim 1.1, with the exception that two control lines (CEM and IMR90) and two patient lines (Pt4 and Pt6) were used.

Cell Culture

A 3 to 5 mm skin punch biopsy was obtained from the forearm of all study participants. The human dermal fibroblasts (HDFs) were expanded and passaged twice prior to being reprogrammed with episomal vectors expressing the transcription factors *OCT3/4*, *SOX2*, *KLF4*, *L-Myc*, *Lin28*, and *p53-shRNA*, according to published methods [420]. Episomal vectors, bearing human *OCT3/4*, *SOX2*, *KLF4*, *L-Myc*, *Lin28*, and *p53-shRNA* were obtained from Addgene (Plasmid 27077, 27078, and 27080). The expression plasmid mixture was electroporated with the Neon Transfection System (Invitrogen). Conditions used were 1,650 V, 10 ms, and 3 time pulses. Colonies were manually passaged onto a feeder layer of irradiated mouse embryonic fibroblasts (MEFs) and grown in MEF-conditioned medium supplemented with 10 ng/mL bFGF (Stemgent). Individual hiPSC clones with similar morphology to human ESCs were selected and further expanded on feeder cells. Only karyotypically normal hiPSCs were expanded and used for this study. All six patient-specific iPSC lines were characterized with pluripotency markers, SSEA4 (DSHB) and GCTM2 (gift from Dr. Martin Pera) by flow cytometry and by staining for alkaline phosphatase (Vector).

A3.3 Preliminary Results

In preliminary studies with two different HCM patient lines of cardiomyocytes, we found increases in the passive tension and contractile force produced by these cells, when compared to wild-type cells. Alternatively, there was no apparent trend in force per area with respect to presence or absence of the HCM mutation, as one patient and one control line demonstrates much higher values than the other lines. We also noted that one of the control lines had a significantly higher spontaneous beating than the other cell lines. This data was compiled from only one experiment per cell line, and there was very little usable data for the Pt4 cell line. Therefore, we cannot make any definitive statements regarding the effect of the HCM mutation on the contractile properties of hPSC-CMs. However, the increased forces seen in the patient lines appear to agree with previous results which observed increased contractility in similarly-derived cells [419].

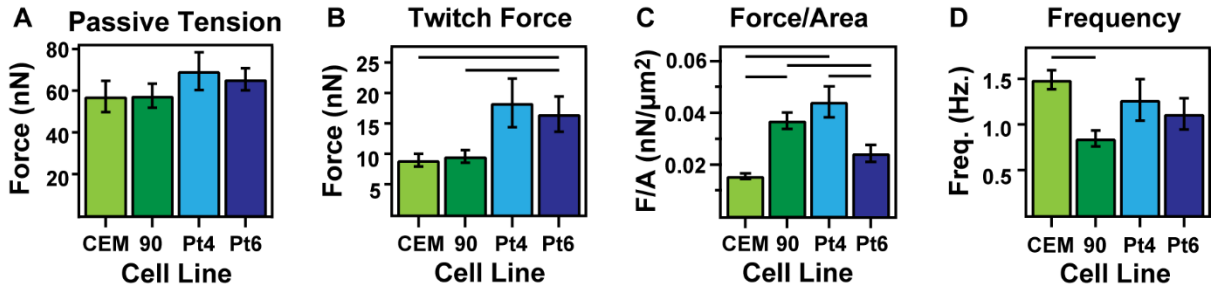

Figure 33 Contractile properties of hPSC-CMs from control and patient cell lines.

A3.4 Future Work

This work will likely be passed onto another student. I suggest that this student confirm these results with additional replicate experiments, as well as that they analyze the twitch kinetics of these cells by assessing upstroke and relaxation twitch velocities. Due to the differences in spontaneous beating frequency between cell lines, I would also suggest that the cells be electrically-stimulated for these experiments. This additional data would give a more complete picture regarding the effect of HCM mutations on the contractile properties of individual hPSC-CMs, and would likely lead to information regarding the development, progression, and potential treatment options for this disease.

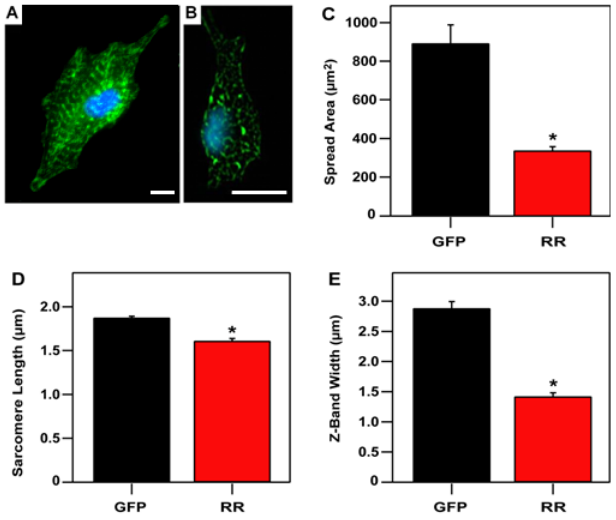

Figure 35 Structural response of neonate cardiomyocytes to RR treatment. Adapted by permission of The Royal Society of Chemistry.

A4 RR Overexpression

A4.1 Background

Ribonucleotide reductase (RR) promotes the generation of 2-deoxy-ATP (dATP) from ATP, which has previously been shown to result in a higher magnitude of force and a faster rate of force production in cardiac muscle by increasing the number of cross-bridges that bind and cycle [306, 307, 421-424].

In preliminary experiments with RR, I tested the hypothesis that cardiomyocyte tensional homeostasis – a feedback mechanism governed by cellular forces – is affected by modulating the amount of force produced by individual myosin heads. To achieve this, neonatal cardiomyocytes were treated with ribonucleotide reductase on top of arrays of microposts; which were used to measure their twitch force, velocity and power in relation to their myofibril structure. Individual micropost deflections were measured with IonOptix© line scanning software and IonOptix© optical equipment, as previously described [127]. I observed that RR-overexpressing cardiomyocytes produced twitch forces that were similar to those produced by cardiomyocytes cultured under control conditions, which indicates that the equilibrium state for cardiac tensional homeostasis was maintained (Figure 34A). Alternatively, twitch velocity and twitch power in the treated cells were significantly lower than control cells (Figure 34). Immunofluorescent analysis of spread area, sarcomere length, and Z-band width revealed that RR-overexpression resulted in lower

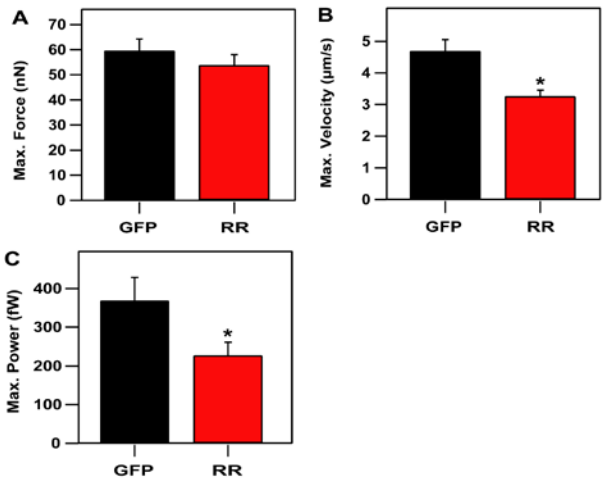

Figure 34 Contractile response of neonate cardiomyocytes to RR treatment. Adapted by permission of The Royal Society of Chemistry.

spreading and poor myofibril structure in treated cells (Figure 33). These results suggested that twitch forces act as an internal cue for tensional homeostasis, which is maintained by altering myofibril structure and, subsequently, cardiac power.

Since hiPSC-CMs are also immature, it is possible that RR treatment would have a similar effect on them. To test this hypothesis, the same procedure used in these preliminary studies will be used to test the effect of RR treatment on the contractile and structural properties of hiPSC-CMs. However, unlike these previous studies, the techniques outlined in methods Aim 1.1 of this work will be employed to measure contractile force, velocity, power, and contractile kinetics at all the microposts underneath a single cell.

A4.2 Methods

These studies will employ hiPSC-CMs derived from the same cell line, and the same cell culture protocols outlined in Aim 1.1 of this work. 60 days following differentiation, the cells will be dispersed and seeded onto arrays of microposts, and analyzed as previously described. Baseline forces were collected immediately preceding the first treatment (Day 0), and two days later (Day 2).

Cell Force Modulation

Viral-mediated enhancement of myofibril forces were achieved by increasing dATP production in cells via transduction with an adenoviral vector for ribonucleotide reductase subunits Rrm1 and Rrm2 (R2R1). RR treatment was conducted 5 days following cell seeding, and was washed out 48 hours following treatment.

A4.3 Preliminary Results

In preliminary studies with hiPSC-CMs from the IMR90 cell line, the R1 and R2 subunits were delivered to the cells in the same vector with the R2

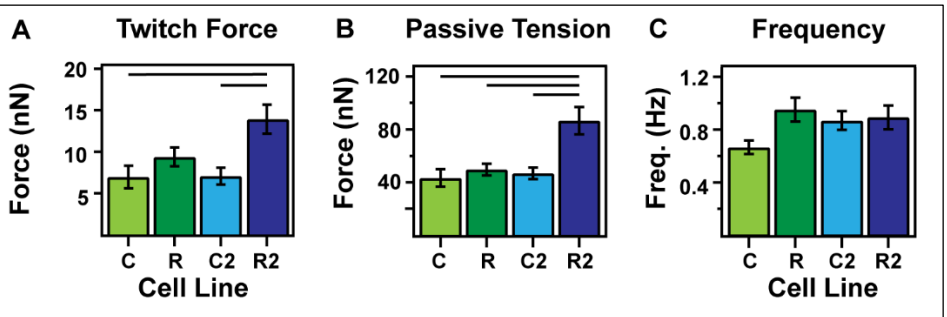

Figure 36 Effect of RR treatment on hiPSC-CM contraction.

unit expressed first (R2R1). As expected, prior to RR treatment, there were no significant differences between the twitch force, passive tension, and twitch frequency of the two cell populations. However, two days following treatment, the twitch forces measured for R2R1 cells were significantly higher when compared to the control cells from both days. Furthermore, measured values of passive tension were significantly higher for RR treated cells on day 2, when compared to all other cell groups. And, there was no difference in twitch frequency between any cell groups. These results suggest a positive, force-enhancing, role of RR on hiPSC-CMs. However, we also found that a large majority of the cells treated with RR were dead on day 2. This led us to the conclusion that the viral load delivered to the cells was likely too high.

A4.4 Future Work

This work will be passed onto another student. In my opinion, that student should establish a titration curve to determine the proper viral load of RR for future experiments. Once this has been done, I suggest that these experiments be repeated, as well as carried out for a longer period of time, in order to determine the longer-term effects of RR on the contractile maturation of hiPSC-CMs.

A5 Stretching hPSC-CMs

A5.1 Background

Cardiomyocytes within the heart are consistently subject to dynamic stresses, both during development and in their fully mature state. The heart experiences active stretching during filling, and self-generated forces during ejection. Previous work has found that extracellular mechanical forces are primarily transmitted across cell membrane via integrin attachments, and are then transmitted to various different mechano-sensitive cell structures via the cytoskeleton [425]. In human cardiomyocytes, there are a number of these structures within the Z-disk, including muscle lim protein (MLP), calsarcin-1, and titin [353, 426]. Alternatively, if these mechanical signals are transmitted to the nucleus they can theoretically alter gene expression or enzymatic activity by physically distorting genomic structures within the nucleus [427, 428]. Or, they can be transmitted to cell-cell junctions, in which case they have been shown to regulate the expression and size of these junctions [266, 429-432].

A number of previous studies have examined the effect of applied strain on the contractile and structural properties of isolated cardiomyocytes [143, 144, 240, 366], as well as the effect of strain on groups of immature cardiomyocytes [118, 299, 302, 303, 310, 405, 431, 433]. In general, these studies have found that applied strain causes immature cardiomyocytes to demonstrate enhanced maturation – as assessed by actin alignment, sarcomeric alignment, gap junction organization, cell area, beating rate, cardiac-specific markers, passive and active force production, etc. – when compared to non-strained cells. Additionally, while static and cyclic straining profiles have both been found to enhance these properties, cyclic strain often does so to a higher degree [405]; as does unidirectional strain when compared to equiaxial or biaxial straining i.e. equal strain in all radial directions, and higher frequency strains as compared to lower frequencies [303].

Methods previously utilized to apply strain to two-dimensional cultures of cells include deforming the substrate below or surrounding the cell of interest [118, 311, 366], clamping the cell between a fixed and a translating rod, and attaching a magnetic bead to the cells, to name a few. Alternatively, a small tissue construct composed of cells can be strained by encapsulating them within an ECM tissue, growing this tissue in a rectangular or ring-shaped mold, and then deforming the tissue via vacuum pressure [300, 405, 431, 434], through an actuator [299, 303, 310, 433], or via magnetic forces [435].

Due to their elastic material properties, silicone micropost arrays can be subject to a wide variety of high-magnitude mechanical forces without losing structural integrity. Such mechanical forces can be simultaneously applied to individual cells or a population of cells by fabricating the posts on top of thin membranes of PDMS, and then straining the underlying membrane. In order to determine the effect of applied strain on individual hiPSC-CMs, these cells will be seeded on top of microposts, and then subjected to physiological strains. This will be achieved by fabricating the micropost arrays onto a thin membrane of PDMS and placing this membrane in a commercial Flexcell

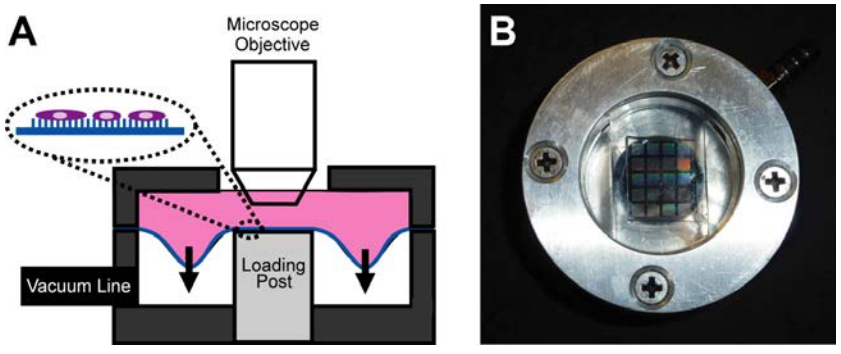

Figure 37 Flexcell Jr. Stageflexer device

Jr. vacuum chamber (Figure 36). In this system, the applied vacuum pressure pulls the membrane over a loading post, whose shape determines the directionality of the applied strain i.e. a rectangular loading post results in biaxial strain, while a circular post results in equibiaxial strain.

A5.2 Methods

Micropost Fabrication

Arrays of microposts will be fabricated on top of thin PDMS membranes in a manner similar to that used to fabricate coverslip-backed microposts described in Aim 1.1 For this fabrication, a metal shim will be used to control the thickness of the resulting membrane, as well as it will act as a frame on which to cast the PDMS master; to facilitate membrane handling. To achieve this, the shim will be placed on top of the PDMS negative, additional PDMS will be poured on top of it, and a flat glass plate will be placed on top of the PDMS. This whole structure will then be placed in an oven for curing. Stamping of these microposts will be performed in the same manner as outlined in the background sections of this work. Prior to straining the cells, the membrane will be cut from the metal shim, and mounted in the stretching device.

Stretch Chamber

These thin membrane microposts will be placed into a FlexCell Jr. chamber for measurement on an upright microscope. For these studies, uniaxial, cyclic strains that mimic the strains present in the heart during development will be applied to the cultured hiPSC-CMs at a frequency of 1 Hz. These values are based on those most-commonly used for previous experiments with cardiomyocytes, but can be altered to allow for a larger degree of studies [299-304]. These strains will be controlled using a LabView interface to control vacuum pressure.

Assessment

Analysis for these strained cells will be the same as outlined in prior sections of this work with the addition of analysis for traction force orientation with respect to the direction of the applied strain. Similarly, cell structure will be analyzed as described in Aim 1.1, with the addition of analysis for actin and sarcomeric alignment.

A5.3 Preliminary Results

In previous work, the effect of applied strain on the structural and contractile properties of human cardiovascular smooth muscle cells was investigated. The results of these experiments demonstrated that applied strain leads to lower traction forces in human smooth muscle cells under 12 and 24 hours of stagnant strain (Figure 37A). Furthermore, we observed that the cytoskeletal proteins within the smooth muscle cells aligned in the direction of the applied strain (Figure 37B & C).

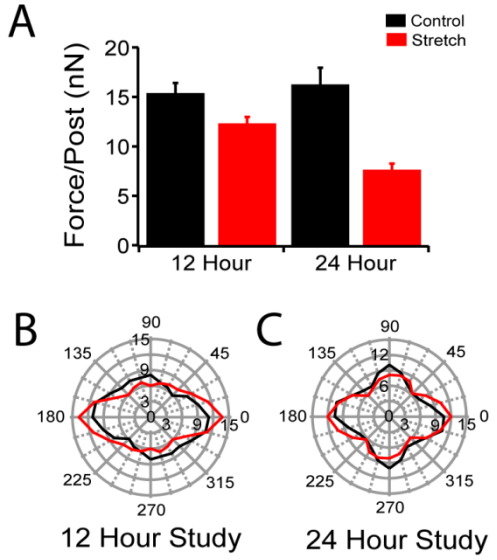

Figure 38 Effect of static strain on hSMC forces and cytoskeletal alignment.

These results suggest that the Flexcell system is capable of strain to a membrane mounted on top of its support column. Furthermore, this strain is translated to microposts mounted on top of the membrane, and even cells on top of these posts. Upon performing these stretching experiments, we also found that the posts remained upright, and could be used for force analysis. Therefore, I believe that this system is capable of delivering similar strains to hPSC-CMs, and that the microposts could be used to assess changes in the contractile properties of these cells, with respect to the applied strain.

A5.4 Future Work

This project has been passed onto another student, who has been exposing hPSC-CMs to cyclic strain profiles using the Flexcell® FX-5000™ Tension System. This system is essentially a larger scale version of the Flexcell Jr. System. This student is currently in the very beginning stages of this project, and has been working on optimizing this new Flexcell system for use with hPSC-CMs seeded on top of micropost membranes and flat PDMS surfaces. I will continue to help oversee this project as long as I can.

APPENDIX B: REFERENCE CELL PROPERTIES

Table 9 Structural and functional properties of aged cardiomyocytes.

								Calcium Handling Properties					*Structural Properties*				*Contractile Properties*			
Author	**Year**	**Cells**	**Age**	**Single/Multi**	**2D/3D**	**E-Stim**	**Substrate**	**F/Fo**	**Vup F/Fo/s**	**Vdecay F/Fo/s**	**Tpeak ms**	**T50 sec**	**SL um**	**Area um x um**	**AR**	**Multinuc. %**	**Velocity um/s**	**Tpeak sec**	**T90 sec**	**Freq. Hz**
Germanguz, I.	2011	hiPSCs	29 60	Multi	2D	Yes	Glass	0.68 0.75 -0.81												
Kiamakura, T.	2012	hiPSCs	30 360	Both	2D	No	TC dish							3277 4067*						1.22 0.537*
Lundy, S.D.	2013	hESCs	20-40 80-120	Single	2D	No	PEI gelatin	0.22 0.24	3.75 9*	0.3 0.8*	342 102*	446 227*	1.65 1.81*	480 1716*		4.2 35.3*		0.3 0.5*	0.65 0.35*	
Sartiani, L.	2007	hESCs	16-25 57-110	Multi	2D	No	Gelatin		4.2 6*											
Shinozawa, T.	2012	hiPSCs	20-30 50-60 80-90	Both	2D	No	TC dish										2 3 5.5*			1.022 0.777 0.588*
Snir, M.	2003	hESCs	7-20 21-35 36-60	Multi	2D	No	0.1% Gelatin							90 80 180	1.9 1.8 3					

Table 10 Structural and functional properties of cardiomyocytes on substrates of different stiffnesses.

								Calcium Handling Properties		*Structural Properties*					*Contractile Properties*			
Author	**Year**	**Cells**	**Age days**	**Single/Multi**	**E-Stim**	**Substrate**	**Stiffness kPa**	**F/Fo**	**T90 ms**	**SL um**	**Area um x um**	**AR**	**Force nN**	**Rest Force nN**	**Stress mN/mm2**	**Resting mN/mm2**	**Velocity um/s**	**Freq. Hz**
Bajaj, P.	2010	ECM	8	Both	No	PA Gel	1 18 50 TC						30.16 71.3*					1-1.3
Bhana, B.	2009	NRVM	N/A	Multi	Yes	PA Gel	3 22 50 144					1.25 2.5 4.25* 3.5*			0.25 0.5 1.5 3*			
Chopra, A.	2011	NRVM	N/A	Single	No	PA Gel	0.1 0.3 5 10 30 30000000				195 225 245 350 375 540	1.2 1.4 1.4 1.66 1.57 1.77			0.04 0.3 1 	0.175 1.05 1.05 		
Engler, A.	2008	EQM and ECM	10	Single	No	Pa Gel	1 11 34				1000 1500 1450							0.8 0.75 0.4
Hersch, N.	2012	ERVM	19 day	Single	No	PDMS	1 15 30 90 150 500			1.9			74 174.5 261.5					
Jacot, J.G.	2008	NRVM	N/A	Single	Yes	PA Gel	1 5 10 25 50	0.25 4 6* 1.5 1		1.69 2.23	600 700 750 650 900	4.1 4.1 4.5 4.75 3.5	100 200 720* 550 375	19 20 45 57.5 55			10 9 8.5 5.75 5	
Rodriguez, A.G.	2011	NRVM	N/A	Single	Yes	PDMS Posts	3 8 10 		100 83	1.76 1.82 1.86 1.95*			20 60 65 120				5.5 3.9 3.2 3.3	
Hazeltine, L.B.	2012	hiPSCs hESCs NRVM	28-32 N/A	Single	No	PA Gel	4.4 18.4 49.4 61.6 76 99.7 4.4 18.4 49.4 61.6 76 99.7 4.4 18.4 49.4 61.6 76 99.7				750 850 1200* 950 945 800				3 4 10 8 21 30* 3 4 15 18 25 35* 5 7 8 9 15 12			0.6 0.55 0.55 0.38 0.42 0.48 0.32 0.4 0.28 0.45 0.45 0.42 0.33 0.3 0.33 0.37 0.34 0.37
Galie, P.A.	2013	rAdult	N/A	Single	Yes	PDMS	7 27 255	2.5 2.4 2.2		1.75-1.81							5 2.3 3.5	

Table 11 Structural and functional properties of aligned cardiomyocytes.

										Calcium Handling Properties					*Structural Properties*				*Contractile Properties*		
Author	**Year**	**Cells**	**Age**	**Single/Multi**	**E-Stim**	**Alignment**	**Pattern**	**Substrate**	**Stiffness**	**F/Fo**	**Trans cm/s**	**Tpeak ms**	**T50 sec**	**T90 ms**	**SL um**	**Area um2**	**Align**	**AR**	**Stress mN/mm2**	**Velocity um/s**	**Freq. Hz**
Bray, M.A.	2008	NRVMs	N/A	Single	No	uCP	1:1 (50 x 50) um 2:1 (35.4 x 70.7) um 3:1 (28.9 x 86.6) um 5:1 (22.3 x 111.8) um 7:1 (18.9 x 132.3) um	PDMS	NR						2.27 2.25 1.98 2.09 1.96						
Chen, A.	2014	hESC		Multi	No	Topology	Flat Line 8 um Wrinkles 50nm - 3um	PS	NR								20% 35% 42%				0.21 0.2 0.27
Feinberg, A.W.	2012	NRVM	N/A	Multi	Yes	uCP	No 20 um aniso 20 um lines	PDMS	NR	2.5 3.4 3.55		62 37 36							0.25 0.75 1.5		
Geisse, N.A.	2009	NRVM	N/A	Single	No	uCP	1:1 (50 x 50) um 2:1 (35.4 x 70.7) um 3:1 (28.9 x 86.6) um 5:1 (22.3 x 111.8) um 7:1 (18.9 x 132.3) um	PDMS	NR							2229 2512 2203 2187 2465					
Kim, DH	2009	NRVM	N/A	Multi	Yes	Grooves	None 150 nm 400 nm 800 nm	PEG gel	NR							341 300 471*		3.73 7.58		5 6.5 3.75	
Kuo, P.L.	2012	NRVM	N/A	Single	No/Yes	uCP	1:1 (50 x 50) um 2:1 (35.4 x 70.7) um 3:1 (28.9 x 86.6) um 5:1 (22.3 x 111.8) um 7:1 (18.9 x 132.3) um 11:1 (14.4 x 173.2)	PA Gel	8 kPa			70 60 60 100		200 200 225 300							
McDevitt, T.C.	2001	NRVM	N/A	Multi	No	uCP	5 um 15 um 30 um 50 um	PS	NR									9.2 4.9 3 1.8			
Pong, T.	2011	NRVM	N/A	Multi	Yes	uCP	None 10 um 20 um	PDMS	NR	0.75-0.9 0.8-0.82 0.95-1.1						1000 800 800	52 619 21	3.5 6.75 8.75			
Sheehy, S.P.	2014	NRVMs	N/A	Monolayer	Yes	uCP	None 20 um	PDMS	NR			49	80	230	2.05				8 kPa		
Wang, P.Y.	2011	NRVM	N/A	Multi	No	Topology	None 450 nm x 100 nm 450 nm x 300 nm	PS/PU	4 MPa -2 GPa							780-850 660-840 660-720	45-47 17-20 5-7	3.25 5-5.25 6.75-7.5			0.17-0.5

Table 12 Structural and functional properties of electrically-stimulated cardiomyocytes.

											Calcium Transient Properties						*Structural Properties*				*Contractile Properties*					
Author	**Year**	**Cells**	**Age Days**	**Structure**	**Pulse Form**	**Pulse (ms)**	**Field (V/cm)**	**Freq. (Hz)**	**Duration (Days)**	**Substrate**	**Tpeak (ms)**	**TRel50 (ms)**	**TRel90 (ms)**	**Vup (F/Fo/s)**	**Transient (cm/s)**	**F/Fo**	**SL (um)**	**Alignment (deg)**	**Area (um^2)**	**AR**	**Force (nN)**	**Stress (mN/mm^2)**	**Vrelax (mN/s)**	**Tpeak (ms)**	**TRel50 (ms)**	**Freq. (Hz)**
Chan, Y.C.	2013	hESCs	23	Single			None			0.1% gelatin										1.9						
					Bi	2	6.6	1	4											3.66						
Lieu, D.K.	2013	hESCs	38-42	Single						0.1% gelatin						1.85										
																1.49										
Hirt, M.N.	2014	NRVM	N/A	Tissue			None			N/A								35		7.4	130	0.1				4
					Bi	2	2	0.5	16-18									35		7.9*	250	0.29				3
							None											55		3-4	56					
		hiPSCs	15-20					0.5													70					
					Bi	2	2	1.5-2	14									37.5		7	83					
Kujala, K.	2012	NRVM	N/A	Monolayer	Bi	100	5.3	1	3	Gelatin																
									2																	
					Mono	2	5		3																	
									3	Collagen																
Lee, P.	2012	hiPSCs	25	Monolayer			None			PDMS	511		365 - 380	5.29			1.98									
					NR	500	NR	NR	2		496		315 - 335	5.55												
						750					403		350 - 360	7.36												
Nunes, S.S.	2013	hESCs	21 - 28	Tissue				None							10	2.5			248 - 857							
					Bi	1	3 - 4	1 - 3	7	N/A					14	2.64			279 - 977							
								1 - 6							16	2.93			208 - 917							
Radisic, M.	2004	NRVM	N/A	Tissue			None			N/A																
					Mono	2	5	1	5													7 fold higher				
Sathaye, A.	2006	NRVM	N/A	Monolayer					4										789							
							None		6										823							
									8	Cover slips									876							
									4										813							
					NR	4	2.5	2	6										878							
									8										941							
Taylor, D.G.	2004	rAdult	N/A				None															11.8				
								0.5			30	190										9.8	22.5	74	130	
								1				168										8.5	25	71	125	
								2				148										7.9	44	66	115	
					Bi	5		3			34	122										7.5	65	60	105	
								4				112										6	66	59	100	
								5				105										6.5	64	58	99	
								6				99										5.2	60	58	98	

Table 13 Structural and functional properties of cardiomyocytes exposed to two or more pro-maturation stimuli.

									Calcium Transient Properties						*Structural Properties*			*Contractile Properties*								
Author	**Year**	**Cells**	**Age**	**Cell Format**	**E-Stim**	**Alignment**	**Pattern**	**Substrate**	**Stiffness kPa**	**Transient cm/s**	**Freq. Hz**	**Tpeak ms**	**T50 ms**	**T90 ms**	**F/Fo**	**SL**	**Alignment**	**Area um x um**	**AR**	**Force nN**	**Velocity nN/s**	**Stress mN/mm2**	**Tpeak ms**	**TRel50 ms**	**TRel90 ms**	**Work pJ**	**Freq Hz**
Chiu	2012	NRVM	N/A	Multi	None	Grooves	Flat	Matrigel	NR								42		3								
					Parallel												11		3.75*								
					Perpendicular												15		3.5								
					None												32		3								
					Parallel		10-100 um										6		5.25								
					Perpendicular												20		4.75								
Hampe, N.	2014	NRVM	N/A	Single	None	uCP	15 x 104 um		15 kPa									1040		75							1
							17 x 86 um																				
							39 x 39 um																				
				Multi			15 x 104 um											1280		119							
Heidi, Au, H.T.	2007	NRVM	N/A	Monolayer	None	Grooves	None	Polyvinyl	NR								47		4								
							3 um										14*		5								
							9.75 um										12*		6.5*								
							13 um										12*		7.5*								
					2.3 V/cm		None										50		4.75								
							13 um										10		5.5								
					4.6 V/cm		None										38		5.5								
							13 um										9		5.75								
Heidi Au, H.T.	2009	NRVM	N/A	Monolayer	No	Grooves?	0.5 um	PS									4		5.6								
							3 um										4		4.25								
							None										42		2.5								
					Perpendicular		0.5 um Perp										4		5.75								
					Parallel		0.5 um Parallel										4		8.9								
					No direction		None										37		5.2								
McCain, M.L.	2014	NRVM	N/A	Single	No	uCP	25 x 50 (2:1)	PA Gel	13							1.76-1.87		1200		300			70			0.45	
									90											1200			110			1.05	
							17 x 68 (4:1)		13											350			88			0.6	
									90											800			86			0.6	
							12 x 96 (8:1)		13											600*			113			0.9	
									90											675			93			0.55	
							10 x 120 (8:1)		13											450			100			0.7	
									90											750			94			0.5	
Pillekamp, F.	2012	hESCs	NR	Co-culture Cluster	No	N/A	N/A													2000	37000			94	163		1.4
					Yes															2800	47000			140	224		1
Rao, C.	2013	hiPSC	NR	Multi	No	Grooves	Flat	PDMS	NR		0.21	275	310	600	2.5		50.11										
					0.5 Hz							240	280	600	2.75												
					1 Hz							200	260	500	2.6												
					No						0.2	225	290	700	2.4		35.6										
					0.5 Hz		10 um					200	290	700	2.1												
					1 Hz							150	225	500	2												
Ribeiro, M.C.	2015	hESCs	23	Single	No	uCP	20 um	PA Gel	5.8 kPa							1.66		1050				0.29					
					1 Hz																						
					2 Hz																						
					3Hz																						
		hiPSCs			No											1.68		1244				0.26					
		hFCMs	N/A		No											1.82		1216				0.39-0.42					
Yin, L.	2004	NRVM	N/A	Multi		Grooves	Flat	PDMS	NR	1.22																	
							120 um			1.29																	

REFERENCES

1. Rodriguez, M.L., et al., *Measuring the contractile forces of human induced pluripotent stem cell-derived cardiomyocytes with arrays of microposts.* J Biomech Eng, 2014. **136**(5): p. 051005.
2. Kuppusamy, K.T., et al., *Let-7 family of microRNA is required for maturation and adult-like metabolism in stem cell-derived cardiomyocytes.* Proc Natl Acad Sci U S A, 2015. **112**(21): p. E2785-94.
3. *Global Status Report on Noncommunicable Diseases*, 2011, World Health Organization: Geneva, Switzerland. p. 176.
4. Go, A.S., et al., *Heart disease and stroke statistics--2013 update: a report from the American Heart Association.* Circulation, 2013. **127**(1): p. e6-e245.
5. National Heart, L., and Blood Institute, *2012 Chart Book on Cardiovascular, Lung, and Blood Diseases*, in *Morbidigy and Mortality*2012, National Institutes of Health.
6. Huang, N.F., R.J. Lee, and S. Li, *Chemical and Physical Regulation of Stem Cells and Progenitor Cells: Potential for Cardiovascular Tissue Engineering.* Tissue Engineering, 2007. **13**(8): p. 1890-1823.
7. Dean, R.G., et al., *Connective tissue growth factor and cardiac fibrosis after myocardial infarction.* J Histochem Cytochem, 2005. **53**(10): p. 1245-56.
8. Harvey, P.A. and L.A. Leinwand, *The cell biology of disease: cellular mechanisms of cardiomyopathy.* J Cell Biol, 2011. **194**(3): p. 355-65.
9. Bellin, M., et al., *Induced pluripotent stem cells: the new patient?* Nat Rev Mol Cell Biol, 2012. **13**(11): p. 713-26.
10. Grskovic, M., et al., *Induced pluripotent stem cells--opportunities for disease modelling and drug discovery.* Nat Rev Drug Discov, 2011. **10**(12): p. 915-29.
11. Dambrot, C., et al., *Cardiomyocyte differentiation of pluripotent stem cells and their use as cardiac disease models.* Biochem J, 2011. **434**(1): p. 25-35.
12. Das, A.K. and R. Pal, *Induced pluripotent stem cells (iPSCs): the emergence of a new champion in stem cell technology-driven biomedical applications.* J Tissue Eng Regen Med, 2010. **4**(6): p. 413-21.
13. Freund, C. and C.L. Mummery, *Prospects for pluripotent stem cell-derived cardiomyocytes in cardiac cell therapy and as disease models.* J Cell Biochem, 2009. **107**(4): p. 592-9.
14. Mercola, M., A. Colas, and E. Willems, *Induced pluripotent stem cells in cardiovascular drug discovery.* Circ Res, 2013. **112**(3): p. 534-48.
15. Miki, K., et al., *Bioengineered myocardium derived from induced pluripotent stem cells improves cardiac function and attenuates cardiac remodeling following chronic myocardial infarction in rats.* Stem Cells Transl Med, 2012. **1**(5): p. 430-7.
16. Kawamura, M., et al., *Feasibility, safety, and therapeutic efficacy of human induced pluripotent stem cell-derived cardiomyocyte sheets in a porcine ischemic cardiomyopathy model.* Circulation, 2012. **126**(11 Suppl 1): p. S29-37.
17. Masumoto, H., et al., *Pluripotent stem cell-engineered cell sheets reassembled with defined cardiovascular populations ameliorate reduction in infarct heart function through cardiomyocyte-mediated neovascularization.* Stem Cells, 2012. **30**(6): p. 1196-205.
18. Mauritz, C., et al., *Induced pluripotent stem cell (iPSC)-derived Flk-1 progenitor cells engraft, differentiate, and improve heart function in a mouse model of acute myocardial infarction.* Eur Heart J, 2011. **32**(21): p. 2634-41.

19. Singla, D.K., et al., *Induced pluripotent stem (iPS) cells repair and regenerate infarcted myocardium.* Mol Pharm, 2011. **8**(5): p. 1573-81.
20. Mosna, F., et al., *Cell therapy for cardiac regeneration after myocardial infarct: which cell is the best?* Cardiovasc Hematol Agents Med Chem, 2010. **8**(4): p. 227-43.
21. Chong, J.J., et al., *Human embryonic-stem-cell-derived cardiomyocytes regenerate non-human primate hearts.* Nature, 2014.
22. Woodcock, E.A. and S.J. Matkovich, *Cardiomyocytes structure, function and associated pathologies.* Int J Biochem Cell Biol, 2005. **37**(9): p. 1746-51.
23. Taber, L.A., *Biomechanics of cardiovascular development.* Annu Rev Biomed Eng, 2001. **3**: p. 1-25.
24. Goenezen, S., M.Y. Rennie, and S. Rugonyi, *Biomechanics of early cardiac development.* Biomech Model Mechanobiol, 2012. **11**(8): p. 1187-204.
25. Taber, L.A., *Mechanical aspects of cardiac development.* Prog Biophys Mol Biol, 1998. **69**(2-3): p. 237-55.
26. Keller, B.B., et al., *Ventricular pressure-area loop characteristics in the stage 16 to 24 chick embryo.* Circ Res, 1991. **68**(1): p. 226-31.
27. Manner, J., *On rotation, torsion, lateralization, and handedness of the embryonic heart loop: new insights from a simulation model for the heart loop of chick embryos.* Anat Rec A Discov Mol Cell Evol Biol, 2004. **278**(1): p. 481-92.
28. Damon, B.J., et al., *Patterns of muscular strain in the embryonic heart wall.* Dev Dyn, 2009. **238**(6): p. 1535-46.
29. Miller, L.A., *Fluid dynamics of ventricular filling in the embryonic heart.* Cell Biochem Biophys, 2011. **61**(1): p. 33-45.
30. Santhanakrishnan, A. and L.A. Miller, *Fluid dynamics of heart development.* Cell Biochem Biophys, 2011. **61**(1): p. 1-22.
31. Hove, J.R., et al., *Intracardiac fluid forces are an essential epigenetic factor for embryonic cardiogenesis.* Nature, 2003. **421**(6919): p. 172-7.
32. Yazawa, M., et al., *Using induced pluripotent stem cells to investigate cardiac phenotypes in Timothy syndrome.* Nature, 2011. **471**(7337): p. 230-U120.
33. Carvajal-Vergara, X., et al., *Patient-specific induced pluripotent stem-cell-derived models of LEOPARD syndrome.* Nature, 2010. **465**(7299): p. 808-U12.
34. Itzhaki, I., et al., *Modelling the long QT syndrome with induced pluripotent stem cells.* Nature, 2011. **471**(7337): p. 225-U113.
35. Kamp, T.J., *An Electrifying iPSC Disease Model: Long QT Syndrome Type 2 and Heart Cells in a Dish.* Cell Stem Cell, 2011. **8**(2): p. 130-131.
36. Moretti, A., et al., *Patient-Specific Induced Pluripotent Stem-Cell Models for Long-QT Syndrome.* New England Journal of Medicine, 2010. **363**(15): p. 1397-1409.
37. Hoekstra, M., et al., *Induced pluripotent stem cell derived cardiomyocytes as models for cardiac arrhythmias.* Front Physiol, 2012. **3**: p. 346.
38. Dick, E., et al., *Evaluating the utility of cardiomyocytes from human pluripotent stem cells for drug screening.* Biochem Soc Trans, 2010. **38**(4): p. 1037-45.
39. Singla, D.K., G.E. Lyons, and T.J. Kamp, *Transplanted embryonic stem cells following mouse myocardial infarction inhibit apoptosis and cardiac remodeling.* Am J Physiol Heart Circ Physiol, 2007. **293**(2): p. H1308-14.
40. Templin, C., et al., *Transplantation and tracking of human-induced pluripotent stem cells in a pig model of myocardial infarction: assessment of cell survival, engraftment, and*

distribution by hybrid single photon emission computed tomography/computed tomography of sodium iodide symporter transgene expression. Circulation, 2012. **126**(4): p. 430-9.
41. Nelson, T.J., et al., *Repair of acute myocardial infarction by human stemness factors induced pluripotent stem cells.* Circulation, 2009. **120**(5): p. 408-16.
42. Blum, B. and N. Benvenisty, *The tumorigenicity of human embryonic stem cells.* Adv Cancer Res, 2008. **100**: p. 133-58.
43. Zhao, T., et al., *Immunogenicity of induced pluripotent stem cells.* Nature, 2011. **474**(7350): p. 212-5.
44. Menard, C., et al., *Transplantation of cardiac-committed mouse embryonic stem cells to infarcted sheep myocardium: a preclinical study.* Lancet, 2005. **366**(9490): p. 1005-12.
45. Laflamme, M.A., et al., *Cardiomyocytes derived from human embryonic stem cells in pro-survival factors enhance function of infarcted rat hearts.* Nat Biotechnol, 2007. **25**(9): p. 1015-24.
46. van Laake, L.W., et al., *Human embryonic stem cell-derived cardiomyocytes survive and mature in the mouse heart and transiently improve function after myocardial infarction.* Stem Cell Res, 2007. **1**(1): p. 9-24.
47. Caspi, O., et al., *Tissue engineering of vascularized cardiac muscle from human embryonic stem cells.* Circ Res, 2007. **100**(2): p. 263-72.
48. Dai, W., et al., *Survival and maturation of human embryonic stem cell-derived cardiomyocytes in rat hearts.* J Mol Cell Cardiol, 2007. **43**(4): p. 504-16.
49. Leor, J., et al., *Human embryonic stem cell transplantation to repair the infarcted myocardium.* Heart, 2007. **93**(10): p. 1278-84.
50. Carpenter, L., et al., *Efficient differentiation of human induced pluripotent stem cells generates cardiac cells that provide protection following myocardial infarction in the rat.* Stem Cells Dev, 2012. **21**(6): p. 977-86.
51. Gnecchi, M., et al., *Paracrine mechanisms in adult stem cell signaling and therapy.* Circ Res, 2008. **103**(11): p. 1204-19.
52. Bursac, N., et al., *Characterizing functional stem cell-cardiomyocyte interactions.* Regen Med, 2010. **5**(1): p. 87-105.
53. Liau, B., D. Zhang, and N. Bursac, *Functional cardiac tissue engineering.* Regen Med, 2012. **7**(2): p. 187-206.
54. Vunjak-Novakovic, G., et al., *Bioengineering heart muscle: a paradigm for regenerative medicine.* Annu Rev Biomed Eng, 2011. **13**: p. 245-67.
55. Kamakura, T., et al., *Ultrastructural Maturation of Human-Induced Pluripotent Stem Cell-Derived Cardiomyocytes in a Long-Term Culture.* Circ J, 2013.
56. Klauke, N., G. Smith, and J.M. Cooper, *Microfluidic systems to examine intercellular coupling of pairs of cardiac myocytes.* Lab Chip, 2007. **7**(6): p. 731-9.
57. Rangappa, S., R. Makkar, and J. Forrester, *Review article: current status of myocardial regeneration: new cell sources and new strategies.* J Cardiovasc Pharmacol Ther, 2010. **15**(4): p. 338-43.
58. Seita, J. and I.L. Weissman, *Hematopoietic stem cell: self-renewal versus differentiation.* Wiley Interdiscip Rev Syst Biol Med, 2010. **2**(6): p. 640-53.
59. Oreffo, R.O., et al., *Mesenchymal stem cells: lineage, plasticity, and skeletal therapeutic potential.* Stem Cell Rev, 2005. **1**(2): p. 169-78.

60. Shantsila, E., T. Watson, and G.Y. Lip, *Endothelial progenitor cells in cardiovascular disorders.* J Am Coll Cardiol, 2007. **49**(7): p. 741-52.
61. Makino, S., et al., *Cardiomyocytes can be generated from marrow stromal cells in vitro.* J Clin Invest, 1999. **103**(5): p. 697-705.
62. Hakuno, D., et al., *Bone marrow-derived regenerated cardiomyocytes (CMG Cells) express functional adrenergic and muscarinic receptors.* Circulation, 2002. **105**(3): p. 380-6.
63. Fukuda, K., *Development of regenerative cardiomyocytes from mesenchymal stem cells for cardiovascular tissue engineering.* Artif Organs, 2001. **25**(3): p. 187-93.
64. Strauer, B.E., et al., *Bone marrow cells to improve ventricular function.* Heart, 2009. **95**(2): p. 98-9.
65. Orlic, D., et al., *Transplanted adult bone marrow cells repair myocardial infarcts in mice.* Ann N Y Acad Sci, 2001. **938**: p. 221-9; discussion 229-30.
66. Orlic, D., et al., *Bone marrow cells regenerate infarcted myocardium.* Nature, 2001. **410**(6829): p. 701-5.
67. Orlic, D., et al., *Mobilized bone marrow cells repair the infarcted heart, improving function and survival.* Proc Natl Acad Sci U S A, 2001. **98**(18): p. 10344-9.
68. Urbanek, K., et al., *Myocardial regeneration by activation of multipotent cardiac stem cells in ischemic heart failure.* Proc Natl Acad Sci U S A, 2005. **102**(24): p. 8692-7.
69. Zhang, X., et al., *Combined transplantation of endothelial progenitor cells and mesenchymal stem cells into a rat model of isoproterenol-induced myocardial injury.* Arch Cardiovasc Dis, 2008. **101**(5): p. 333-42.
70. Price, M.J., et al., *Intravenous mesenchymal stem cell therapy early after reperfused acute myocardial infarction improves left ventricular function and alters electrophysiologic properties.* Int J Cardiol, 2006. **111**(2): p. 231-9.
71. Kamihata, H., et al., *Implantation of bone marrow mononuclear cells into ischemic myocardium enhances collateral perfusion and regional function via side supply of angioblasts, angiogenic ligands, and cytokines.* Circulation, 2001. **104**(9): p. 1046-52.
72. Hatzistergos, K.E., et al., *Bone marrow mesenchymal stem cells stimulate cardiac stem cell proliferation and differentiation.* Circ Res, 2010. **107**(7): p. 913-22.
73. Quevedo, H.C., et al., *Allogeneic mesenchymal stem cells restore cardiac function in chronic ischemic cardiomyopathy via trilineage differentiating capacity.* Proc Natl Acad Sci U S A, 2009. **106**(33): p. 14022-7.
74. Shake, J.G., et al., *Mesenchymal stem cell implantation in a swine myocardial infarct model: engraftment and functional effects.* Ann Thorac Surg, 2002. **73**(6): p. 1919-25; discussion 1926.
75. Amado, L.C., et al., *Cardiac repair with intramyocardial injection of allogeneic mesenchymal stem cells after myocardial infarction.* Proc Natl Acad Sci U S A, 2005. **102**(32): p. 11474-9.
76. Murry, C.E., et al., *Haematopoietic stem cells do not transdifferentiate into cardiac myocytes in myocardial infarcts.* Nature, 2004. **428**(6983): p. 664-8.
77. Silva, G.V., et al., *Mesenchymal stem cells differentiate into an endothelial phenotype, enhance vascular density, and improve heart function in a canine chronic ischemia model.* Circulation, 2005. **111**(2): p. 150-6.
78. Karantalis, V., et al., *Cell-based therapy for prevention and reversal of myocardial remodeling.* Am J Physiol Heart Circ Physiol, 2012. **303**(3): p. H256-70.

79. Buckingham, M., *Skeletal muscle formation in vertebrates.* Curr Opin Genet Dev, 2001. **11**(4): p. 440-8.
80. Siminiak, T., P. Kalmucki, and M. Kurpisz, *Autologous skeletal myoblasts for myocardial regeneration.* J Interv Cardiol, 2004. **17**(6): p. 357-65.
81. Reinecke, H., V. Poppa, and C.E. Murry, *Skeletal muscle stem cells do not transdifferentiate into cardiomyocytes after cardiac grafting.* J Mol Cell Cardiol, 2002. **34**(2): p. 241-9.
82. Roell, W., et al., *Engraftment of connexin 43-expressing cells prevents post-infarct arrhythmia.* Nature, 2007. **450**(7171): p. 819-24.
83. Beltrami, A.P., et al., *Adult cardiac stem cells are multipotent and support myocardial regeneration.* Cell, 2003. **114**(6): p. 763-76.
84. Bearzi, C., et al., *Human cardiac stem cells.* Proc Natl Acad Sci U S A, 2007. **104**(35): p. 14068-73.
85. Leri, A., J. Kajstura, and P. Anversa, *Cardiac stem cells and mechanisms of myocardial regeneration.* Physiological Reviews, 2005. **85**(4): p. 1373-416.
86. Barile, L., et al., *Cardiac stem cells: isolation, expansion and experimental use for myocardial regeneration.* Nat Clin Pract Cardiovasc Med, 2007. **4 Suppl 1**: p. S9-S14.
87. Beltrami, A.P., et al., *Evidence that human cardiac myocytes divide after myocardial infarction.* N Engl J Med, 2001. **344**(23): p. 1750-7.
88. Thomson, J.A., et al., *Embryonic stem cell lines derived from human blastocysts.* Science, 1998. **282**(5391): p. 1145-7.
89. Doetschman, T.C., et al., *The in vitro development of blastocyst-derived embryonic stem cell lines: formation of visceral yolk sac, blood islands and myocardium.* J Embryol Exp Morphol, 1985. **87**: p. 27-45.
90. Takahashi, T., et al., *Ascorbic acid enhances differentiation of embryonic stem cells into cardiac myocytes.* Circulation, 2003. **107**(14): p. 1912-6.
91. Behfar, A., et al., *Stem cell differentiation requires a paracrine pathway in the heart.* FASEB J, 2002. **16**(12): p. 1558-66.
92. Sachinidis, A., et al., *Generation of cardiomyocytes from embryonic stem cells experimental studies.* Herz, 2002. **27**(7): p. 589-97.
93. Kehat, I., et al., *High-resolution electrophysiological assessment of human embryonic stem cell-derived cardiomyocytes: a novel in vitro model for the study of conduction.* Circ Res, 2002. **91**(8): p. 659-61.
94. Hescheler, J., et al., *Embryonic stem cells: a model to study structural and functional properties in cardiomyogenesis.* Cardiovasc Res, 1997. **36**(2): p. 149-62.
95. Fijnvandraat, A.C., et al., *Cardiomyocytes purified from differentiated embryonic stem cells exhibit characteristics of early chamber myocardium.* J Mol Cell Cardiol, 2003. **35**(12): p. 1461-72.
96. Kehat, I., et al., *Electromechanical integration of cardiomyocytes derived from human embryonic stem cells.* Nat Biotechnol, 2004. **22**(10): p. 1282-9.
97. Takahashi, K. and S. Yamanaka, *Induction of pluripotent stem cells from mouse embryonic and adult fibroblast cultures by defined factors.* Cell, 2006. **126**(4): p. 663-76.
98. Yu, J., et al., *Induced pluripotent stem cell lines derived from human somatic cells.* Science, 2007. **318**(5858): p. 1917-20.
99. Okita, K., et al., *Generation of mouse induced pluripotent stem cells without viral vectors.* Science, 2008. **322**(5903): p. 949-53.

100. Narsinh, K.H., et al., *Generation of adult human induced pluripotent stem cells using nonviral minicircle DNA vectors.* Nature Protocols, 2011. **6**(1): p. 78-88.
101. Merkl, C., et al., *Efficient generation of rat induced pluripotent stem cells using a non-viral inducible vector.* PLoS One, 2013. **8**(1): p. e55170.
102. Aasen, T., et al., *Efficient and rapid generation of induced pluripotent stem cells from human keratinocytes.* Nat Biotechnol, 2008. **26**(11): p. 1276-84.
103. Loh, Y.H., et al., *Generation of induced pluripotent stem cells from human blood.* Blood, 2009. **113**(22): p. 5476-9.
104. Loh, Y.H., et al., *Reprogramming of T cells from human peripheral blood.* Cell Stem Cell, 2010. **7**(1): p. 15-9.
105. Staerk, J., et al., *Reprogramming of human peripheral blood cells to induced pluripotent stem cells.* Cell Stem Cell, 2010. **7**(1): p. 20-4.
106. Sun, N., et al., *Feeder-free derivation of induced pluripotent stem cells from adult human adipose stem cells.* Proc Natl Acad Sci U S A, 2009. **106**(37): p. 15720-5.
107. Zhou, J.M., et al., *Generation and Characterization of Human Cryptorchid-Specific Induced Pluripotent Stem Cells from Urine.* Stem Cells Dev, 2013. **22**(5).
108. Zhou, T., et al., *Generation of Induced Pluripotent Stem Cells from Urine.* Journal of the American Society of Nephrology, 2011. **22**(7): p. 1221-1228.
109. Miyoshi, K., et al., *Generation of human induced pluripotent stem cells from oral mucosa.* Journal of Bioscience and Bioengineering, 2010. **110**(3): p. 345-350.
110. Zhang, J., et al., *Functional cardiomyocytes derived from human induced pluripotent stem cells.* Circ Res, 2009. **104**(4): p. e30-41.
111. Zwi-Dantsis, L. and L. Gepstein, *Induced pluripotent stem cells for cardiac repair.* Cell Mol Life Sci, 2012. **69**(19): p. 3285-99.
112. Zwi-Dantsis, L., et al., *Derivation and cardiomyocyte differentiation of induced pluripotent stem cells from heart failure patients.* Eur Heart J, 2012.
113. Spach, M.S., et al., *Cell size and communication: role in structural and electrical development and remodeling of the heart.* Heart Rhythm, 2004. **1**(4): p. 500-15.
114. Feinberg, A.W., et al., *Controlling the contractile strength of engineered cardiac muscle by hierarchal tissue architecture.* Biomaterials, 2012. **33**(23): p. 5732-41.
115. Lundy, S.D., et al., *Structural and functional maturation of cardiomyocytes derived from human pluripotent stem cells.* Stem Cells Dev, 2013. **22**(14): p. 1991-2002.
116. Hazeltine, L.B., et al., *Effects of substrate mechanics on contractility of cardiomyocytes generated from human pluripotent stem cells.* Int J Cell Biol, 2012. **2012**: p. 508294.
117. Carson, D., *Engineering Combinatorial Microenvironments for Structural and Functional Maturation of Human Stem Cell-Derived Cardiomyocytes*, in *Bioengineering*2013, University of Washington.
118. Foldes, G., et al., *Modulation of human embryonic stem cell-derived cardiomyocyte growth: a testbed for studying human cardiac hypertrophy?* J Mol Cell Cardiol, 2011. **50**(2): p. 367-76.
119. Snir, M., et al., *Assessment of the ultrastructural and proliferative properties of human embryonic stem cell-derived cardiomyocytes.* Am J Physiol Heart Circ Physiol, 2003. **285**(6): p. H2355-63.
120. Ribeiro, M.C., et al., *Functional maturation of human pluripotent stem cell derived cardiomyocytes in vitro - Correlation between contraction force and electrophysiology.* Biomaterials, 2015. **51**: p. 138-50.

121. Zhang, D.H., et al., *Tissue-engineered cardiac patch for advanced functional maturation of human ESC-derived cardiomyocytes.* Biomaterials, 2013. **34**(23): p. 5813-5820.
122. Chan, Y.C., et al., *Electrical stimulation promotes maturation of cardiomyocytes derived from human embryonic stem cells.* J Cardiovasc Transl Res, 2013. **6**(6): p. 989-99.
123. Lee, P., et al., *Simultaneous voltage and calcium mapping of genetically purified human induced pluripotent stem cell-derived cardiac myocyte monolayers.* Circulation Research, 2012. **110**(12): p. 1556-63.
124. Rao, C., et al., *The effect of microgrooved culture substrates on calcium cycling of cardiac myocytes derived from human induced pluripotent stem cells.* Biomaterials, 2013. **34**(10): p. 2399-411.
125. Kita-Matsuo, H., et al., *Lentiviral vectors and protocols for creation of stable hESC lines for fluorescent tracking and drug resistance selection of cardiomyocytes.* PLoS One, 2009. **4**(4): p. e5046.
126. Jacot, J.G., A.D. McCulloch, and J.H. Omens, *Substrate stiffness affects the functional maturation of neonatal rat ventricular myocytes.* Biophys J, 2008. **95**(7): p. 3479-87.
127. Rodriguez, A.G., et al., *Substrate Stiffness Increases Twitch Power of Neonatal Cardiomyocytes in Correlation with Changes in Myofibril Structure and Intracellular Calcium.* Biophys J, 2011. **101**(10): p. 2455-2464.
128. *Rodriguez, A.G., et al., *Enhanced contractility with 2-deoxy-ATP and EMD 57033 is correlated with reduced myofibril structure and twitch power in neonatal cardiomyocytes.* Integr Biol, 2013. **5**(11): p. 1366-1373.
129. Sheehy, S.P., et al., *Quality metrics for stem cell-derived cardiac myocytes.* Stem Cell Reports, 2014. **2**(3): p. 282-94.
130. Bhana, B., et al., *Influence of substrate stiffness on the phenotype of heart cells.* Biotechnol Bioeng, 2010. **105**(6): p. 1148-60.
131. Chopra, A., et al., *Contractility dependent regulation of the N-cadherin complex formation and myocyte structural organization.* Faseb Journal, 2011. **25**.
132. Sathaye, A., et al., *Electrical pacing counteracts intrinsic shortening of action potential duration of neonatal rat ventricular cells in culture.* J Mol Cell Cardiol, 2006. **41**(4): p. 633-41.
133. Bray, M.A., S.P. Sheehy, and K.K. Parker, *Sarcomere alignment is regulated by myocyte shape.* Cell Motil Cytoskeleton, 2008. **65**(8): p. 641-51.
134. Galie, P.A., et al., *Substrate stiffness affects sarcomere and costamere structure and electrophysiological function of isolated adult cardiomyocytes.* Cardiovasc Pathol, 2013. **22**(3): p. 219-27.
135. Geisse, N.A., S.P. Sheehy, and K.K. Parker, *Control of myocyte remodeling in vitro with engineered substrates.* In Vitro Cell Dev Biol Anim, 2009. **45**(7): p. 343-50.
136. Kim, D.H., et al., *Nanoscale cues regulate the structure and function of macroscopic cardiac tissue constructs.* Proc Natl Acad Sci U S A, 2010. **107**(2): p. 565-570.
137. McDevitt, T.C., et al., *In vitro generation of differentiated cardiac myofibers on micropatterned laminin surfaces.* Journal of Biomedical Materials Research, 2002. **60**(3): p. 472-479.
138. Pong, T., et al., *Hierarchical architecture influences calcium dynamics in engineered cardiac muscle.* Exp Biol Med (Maywood), 2011. **236**(3): p. 366-73.

139. Chiu, L.L.Y., K. Janic, and M. Radisic, *Engineering of oriented myocardium on three-dimensional micropatterned collagen-chitosan hydrogel.* International Journal of Artificial Organs, 2012. **35**(4): p. 237-250.
140. Hampe, N., et al., *Defined 2-D microtissues on soft elastomeric silicone rubber using lift-off epoxy-membranes for biomechanical analyses.* Soft Matter, 2014. **10**(14): p. 2431-43.
141. Heidi Au, H.T., et al., *Cell culture chips for simultaneous application of topographical and electrical cues enhance phenotype of cardiomyocytes.* Lab Chip, 2009. **9**(4): p. 564-75.
142. McCain, M.L., et al., *Matrix elasticity regulates the optimal cardiac myocyte shape for contractility.* Am J Physiol Heart Circ Physiol, 2014. **306**(11): p. H1525-39.
143. Garcia-Webb, M.G., et al., *A modular instrument for exploring the mechanics of cardiac myocytes.* Am J Physiol Heart Circ Physiol, 2007. **293**(1): p. H866-74.
144. Le Guennec, J.Y., et al., *A new method of attachment of isolated mammalian ventricular myocytes for tension recording: length dependence of passive and active tension.* J Mol Cell Cardiol, 1990. **22**(10): p. 1083-93.
145. Nishimura, S., et al., *Single cell mechanics of rat cardiomyocytes under isometric, unloaded, and physiologically loaded conditions.* Am J Physiol Heart Circ Physiol, 2004. **287**(1): p. H196-202.
146. Yasuda, S.I., et al., *A novel method to study contraction characteristics of a single cardiac myocyte using carbon fibers.* American Journal of Physiology-Heart and Circulatory Physiology, 2001. **281**(3): p. H1442-H1446.
147. Engler, A.J., et al., *Embryonic cardiomyocytes beat best on a matrix with heart-like elasticity: scar-like rigidity inhibits beating.* J Cell Sci, 2008. **121**(Pt 22): p. 3794-802.
148. van der Velden, J., et al., *Force production in mechanically isolated cardiac myocytes from human ventricular muscle tissue.* Cardiovasc Res, 1998. **38**(2): p. 414-23.
149. Robertson, C., D.D. Tran, and S.C. George, *Concise review: maturation phases of human pluripotent stem cell-derived cardiomyocytes.* Stem Cells, 2013. **31**(5): p. 829-37.
150. Gerdes, A.M., et al., *Structural remodeling of cardiac myocytes in patients with ischemic cardiomyopathy.* Circulation, 1992. **86**(2): p. 426-30.
151. Yang, X., L. Pabon, and C.E. Murry, *Engineering adolescence: maturation of human pluripotent stem cell-derived cardiomyocytes.* Circ Res, 2014. **114**(3): p. 511-23.
152. Keung, W., K.R. Boheler, and R.A. Li, *Developmental cues for the maturation of metabolic, electrophysiological and calcium handling properties of human pluripotent stem cell-derived cardiomyocytes.* Stem Cell Res Ther, 2014. **5**(1): p. 17.
153. Olivetti, G., et al., *Aging, cardiac hypertrophy and ischemic cardiomyopathy do not affect the proportion of mononucleated and multinucleated myocytes in the human heart.* J Mol Cell Cardiol, 1996. **28**(7): p. 1463-77.
154. Radisic, M., et al., *Functional assembly of engineered myocardium by electrical stimulation of cardiac myocytes cultured on scaffolds.* Proc Natl Acad Sci U S A, 2004. **101**(52): p. 18129-34.
155. Nakao, K., et al., *Myosin heavy chain gene expression in human heart failure.* J Clin Invest, 1997. **100**(9): p. 2362-70.
156. Lowes, B.D., et al., *Changes in gene expression in the intact human heart. Downregulation of alpha-myosin heavy chain in hypertrophied, failing ventricular myocardium.* J Clin Invest, 1997. **100**(9): p. 2315-24.
157. Korte, F.S., et al., *Power output is linearly related to MyHC content in rat skinned myocytes and isolated working hearts.* Am J Physiol Heart Circ Physiol, 2005. **289**(2): p. H801-12.

158. Lahmers, S., et al., *Developmental control of titin isoform expression and passive stiffness in fetal and neonatal myocardium.* Circ Res, 2004. **94**(4): p. 505-13.
159. Opitz, C.A., et al., *Developmentally regulated switching of titin size alters myofibrillar stiffness in the perinatal heart.* Circ Res, 2004. **94**(7): p. 967-75.
160. Warren, C.M., et al., *Titin isoform changes in rat myocardium during development.* Mech Dev, 2004. **121**(11): p. 1301-12.
161. Granzier, H.L. and T.C. Irving, *Passive tension in cardiac muscle: contribution of collagen, titin, microtubules, and intermediate filaments.* Biophys J, 1995. **68**(3): p. 1027-44.
162. Metzger, J.M., et al., *Sarcomere thin filament regulatory isoforms. Evidence of a dominant effect of slow skeletal troponin I on cardiac contraction.* J Biol Chem, 2003. **278**(15): p. 13118-23.
163. Reiser, P.J., et al., *Tension production and thin-filament protein isoforms in developing rat myocardium.* Am J Physiol, 1994. **267**(4 Pt 2): p. H1589-96.
164. Siedner, S., et al., *Developmental changes in contractility and sarcomeric proteins from the early embryonic to the adult stage in the mouse heart.* J Physiol, 2003. **548**(Pt 2): p. 493-505.
165. Gordon, A.M., E. Homsher, and M. Regnier, *Regulation of contraction in striated muscle.* Physiological Reviews, 2000. **80**(2): p. 853-924.
166. Campbell, K.S., *Interactions between connected half-sarcomeres produce emergent mechanical behavior in a mathematical model of muscle.* PLoS Comput Biol, 2009. **5**(11): p. e1000560.
167. Iribe, G., M. Helmes, and P. Kohl, *Force-length relations in isolated intact cardiomyocytes subjected to dynamic changes in mechanical load.* Am J Physiol Heart Circ Physiol, 2007. **292**(3): p. H1487-97.
168. Lin, G., K.S.J. Pister, and K.P. Roos, *Surface micromachined polysilicon heart cell force transducer.* Journal of Microelectromechanical Systems, 2000. **9**(1): p. 9-17.
169. Walker, C.A. and F.G. Spinale, *The structure and function of the cardiac myocyte: a review of fundamental concepts.* J Thorac Cardiovasc Surg, 1999. **118**(2): p. 375-82.
170. Li, J., et al., *Cardiac-specific loss of N-cadherin leads to alteration in connexins with conduction slowing and arrhythmogenesis.* Circ Res, 2005. **97**(5): p. 474-81.
171. Xu, X.Q., et al., *Global expression profile of highly enriched cardiomyocytes derived from human embryonic stem cells.* Stem Cells, 2009. **27**(9): p. 2163-74.
172. Cao, F., et al., *Transcriptional and functional profiling of human embryonic stem cell-derived cardiomyocytes.* PLoS One, 2008. **3**(10): p. e3474.
173. Bers, D.M., *Cardiac excitation-contraction coupling.* Nature, 2002. **415**(6868): p. 198-205.
174. Dolnikov, K., et al., *Functional properties of human embryonic stem cell-derived cardiomyocytes: intracellular Ca2+ handling and the role of sarcoplasmic reticulum in the contraction.* Stem Cells, 2006. **24**(2): p. 236-45.
175. Gomez, J.P., D. Potreau, and G. Raymond, *Intracellular calcium transients from newborn rat cardiomyocytes in primary culture.* Cell Calcium, 1994. **15**(4): p. 265-75.
176. Husse, B. and M. Wussling, *Developmental changes of calcium transients and contractility during the cultivation of rat neonatal cardiomyocytes.* Mol Cell Biochem, 1996. **163-164**: p. 13-21.

177. Li, S., G. Chen, and R.A. Li, *Calcium signalling of human pluripotent stem cell-derived cardiomyocytes.* J Physiol, 2013. **591**(Pt 21): p. 5279-90.
178. Lieu, D.K., et al., *Absence of transverse tubules contributes to non-uniform Ca(2+) wavefronts in mouse and human embryonic stem cell-derived cardiomyocytes.* Stem Cells Dev, 2009. **18**(10): p. 1493-500.
179. Satin, J., et al., *Calcium handling in human embryonic stem cell-derived cardiomyocytes.* Stem Cells, 2008. **26**(8): p. 1961-72.
180. Liu, J., et al., *Functional sarcoplasmic reticulum for calcium handling of human embryonic stem cell-derived cardiomyocytes: insights for driven maturation.* Stem Cells, 2007. **25**(12): p. 3038-44.
181. Binah, O., et al., *Functional and developmental properties of human embryonic stem cells-derived cardiomyocytes.* J Electrocardiol, 2007. **40**(6 Suppl): p. S192-6.
182. Germanguz, I., et al., *Molecular characterization and functional properties of cardiomyocytes derived from human inducible pluripotent stem cells.* J Cell Mol Med, 2011. **15**(1): p. 38-51.
183. Caspi, O., et al., *In Vitro Electrophysiological Drug Testing Using Human Embryonic Stem Cell Derived Cardiomyocytes.* Stem Cells Dev, 2009. **18**(1): p. 161-172.
184. Satin, J., et al., *Mechanism of spontaneous excitability in human embryonic stem cell derived cardiomyocytes.* Journal of Physiology-London, 2004. **559**(2): p. 479-496.
185. Nanthakumar, K., et al., *Optical mapping of Langendorff-perfused human hearts: establishing a model for the study of ventricular fibrillation in humans.* American Journal of Physiology-Heart and Circulatory Physiology, 2007. **293**(1): p. H875-H880.
186. Fu, J.D., et al., *Na+/Ca2+ exchanger is a determinant of excitation-contraction coupling in human embryonic stem cell-derived ventricular cardiomyocytes.* Stem Cells and Development, 2010. **19**(6): p. 773-82.
187. Brodie, B.R., et al., *Six-month clinical and angiographic follow-up after direct angioplasty for acute myocardial infarction. Final results from the Primary Angioplasty Registry.* Circulation, 1994. **90**(1): p. 156-62.
188. Ivashchenko, C.Y., et al., *Human-induced pluripotent stem cell-derived cardiomyocytes exhibit temporal changes in phenotype.* Am J Physiol Heart Circ Physiol, 2013. **305**(6): p. H913-22.
189. Lieu, D.K., et al., *Mechanism-based facilitated maturation of human pluripotent stem cell-derived cardiomyocytes.* Circ Arrhythm Electrophysiol, 2013. **6**(1): p. 191-201.
190. Sartiani, L., et al., *Developmental changes in cardiomyocytes differentiated from human embryonic stem cells: a molecular and electrophysiological approach.* Stem Cells, 2007. **25**(5): p. 1136-44.
191. Kuo, P.L., et al., *Myocyte Shape Regulates Lateral Registry of Sarcomeres and Contractility.* American Journal of Pathology, 2012. **181**(6): p. 2030-2037.
192. Yin, L., H. Bien, and E. Entcheva, *Scaffold topography alters intracellular calcium dynamics in cultured cardiomyocyte networks.* Am J Physiol Heart Circ Physiol, 2004. **287**(3): p. H1276-85.
193. Taylor, D.G., et al., *Quantification of the rat left ventricle force and Ca2+ -frequency relationships: similarities to dog and human.* Cardiovasc Res, 2004. **61**(1): p. 77-86.
194. Nerbonne, J.M. and R.S. Kass, *Molecular physiology of cardiac repolarization.* Physiological Reviews, 2005. **85**(4): p. 1205-53.

195. Reppel, M., et al., *Microelectrode arrays: a new tool to measure embryonic heart activity.* J Electrocardiol, 2004. **37 Suppl**: p. 104-9.
196. Sperelakis, N. and K. Shigenobu, *Changes in membrane properties of chick embryonic hearts during development.* J Gen Physiol, 1972. **60**(4): p. 430-53.
197. Toda, N., *Age-related changes in the transmembrane potential of isolated rabbit sino-atrial nodes and atria.* Cardiovasc Res, 1980. **14**(1): p. 58-63.
198. Blazeski, A., et al., *Electrophysiological and contractile function of cardiomyocytes derived from human embryonic stem cells.* Progress in Biophysics & Molecular Biology, 2012. **110**(2-3): p. 178-195.
199. Rodriguez, M.L., S.J. Han, and N.J. Sniadecki, *A Multi-Physics Finite Element Model of the Traction Forces in a Three-Dimensional Smooth Muscle Cell. ,* in *ASME SBC*2011: Farmington, PA.
200. Mummery, C., et al., *Differentiation of human embryonic stem cells to cardiomyocytes: role of coculture with visceral endoderm-like cells.* Circulation, 2003. **107**(21): p. 2733-40.
201. Du, D.T., et al., *Action potential morphology of human induced pluripotent stem cell-derived cardiomyocytes does not predict cardiac chamber specificity and is dependent on cell density.* Biophys J, 2015. **108**(1): p. 1-4.
202. Heras-Bautista, C.O., et al., *The influence of physiological matrix conditions on permanent culture of induced pluripotent stem cell-derived cardiomyocytes.* Biomaterials, 2014. **35**(26): p. 7374-85.
203. Chiu, L.L., et al., *Biphasic electrical field stimulation aids in tissue engineering of multicell-type cardiac organoids.* Tissue Eng Part A, 2011. **17**(11-12): p. 1465-77.
204. Wang, J., et al., *Effect of engineered anisotropy on the susceptibility of human pluripotent stem cell-derived ventricular cardiomyocytes to arrhythmias.* Biomaterials, 2013. **34**(35): p. 8878-86.
205. Ma, J., et al., *High purity human-induced pluripotent stem cell-derived cardiomyocytes: electrophysiological properties of action potentials and ionic currents.* Am J Physiol Heart Circ Physiol, 2011. **301**(5): p. H2006-17.
206. Levy, D., et al., *The progression from hypertension to congestive heart failure.* JAMA, 1996. **275**(20): p. 1557-62.
207. Bursac, N., et al., *Cardiomyocyte cultures with controlled macroscopic anisotropy - A model for functional electrophysiological studies of cardiac muscle.* Circulation Research, 2002. **91**(12): p. E45-E54.
208. Pekkanen-Mattila, M., et al., *Human embryonic stem cell-derived cardiomyocytes: demonstration of a portion of cardiac cells with fairly mature electrical phenotype.* Exp Biol Med (Maywood), 2010. **235**(4): p. 522-30.
209. Zhu, W.Z., et al., *Neuregulin/ErbB signaling regulates cardiac subtype specification in differentiating human embryonic stem cells.* Circ Res, 2010. **107**(6): p. 776-86.
210. Xu, C., et al., *Efficient generation and cryopreservation of cardiomyocytes derived from human embryonic stem cells.* Regen Med, 2011. **6**(1): p. 53-66.
211. Schram, G., et al., *Differential distribution of cardiac ion channel expression as a basis for regional specialization in electrical function.* Circ Res, 2002. **90**(9): p. 939-50.
212. Wang, K., et al., *Biophysical properties of slow potassium channels in human embryonic stem cell derived cardiomyocytes implicate subunit stoichiometry.* J Physiol, 2011. **589**(Pt 24): p. 6093-104.

213. Peng, S., et al., *The action potential and comparative pharmacology of stem cell-derived human cardiomyocytes.* J Pharmacol Toxicol Methods, 2010. **61**(3): p. 277-86.
214. Jacobson, S.L. and H.M. Piper, *Cell cultures of adult cardiomyocytes as models of the myocardium.* J Mol Cell Cardiol, 1986. **18**(7): p. 661-78.
215. Gaspar, J.A., et al., *Unique metabolic features of stem cells, cardiomyocytes, and their progenitors.* Circulation Research, 2014. **114**(8): p. 1346-60.
216. Kolwicz, S.C., Jr., S. Purohit, and R. Tian, *Cardiac metabolism and its interactions with contraction, growth, and survival of cardiomyocytes.* Circulation Research, 2013. **113**(5): p. 603-16.
217. Lopaschuk, G.D. and J.S. Jaswal, *Energy metabolic phenotype of the cardiomyocyte during development, differentiation, and postnatal maturation.* J Cardiovasc Pharmacol, 2010. **56**(2): p. 130-40.
218. Harris, D.A. and A.M. Das, *Control of mitochondrial ATP synthesis in the heart.* Biochem J, 1991. **280 (Pt 3)**: p. 561-73.
219. Piquereau, J., et al., *Postnatal development of mouse heart: formation of energetic microdomains.* J Physiol, 2010. **588**(Pt 13): p. 2443-54.
220. St John, J.C., et al., *The expression of mitochondrial DNA transcription factors during early cardiomyocyte in vitro differentiation from human embryonic stem cells.* Cloning Stem Cells, 2005. **7**(3): p. 141-53.
221. Sen, S. and S. Kumar, *Combining mechanical and optical approaches to dissect cellular mechanobiology.* J Biomech, 2010. **43**(1): p. 45-54.
222. Van Vliet, K.J., G. Bao, and S. Suresh, *The biomechanics toolbox: experimental approaches for living cells and biomolecules.* Acta Materialia, 2003. **51**(19): p. 5881-5905.
223. Nahmias, Y. and S. Bhatia, *Methods in Bioengineering: Microdevices in Biology and Medicine*2009, Norwood, MA: Artech House. 1-260.
224. Pelling, A.E. and M.A. Horton, *An historical perspective on cell mechanics.* Pflugers Arch, 2008. **456**(1): p. 3-12.
225. Shin, D. and K. Athanasiou, *Cytoindentation for obtaining cell biomechanical properties.* J Orthop Res, 1999. **17**(6): p. 880-90.
226. Daily, B., E.L. Elson, and G.I. Zahalak, *Cell poking. Determination of the elastic area compressibility modulus of the erythrocyte membrane.* Biophys J, 1984. **45**(4): p. 671-82.
227. Krayer, J., S. Tatic-Lucic, and S. Neti, *Micro-arheometer: High throughput system for measuring of viscoelastic properties of single biological cells.* Sensors and Actuators B-Chemical, 2006. **118**(1-2): p. 20-27.
228. Delbridge, L.M. and K.P. Roos, *Optical methods to evaluate the contractile function of unloaded isolated cardiac myocytes.* J Mol Cell Cardiol, 1997. **29**(1): p. 11-25.
229. Kamgoue, A., et al., *Quantification of cardiomyocyte contraction based on image correlation analysis.* Cytometry A, 2009. **75**(4): p. 298-308.
230. Chen, A., et al., *Integrated platform for functional monitoring of biomimetic heart sheets derived from human pluripotent stem cells.* Biomaterials, 2014. **35**(2): p. 675-83.
231. Yang, M.T., N.J. Sniadecki, and C.S. Chen, *Geometric considerations of micro- to nanoscale elastomeric post arrays to study cellular traction forces.* Advanced Materials, 2007. **19**(20): p. 3119-+.
232. Wang, I.N., et al., *Apelin enhances directed cardiac differentiation of mouse and human embryonic stem cells.* PLoS One, 2012. **7**(6): p. e38328.

233. Liu, J., et al., *Atomic force mechanobiology of pluripotent stem cell-derived cardiomyocytes.* PLoS One, 2012. **7**(5): p. e37559.
234. Taylor, R.E., et al., *Sacrificial layer technique for axial force post assay of immature cardiomyocytes.* Biomed Microdevices, 2013. **15**(1): p. 171-81.
235. Sun, N., et al., *Patient-specific induced pluripotent stem cells as a model for familial dilated cardiomyopathy.* Sci Transl Med, 2012. **4**(130): p. 130ra47.
236. Shinozawa, T., et al., *Determination of appropriate stage of human-induced pluripotent stem cell-derived cardiomyocytes for drug screening and pharmacological evaluation in vitro.* J Biomol Screen, 2012. **17**(9): p. 1192-203.
237. Kim, K., et al., *Calibrated micropost arrays for biomechanical characterisation of cardiomyocytes.* Micro & Nano Letters, 2011. **6**(5): p. 317-322.
238. Hasenfuss, G., et al., *Energetics of Isometric Force Development in Control and Volume-Overload Human Myocardium - Comparison with Animal Species.* Circulation Research, 1991. **68**(3): p. 836-846.
239. Holt, E., et al., *Electrical stimulation of adult rat cardiomyocytes in culture improves contractile properties and is associated with altered calcium handling.* Basic Res Cardiol, 1997. **92**(5): p. 289-98.
240. Korte, F.S. and K.S. McDonald, *Sarcomere length dependence of rat skinned cardiac myocyte mechanical properties: dependence on myosin heavy chain.* J Physiol, 2007. **581**(Pt 2): p. 725-39.
241. Huang, X., et al., *Age-related down-regulation of HCN channels in rat sinoatrial node.* Basic Res Cardiol, 2007. **102**(5): p. 429-35.
242. Layland, J. and J.C. Kentish, *Positive force- and [Ca2+]i-frequency relationships in rat ventricular trabeculae at physiological frequencies.* Am J Physiol, 1999. **276**(1 Pt 2): p. H9-H18.
243. Dolnikov, K., et al., *Functional properties of human embryonic stem cell-derived cardiomyocytes.* Ann N Y Acad Sci, 2005. **1047**: p. 66-75.
244. Yin, S., et al., *Measuring single cardiac myocyte contractile force via moving a magnetic bead.* Biophys J, 2005. **88**(2): p. 1489-95.
245. Hersch, N., et al., *The constant beat: cardiomyocytes adapt their forces by equal contraction upon environmental stiffening.* Biology Open, 2013. **2**: p. 351-361.
246. Jacot, J.G., J.C. Martin, and D.L. Hunt, *Mechanobiology of cardiomyocyte development.* J Biomech, 2010. **43**(1): p. 93-8.
247. Borbely, A., et al., *Cardiomyocyte stiffness in diastolic heart failure.* Circulation, 2005. **111**(6): p. 774-81.
248. Nishimura, S., et al., *Expression of green fluorescent protein impairs the force-generating ability of isolated rat ventricular cardiomyocytes.* Molecular and Cellular Biochemistry, 2006. **286**(1-2): p. 59-65.
249. Domke, J., et al., *Mapping the mechanical pulse of single cardiomyocytes with the atomic force microscope.* Eur Biophys J, 1999. **28**(3): p. 179-86.
250. Chang, W.T., et al., *Characterization of the Mechanodynamic Response of Cardiomyocytes with Atomic Force Microscopy.* Anal Chem, 2012. **85**: p. 1395-1400.
251. Brixius, K., et al., *Force/shortening-frequency relationship in multicellular muscle strips and single cardiomyocytes of human failing and nonfailing hearts.* J Card Fail, 2001. **7**(4): p. 335-41.

252. Edes, I.F., et al., *Rate of tension redevelopment is not modulated by sarcomere length in permeabilized human, murine, and porcine cardiomyocytes.* Am J Physio Reg Int Comp Physio, 2007. **293**(1): p. R20-R29.
253. Tanaka, Y., et al., *Demonstration of a PDMS-based bio-microactuator using cultured cardiomyocytes to drive polymer micropillars.* Lab on a Chip, 2006. **6**(2): p. 230-235.
254. Vannier, C., H. Chevassus, and G. Vassort, *Ca-dependence of isometric force kinetics in single skinned ventricular cardiomyocytes from rats.* Cardiovasc Res, 1996. **32**(3): p. 580-586.
255. Borg, T.K., et al., *Recognition of extracellular matrix components by neonatal and adult cardiac myocytes.* Dev Biol, 1984. **104**(1): p. 86-96.
256. Xi, J., et al., *Comparison of contractile behavior of native murine ventricular tissue and cardiomyocytes derived from embryonic or induced pluripotent stem cells.* FASEB J, 2010. **24**(8): p. 2739-51.
257. Eschenhagen, T., et al., *Three-dimensional reconstitution of embryonic cardiomyocytes in a collagen matrix: a new heart muscle model system.* FASEB J, 1997. **11**(8): p. 683-94.
258. Pillekamp, F., et al., *Force measurements of human embryonic stem cell-derived cardiomyocytes in an in vitro transplantation model.* Stem Cells, 2007. **25**(1): p. 174-80.
259. Kim, J., et al., *Quantitative evaluation of cardiomyocyte contractility in a 3D microenvironment.* J Biomech, 2008. **41**(11): p. 2396-401.
260. Park, J., et al., *Real-time measurement of the contractile forces of self-organized cardiomyocytes on hybrid biopolymer microcantilevers.* Anal Chem, 2005. **77**(20): p. 6571-6580.
261. Boudou, T., et al., *A Microfabricated Platform to Measure and Manipulate the Mechanics of Engineered Cardiac Microtissues.* Tissue Eng Part A, 2011. **18**(9-10): p. 910-919.
262. Legant, W.R., et al., *Microfabricated tissue gauges to measure and manipulate forces from 3D microtissues.* Proc Natl Acad Sci U S A, 2009. **106**(25): p. 10097-102.
263. Ganz, A., et al., *Traction forces exerted through N-cadherin contacts.* Biology of the Cell, 2006. **98**(12): p. 721-730.
264. Ladoux, B., et al., *Force mapping in epithelial cell migration.* Molecular Biology of the Cell, 2004. **15**: p. 161a-162a.
265. Saez, A., et al., *Traction forces exerted by epithelial cell sheets.* Journal of Physics-Condensed Matter, 2010. **22**(19).
266. Liu, Z., et al., *Mechanical tugging force regulates the size of cell-cell junctions.* Proc Natl Acad Sci U S A, 2010. **107**(22): p. 9944-9.
267. Ghibaudo, M., et al., *Traction forces and rigidity sensing regulate cell functions.* Soft Matter, 2008. **4**(9): p. 1836-1843.
268. Han, S.J., et al., *Decoupling substrate stiffness, spread area, and micropost density: a close spatial relationship between traction forces and focal adhesions.* Biophys J, 2012. **103**(4): p. 640-8.
269. Ting, L.H., et al., *Flow mechanotransduction regulates traction forces, intercellular forces, and adherens junctions.* Am J Physiol Heart Circ Physiol, 2012. **302**(11): p. H2220-9.
270. Lemmon, C.A., et al., *Shear force at the cell-matrix interface: enhanced analysis for microfabricated post array detectors.* Mech Chem Biosyst, 2005. **2**(1): p. 1-16.
271. Liang, X.M., et al., *Platelet retraction force measurements using flexible post force sensors.* Lab Chip, 2010. **10**(8): p. 991-8.

272. Sniadecki, N.J., et al., *Magnetic microposts as an approach to apply forces to living cells.* Proc Natl Acad Sci USA, 2007. **104**(37): p. 14553-14558.
273. Fu, J., et al., *Mechanical regulation of cell function with geometrically modulated elastomeric substrates.* Nat Methods, 2010. **7**(9): p. 733-736.
274. Tee, S.Y., et al., *Cell shape and substrate rigidity both regulate cell stiffness.* Biophys J, 2011. **100**(5): p. L25-7.
275. Sun, Y., et al., *Mechanics regulates fate decisions of human embryonic stem cells.* PLoS One, 2012. **7**(5): p. e37178.
276. Sochol, R.D., et al., *Effects of micropost spacing and stiffness on cell motility.* Micro & Nano Letters, 2011. **6**(5): p. 323-326.
277. Sochol, R.D., et al., *Unidirectional mechanical cellular stimuli via micropost array gradients.* Soft Matter, 2011. **7**(10): p. 4606-4609.
278. Lam, R.H.W., et al., *Elastomeric microposts integrated into microfluidics for flow-mediated endothelial mechanotransduction analysis.* Lab on a Chip, 2012. **12**(10): p. 1865-1873.
279. Zhao, Y., et al., *Cellular force measurements using single-spaced polymeric microstructures: isolating cells from base substrate.* Journal of Micromechanics and Microengineering, 2005. **15**(9): p. 1649-1656.
280. Zhao, Y. and X. Zhang, *Cellular mechanics study in cardiac myocytes using PDMS pillars array.* Sensors and Actuators a-Physical, 2006. **125**(2): p. 398-404.
281. Rodriguez, A.G., et al., *Enhanced contractility with 2 deoxy-ATP and EMD 57033 leads to reduced myofibril structure and twitch power in neonatal cardiomyocytes.* Integrative Biology, 2013.
282. Kresh, J.Y. and A. Chopra, *Intercellular and extracellular mechanotransduction in cardiac myocytes.* Pflugers Arch, 2011. **462**(1): p. 75-87.
283. Parker, K.K. and D.E. Ingber, *Extracellular matrix, mechanotransduction and structural hierarchies in heart tissue engineering.* Philos Trans R Soc Lond B Biol Sci, 2007. **362**(1484): p. 1267-79.
284. Terracio, L., et al., *Expression of collagen binding integrins during cardiac development and hypertrophy.* Circ Res, 1991. **68**(3): p. 734-44.
285. Lundgren, E., et al., *Extracellular matrix components influence the survival of adult cardiac myocytes in vitro.* Exp Cell Res, 1985. **158**(2): p. 371-81.
286. Lundgren, E., L. Terracio, and T.K. Borg, *Adhesion of cardiac myocytes to extracellular matrix components.* Basic Res Cardiol, 1985. **80 Suppl 1**: p. 69-74.
287. Bird, S.D., et al., *The human adult cardiomyocyte phenotype.* Cardiovasc Res, 2003. **58**(2): p. 423-34.
288. Sniadecki, N.J. and C.S. Chen, *Microfabricated Silicone Elastomeric Post Arrays for Measuring Traction Forces of Adherent Cells*, in *Methods in Cell Biology: Cell Mechanics*, Y. Wang and D.E. Discher, Editors. 2007, Elsevier Inc.: San Diego, CA. p. 313-328.
289. Schoen, I., et al., *Probing cellular traction forces by micropillar arrays: contribution of substrate warping to pillar deflection.* Nano Lett, 2010. **10**(5): p. 1823-30.
290. Wu, X., et al., *Cardiomyocyte contractile status is associated with differences in fibronectin and integrin interactions.* Am J Physiol Heart Circ Physiol, 2010. **298**(6): p. H2071-81.
291. Prowse, A.B., et al., *Stem cell integrins: implications for ex-vivo culture and cellular therapies.* Stem Cell Res, 2011. **6**(1): p. 1-12.

292. Ross, R.S. and T.K. Borg, *Integrins and the myocardium.* Circ Res, 2001. **88**(11): p. 1112-9.
293. Maitra, N., et al., *Expression of alpha and beta integrins during terminal differentiation of cardiomyocytes.* Cardiovasc Res, 2000. **47**(4): p. 715-25.
294. van Laake, L.W., et al., *Extracellular matrix formation after transplantation of human embryonic stem cell-derived cardiomyocytes.* Cell Mol Life Sci, 2010. **67**(2): p. 277-90.
295. Kass, D.A., J.G.F. Bronzwaer, and W.J. Paulus, *What mechanisms underlie diastolic dysfunction in heart failure?* Circulation Research, 2004. **94**(12): p. 1533-1542.
296. Hamdani, N., et al., *Sarcomeric dysfunction in heart failure.* Cardiovasc Res, 2008. **77**(4): p. 649-658.
297. McCain, M.L. and K.K. Parker, *Mechanotransduction: the role of mechanical stress, myocyte shape, and cytoskeletal architecture on cardiac function.* Pflugers Arch, 2011. **462**(1): p. 89-104.
298. Parker, K.K., et al., *Myofibrillar architecture in engineered cardiac myocytes.* Circ Res, 2008. **103**(4): p. 340-2.
299. Fink, C., et al., *Chronic stretch of engineered heart tissue induces hypertrophy and functional improvement.* FASEB J, 2000. **14**(5): p. 669-79.
300. Throm Quinlan, A.M., et al., *Combining dynamic stretch and tunable stiffness to probe cell mechanobiology in vitro.* PLoS One, 2011. **6**(8): p. e23272.
301. Kurazumi, H., et al., *The effects of mechanical stress on the growth, differentiation, and paracrine factor production of cardiac stem cells.* PLoS One, 2011. **6**(12): p. e28890.
302. Gwak, S.J., et al., *The effect of cyclic strain on embryonic stem cell-derived cardiomyocytes.* Biomaterials, 2008. **29**(7): p. 844-56.
303. Shimko, V.F. and W.C. Claycomb, *Effect of Mechanical Loading on Three-Dimensional Cultures of Embryonic Stem Cell-Derived Cardiomyocytes.* Tissue Engineering, 2008. **14**(1): p. 49-58.
304. Cassino, T.R., et al., *Mechanical Loading of Stem Cells for Improvement of Transplantation Outcome: The Role of Loading History.* Tissue Eng Part A, 2012.
305. Hirt, M.N., et al., *Functional improvement and maturation of rat and human engineered heart tissue by chronic electrical stimulation.* J Mol Cell Cardiol, 2014. **74C**: p. 151-161.
306. Korte, F.S., et al., *Upregulation of cardiomyocyte ribonucleotide reductase increases intracellular 2 deoxy-ATP, contractility, and relaxation.* J Mol Cell Cardiol, 2011. **51**(6): p. 894-901.
307. Nowakowski, S.G., et al., *Transgenic overexpression of ribonucleotide reductase improves cardiac performance.* Proc Natl Acad Sci U S A, 2013. **110**(15): p. 6187-92.
308. Lee, Y.K., et al., *Triiodothyronine promotes cardiac differentiation and maturation of embryonic stem cells via the classical genomic pathway.* Mol Endocrinol, 2010. **24**(9): p. 1728-36.
309. Nunes, S.S., et al., *Biowire: a platform for maturation of human pluripotent stem cell-derived cardiomyocytes.* Nat Methods, 2013. **10**(8): p. 781-7.
310. Zimmermann, W.H., et al., *Tissue engineering of a differentiated cardiac muscle construct.* Circ Res, 2002. **90**(2): p. 223-30.
311. Gopalan, S.M., et al., *Anisotropic stretch-induced hypertrophy in neonatal ventricular myocytes micropatterned on deformable elastomers.* Biotechnol Bioeng, 2003. **81**(5): p. 578-87.

312. Kandow, C.E., et al., *Polyacrylamide hydrogels for cell mechanics: steps toward optimization and alternative uses.* Methods Cell Biol, 2007. **83**: p. 29-46.
313. Pelham, R.J., Jr. and Y. Wang, *Cell locomotion and focal adhesions are regulated by substrate flexibility.* Proc Natl Acad Sci U S A, 1997. **94**(25): p. 13661-5.
314. Tse, J.R. and A.J. Engler, *Preparation of hydrogel substrates with tunable mechanical properties.* Curr Protoc Cell Biol, 2010. **Chapter 10**: p. Unit 10 16.
315. Saha, K., et al., *Surface creasing instability of soft polyacrylamide cell culture substrates.* Biophys J, 2010. **99**(12): p. L94-6.
316. Hersch, N., et al., *The constant beat: cardiomyocytes adapt their forces by equal contraction upon environmental stiffening.* Biol Open, 2013. **2**(3): p. 351-61.
317. Palchesko, R.N., et al., *Development of polydimethylsiloxane substrates with tunable elastic modulus to study cell mechanobiology in muscle and nerve.* PLoS One, 2012. **7**(12): p. e51499.
318. Li, Y., et al., *Engineering cell alignment in vitro.* Biotechnol Adv, 2014. **32**(2): p. 347-65.
319. Matsuda, T., et al., *N-cadherin-mediated cell adhesion determines the plasticity for cell alignment in response to mechanical stretch in cultured cardiomyocytes.* Biochem Biophys Res Commun, 2005. **326**(1): p. 228-32.
320. Au, H.T., et al., *Interactive effects of surface topography and pulsatile electrical field stimulation on orientation and elongation of fibroblasts and cardiomyocytes.* Biomaterials, 2007. **28**(29): p. 4277-93.
321. Legant, W.R., C.S. Chen, and V. Vogel, *Force-induced fibronectin assembly and matrix remodeling in a 3D microtissue model of tissue morphogenesis.* Integr Biol (Camb), 2012. **4**(10): p. 1164-74.
322. Schaaf, S., et al., *Human engineered heart tissue as a versatile tool in basic research and preclinical toxicology.* PLoS One, 2011. **6**(10): p. e26397.
323. Salick, M.R., et al., *Micropattern width dependent sarcomere development in human ESC-derived cardiomyocytes.* Biomaterials, 2014. **35**(15): p. 4454-64.
324. Khademhosseini, A., et al., *Microfluidic patterning for fabrication of contractile cardiac organoids.* Biomedical Microdevices, 2007. **9**(2): p. 149-157.
325. Wang, P.Y., et al., *Modulation of alignment, elongation and contraction of cardiomyocytes through a combination of nanotopography and rigidity of substrates.* Acta Biomater, 2011. **7**(9): p. 3285-93.
326. Motlagh, D., et al., *Microfabricated grooves recapitulate neonatal myocyte connexin43 and N-cadherin expression and localization.* J Biomed Mater Res A, 2003. **67**(1): p. 148-57.
327. den Braber, E.T., et al., *Orientation of ECM protein deposition, fibroblast cytoskeleton, and attachment complex components on silicone microgrooved surfaces.* Journal of Biomedical Materials Research, 1998. **40**(2): p. 291-300.
328. denBraber, E.T., et al., *Quantitative analysis of fibroblast morphology on microgrooved surfaces with various groove and ridge dimensions.* Biomaterials, 1996. **17**(21): p. 2037-2044.
329. Tandon, N., et al., *Optimization of electrical stimulation parameters for cardiac tissue engineering.* Journal of Tissue Engineering and Regenerative Medicine, 2011. **5**(6): p. E115-E125.

330. Beauchamp, P., et al., *Electrical coupling and propagation in engineered ventricular myocardium with heterogeneous expression of connexin43.* Circulation Research, 2012. **110**(11): p. 1445-53.
331. McCain, M.L., et al., *Cell-to-cell coupling in engineered pairs of rat ventricular cardiomyocytes: relation between Cx43 immunofluorescence and intercellular electrical conductance.* Am J Physiol Heart Circ Physiol, 2012. **302**(2): p. H443-50.
332. Ma, Z., et al., *Cardiogenic Regulation of Stem-Cell Electrical Properties in a Laser-Patterned Biochip.* Cell Mol Bioeng, 2012. **5**(3): p. 327-336.
333. Legrice, I.J., Y. Takayama, and J.W. Covell, *Transverse-Shear Along Myocardial Cleavage Planes Provides a Mechanism for Normal Systolic Wall Thickening.* Circulation Research, 1995. **77**(1): p. 182-193.
334. Tung, L., N. Sliz, and M.R. Mulligan, *Influence of Electrical Axis of Stimulation on Excitation of Cardiac-Muscle-Cells.* Circulation Research, 1991. **69**(3): p. 722-730.
335. Barash, Y., et al., *Electric Field Stimulation Integrated into Perfusion Bioreactor for Cardiac Tissue Engineering.* Tissue Engineering Part C-Methods, 2010. **16**(6): p. 1417-1426.
336. Pillekamp, F., et al., *Contractile properties of early human embryonic stem cell-derived cardiomyocytes: beta-adrenergic stimulation induces positive chronotropy and lusitropy but not inotropy.* Stem Cells and Development, 2012. **21**(12): p. 2111-21.
337. Kujala, K., et al., *Electrical Field Stimulation with a Novel Platform: Effect on Cardiomyocyte Gene Expression but not on Orientation.* Int J Biomed Sci, 2012. **8**(2): p. 109-20.
338. Wharton, J.M., et al., *Electrophysiological effects of monophasic and biphasic stimuli in normal and infarcted dogs.* Pacing Clin Electrophysiol, 1990. **13**(9): p. 1158-72.
339. Flaker, G.C., et al., *Superiority of biphasic shocks in the defibrillation of dogs by epicardial patches and catheter electrodes.* Am Heart J, 1989. **118**(2): p. 288-91.
340. Tung, L. and J.R. Borderies, *Analysis of electric field stimulation of single cardiac muscle cells.* Biophys J, 1992. **63**(2): p. 371-86.
341. Kavanagh, K.M., et al., *Monophasic versus biphasic cardiac stimulation: mechanism of decreased energy requirements.* Pacing Clin Electrophysiol, 1990. **13**(10): p. 1268-76.
342. Zhu, W.Z., B. Van Biber, and M.A. Laflamme, *Methods for the derivation and use of cardiomyocytes from human pluripotent stem cells*, in *Human Pluripotent Stem Cells: Methods and Protocols*, J.M. Walker, Editor 2011, Humana Press: New York, NY.
343. Desai, R.A., N.M. Rodriguez, and C.S. Chen, *"Stamp-off" to micropattern sparse, multicomponent features.* Methods Cell Biol, 2014. **119**: p. 3-16.
344. Park, H., et al., *Biomimetic scaffold combined with electrical stimulation and growth factor promotes tissue engineered cardiac development.* Exp Cell Res, 2014. **321**(2): p. 297-306.
345. Brady, A.J., S.T. Tan, and N.V. Ricchiuti, *Contractile force measured in unskinned isolated adult rat heart fibres.* Nature, 1979. **282**(5740): p. 728-9.
346. Tasche, C., E. Meyhofer, and B. Brenner, *A force transducer for measuring mechanical properties of single cardiac myocytes.* American Journal of Physiology-Heart and Circulatory Physiology, 1999. **277**(6): p. H2400-H2408.
347. New, R.B., et al., *Isolated left ventricular myocyte contractility in patients undergoing cardiac operations.* J Thorac Cardiovasc Surg, 1998. **116**(3): p. 495-502.
348. Lin, G., et al., *Miniature heart cell force transducer system implemented in MEMS technology.* IEEE Trans Biomed Eng, 2001. **48**(9): p. 996-1006.

349. Weng, S. and J. Fu, *Synergistic regulation of cell function by matrix rigidity and adhesive pattern.* Biomaterials, 2011. **32**(36): p. 9584-93.
350. Majkut, S.F. and D.E. Discher, *Cardiomyocytes from late embryos and neonates do optimal work and striate best on substrates with tissue-level elasticity: metrics and mathematics.* Biomech Model Mechanobiol, 2012. **11**(8): p. 1219-25.
351. Berry, M.F., et al., *Mesenchymal stem cell injection after myocardial infarction improves myocardial compliance.* Am J Physiol Heart Circ Physiol, 2006. **290**(6): p. H2196-203.
352. McCain, M.L., et al., *Cooperative coupling of cell-matrix and cell-cell adhesions in cardiac muscle.* Proc Natl Acad Sci U S A, 2012. **109**(25): p. 9881-6.
353. Sheehy, S.P., A. Grosberg, and K.K. Parker, *The contribution of cellular mechanotransduction to cardiomyocyte form and function.* Biomech Model Mechanobiol, 2012. **11**(8): p. 1227-39.
354. Maillet, M., J.H. van Berlo, and J.D. Molkentin, *Molecular basis of physiological heart growth: fundamental concepts and new players.* Nat Rev Mol Cell Biol, 2013. **14**(1): p. 38-48.
355. Forte, G., et al., *Substrate stiffness modulates gene expression and phenotype in neonatal cardiomyocytes in vitro.* Tissue Eng Part A, 2012. **18**(17-18): p. 1837-48.
356. Chopra, A., et al., *Cardiac myocyte remodeling mediated by N-cadherin-dependent mechanosensing.* American Journal of Physiology-Heart and Circulatory Physiology, 2011. **300**(4): p. H1252-H1266.
357. Chopra, A., et al., *alpha-Catenin localization and sarcomere self-organization on N-cadherin adhesive patterns are myocyte contractility driven.* PLoS One, 2012. **7**(10): p. e47592.
358. Georges, P.C. and P.A. Janmey, *Cell type-specific response to growth on soft materials.* J Appl Physiol (1985), 2005. **98**(4): p. 1547-53.
359. Herron, T.J., P. Lee, and J. Jalife, *Optical imaging of voltage and calcium in cardiac cells & tissues.* Circulation Research, 2012. **110**(4): p. 609-23.
360. van Spreeuwel, A.C., et al., *The influence of matrix (an)isotropy on cardiomyocyte contraction in engineered cardiac microtissues.* Integr Biol (Camb), 2014. **6**(4): p. 422-9.
361. Gerdes, A.M., *Cardiac myocyte remodeling in hypertrophy and progression to failure.* Journal of Cardiac Failure, 2002. **8**(6): p. S264-S268.
362. Gerdes, A.M. and J.M. Capasso, *Structural remodeling and mechanical dysfunction of cardiac myocytes in heart failure.* J Mol Cell Cardiol, 1995. **27**(3): p. 849-56.
363. Yasui, K., et al., *Cell-to-cell interaction prevents cell death in cultured neonatal rat ventricular myocytes.* Cardiovasc Res, 2000. **48**(1): p. 68-76.
364. Reaume, A.G., et al., *Cardiac malformation in neonatal mice lacking connexin43.* Science, 1995. **267**(5205): p. 1831-4.
365. Yamamoto, S., et al., *Spontaneous death of isolated adult rat cardiocytes in culture in association with internucleosomal cleavage of genomic DNA.* Apoptosis, 1997. **2**(2): p. 178-88.
366. Tang, X., et al., *How far cardiac cells can see each other mechanically.* Soft Matter, 2011. **7**(13): p. 6151-6158.
367. Hershman, K.M. and E.S. Levitan, *Cell-cell contact between adult rat cardiac myocytes regulates Kv1.5 and Kv4.2 K+ channel mRNA expression.* Am J Physiol, 1998. **275**(6 Pt 1): p. C1473-80.

368. Pedrotty, D.M., et al., *Structural coupling of cardiomyocytes and noncardiomyocytes: quantitative comparisons using a novel micropatterned cell pair assay.* Am J Physiol Heart Circ Physiol, 2008. **295**(1): p. H390-400.
369. Luo, Y. and G.L. Radice, *Cadherin-mediated adhesion is essential for myofibril continuity across the plasma membrane but not for assembly of the contractile apparatus.* Journal of Cell Science, 2003. **116**(8): p. 1471-1479.
370. Mezzano, V., J. Pellman, and F. Sheikh, *Cell junctions in the specialized conduction system of the heart.* Cell Commun Adhes, 2014. **21**(3): p. 149-59.
371. Garrod, D. and M. Chidgey, *Desmosome structure, composition and function.* Biochim Biophys Acta, 2008. **1778**(3): p. 572-87.
372. Howard, C.M. and T.A. Baudino, *Dynamic cell-cell and cell-ECM interactions in the heart.* J Mol Cell Cardiol, 2014. **70**: p. 19-26.
373. Eppenberger, H.M. and C. Zuppinger, *In vitro reestablishment of cell-cell contacts in adult rat cardiomyocytes. Functional role of transmembrane components in the formation of new intercalated disk-like cell contacts.* Faseb Journal, 1999. **13**: p. S83-S89.
374. Geisler, S.B., et al., *Ordered Assembly of the Adhesive and Electrochemical Connections within Newly Formed Intercalated Disks in Primary Cultures of Adult Rat Cardiomyocytes.* Journal of Biomedicine and Biotechnology, 2010.
375. Matsuda, T., et al., *N-cadherin signals through Rac1 determine the localization of connexin 43 in cardiac myocytes.* J Mol Cell Cardiol, 2006. **40**(4): p. 495-502.
376. Kostin, S., et al., *Spatiotemporal development and distribution of intercellular junctions in adult rat cardiomyocytes in culture.* Circulation Research, 1999. **85**(2): p. 154-67.
377. Kostetskii, I., et al., *Induced deletion of the N-cadherin gene in the heart leads to dissolution of the intercalated disc structure.* Circulation Research, 2005. **96**(3): p. 346-354.
378. Hertig, C.M., et al., *N-cadherin in adult rat cardiomyocytes in culture. I. Functional role of N-cadherin and impairment of cell-cell contact by a truncated N-cadherin mutant.* Journal of Cell Science, 1996. **109 (Pt 1)**: p. 1-10.
379. Delmar, M. and W.J. McKenna, *The cardiac desmosome and arrhythmogenic cardiomyopathies: from gene to disease.* Circulation Research, 2010. **107**(6): p. 700-14.
380. Luna, J.I., et al., *Multiscale biomimetic topography for the alignment of neonatal and embryonic stem cell-derived heart cells.* Tissue Eng Part C Methods, 2011. **17**(5): p. 579-88.
381. Kruger, M., et al., *Thyroid hormone regulates developmental titin isoform transitions via the phosphatidylinositol-3-kinase/ AKT pathway.* Circ Res, 2008. **102**(4): p. 439-47.
382. Klein, I. and K. Ojamaa, *Thyroid hormone and the cardiovascular system.* N Engl J Med, 2001. **344**(7): p. 501-9.
383. Dillmann, W.H., *Cellular action of thyroid hormone on the heart.* Thyroid, 2002. **12**(6): p. 447-52.
384. Chattergoon, N.N., et al., *Thyroid hormone drives fetal cardiomyocyte maturation.* FASEB J, 2012. **26**(1): p. 397-408.
385. Makinde, A.O., P.F. Kantor, and G.D. Lopaschuk, *Maturation of fatty acid and carbohydrate metabolism in the newborn heart.* Mol Cell Biochem, 1998. **188**(1-2): p. 49-56.
386. Zaha, V.G. and L.H. Young, *AMP-activated protein kinase regulation and biological actions in the heart.* Circ Res, 2012. **111**(6): p. 800-14.

387. Makinde, A.O., J. Gamble, and G.D. Lopaschuk, *Upregulation of 5'-AMP-activated protein kinase is responsible for the increase in myocardial fatty acid oxidation rates following birth in the newborn rabbit.* Circ Res, 1997. **80**(4): p. 482-9.
388. Hu, X., et al., *AMP activated protein kinase-alpha2 regulates expression of estrogen-related receptor-alpha, a metabolic transcription factor related to heart failure development.* Hypertension, 2011. **58**(4): p. 696-703.
389. Ventura-Clapier, R., A. Garnier, and V. Veksler, *Transcriptional control of mitochondrial biogenesis: the central role of PGC-1alpha.* Cardiovasc Res, 2008. **79**(2): p. 208-17.
390. Adam, T., L.H. Opie, and M.F. Essop, *AMPK activation represses the human gene promoter of the cardiac isoform of acetyl-CoA carboxylase: Role of nuclear respiratory factor-1.* Biochem Biophys Res Commun, 2010. **398**(3): p. 495-9.
391. Terai, K., et al., *AMP-activated protein kinase protects cardiomyocytes against hypoxic injury through attenuation of endoplasmic reticulum stress.* Mol Cell Biol, 2005. **25**(21): p. 9554-75.
392. Stuck, B.J., et al., *Metabolic switch and hypertrophy of cardiomyocytes following treatment with angiotensin II are prevented by AMP-activated protein kinase.* J Biol Chem, 2008. **283**(47): p. 32562-9.
393. Rodriguez, M.L., et al., *Measuring the Contractile Forces of Human Induced Pluripotent Stem Cell-Derived Cardiomyocytes with Arrays of Microposts.* J Biomechanical Engineering, 2014.
394. Yang, X., et al., *Tri-iodo-l-thyronine promotes the maturation of human cardiomyocytes-derived from induced pluripotent stem cells.* J Mol Cell Cardiol, 2014. **72**: p. 296-304.
395. Oliveira, S.M., et al., *AMP-activated protein kinase phosphorylates cardiac troponin I and alters contractility of murine ventricular myocytes.* Circ Res, 2012. **110**(9): p. 1192-201.
396. Nixon, B.R., et al., *AMP-activated protein kinase phosphorylates cardiac troponin I at Ser-150 to increase myofilament calcium sensitivity and blunt PKA-dependent function.* J Biol Chem, 2012. **287**(23): p. 19136-47.
397. Rog-Zielinska, E.A., et al., *Glucocorticoids promote structural and functional maturation of foetal cardiomyocytes: a role for PGC-1alpha.* Cell Death Differ, 2014.
398. Montessuit, C., et al., *Effects of insulin-like growth factor-I on the maturation of metabolism in neonatal rat cardiomyocytes.* Pflugers Arch, 2006. **452**(4): p. 380-6.
399. Ito, H., et al., *Insulin-like growth factor-I induces hypertrophy with enhanced expression of muscle specific genes in cultured rat cardiomyocytes.* Circulation, 1993. **87**(5): p. 1715-21.
400. Xia, Y., et al., *Electrical stimulation of neonatal cardiomyocytes results in the sequential activation of nuclear genes governing mitochondrial proliferation and differentiation.* Proc Natl Acad Sci U S A, 1997. **94**(21): p. 11399-404.
401. Lasher, R.A., et al., *Electrical stimulation directs engineered cardiac tissue to an age-matched native phenotype.* J Tissue Eng, 2012. **3**(1): p. 2041731412455354.
402. Fu, J.D., et al., *Distinct roles of microRNA-1 and -499 in ventricular specification and functional maturation of human embryonic stem cell-derived cardiomyocytes.* PLoS One, 2011. **6**(11): p. e27417.
403. Callis, T.E., et al., *MicroRNA-208a is a regulator of cardiac hypertrophy and conduction in mice.* J Clin Invest, 2009. **119**(9): p. 2772-86.
404. van Rooij, E., et al., *Control of stress-dependent cardiac growth and gene expression by a microRNA.* Science, 2007. **316**(5824): p. 575-9.

405. Tulloch, N.L., et al., *Growth of engineered human myocardium with mechanical loading and vascular coculture.* Circ Res, 2011. **109**(1): p. 47-59.
406. Serradifalco, C., G. Zummo, and V. Di Felice, *MicroRNA and Cardiac Stem Cell Therapy.* J Clin Exp Cardiolog, 2012. **11**.
407. Wilson, K.D., et al., *Dynamic microRNA expression programs during cardiac differentiation of human embryonic stem cells: role for miR-499.* Circ Cardiovasc Genet, 2010. **3**(5): p. 426-35.
408. Gan, L., S. Schwengberg, and B. Denecke, *MicroRNA profiling during cardiomyocyte-specific differentiation of murine embryonic stem cells based on two different miRNA array platforms.* PLoS One, 2011. **6**(10): p. e25809.
409. Espinoza-Lewis, R.A. and D.Z. Wang, *MicroRNAs in heart development.* Curr Top Dev Biol, 2012. **100**: p. 279-317.
410. Burridge, P.W., et al., *Production of de novo cardiomyocytes: human pluripotent stem cell differentiation and direct reprogramming.* Cell Stem Cell, 2012. **10**(1): p. 16-28.
411. Beqqali, A., et al., *Genome-wide transcriptional profiling of human embryonic stem cells differentiating to cardiomyocytes.* Stem Cells, 2006. **24**(8): p. 1956-67.
412. Davis, R.P., et al., *Pluripotent stem cell models of cardiac disease and their implication for drug discovery and development.* Trends Mol Med, 2011. **17**(9): p. 475-84.
413. Cameron, I.L., et al., *Environmental magnetic fields: influences on early embryogenesis.* J Cell Biochem, 1993. **51**(4): p. 417-25.
414. Berger, H.J., et al., *Continual electric field stimulation preserves contractile function of adult ventricular myocytes in primary culture.* Am J Physiol, 1994. **266**(1 Pt 2): p. H341-9.
415. Maron, B.J., et al., *Prevalence of hypertrophic cardiomyopathy in a general population of young adults. Echocardiographic analysis of 4111 subjects in the CARDIA Study. Coronary Artery Risk Development in (Young) Adults.* Circulation, 1995. **92**(4): p. 785-9.
416. Maron, B.J. and A. Pelliccia, *The heart of trained athletes: cardiac remodeling and the risks of sports, including sudden death.* Circulation, 2006. **114**(15): p. 1633-44.
417. Wang, L., J.G. Seidman, and C.E. Seidman, *Narrative review: harnessing molecular genetics for the diagnosis and management of hypertrophic cardiomyopathy.* Ann Intern Med, 2010. **152**(8): p. 513-20, W181.
418. Marian, A.J., *Pathogenesis of diverse clinical and pathological phenotypes in hypertrophic cardiomyopathy.* Lancet, 2000. **355**(9197): p. 58-60.
419. Lan, F., et al., *Abnormal calcium handling properties underlie familial hypertrophic cardiomyopathy pathology in patient-specific induced pluripotent stem cells.* Cell Stem Cell, 2013. **12**(1): p. 101-13.
420. Okita, K., et al., *A more efficient method to generate integration-free human iPS cells.* Nat Methods, 2011. **8**(5): p. 409-12.
421. Regnier, M. and E. Homsher, *The effect of ATP analogs on posthydrolytic and force development steps in skinned skeletal muscle fibers.* Biophys J, 1998. **74**(6): p. 3059-71.
422. Regnier, M., D.M. Lee, and E. Homsher, *ATP analogs and muscle contraction: mechanics and kinetics of nucleoside triphosphate binding and hydrolysis.* Biophys J, 1998. **74**(6): p. 3044-58.
423. Regnier, M., D.A. Martyn, and P.B. Chase, *Calcium regulation of tension redevelopment kinetics with 2-deoxy-ATP or low [ATP] in rabbit skeletal muscle.* Biophys J, 1998. **74**(4): p. 2005-15.

424. Regnier, M., et al., *2-deoxy-ATP enhances contractility of rat cardiac muscle.* Circ Res, 2000. **86**(12): p. 1211-7.
425. Wang, N., J.P. Butler, and D.E. Ingber, *Mechanotransduction across the cell surface and through the cytoskeleton.* Science, 1993. **260**(5111): p. 1124-7.
426. Frank, D., et al., *Gene expression pattern in biomechanically stretched cardiomyocytes: evidence for a stretch-specific gene program.* Hypertension, 2008. **51**(2): p. 309-18.
427. Maniotis, A.J., C.S. Chen, and D.E. Ingber, *Demonstration of mechanical connections between integrins, cytoskeletal filaments, and nucleoplasm that stabilize nuclear structure.* Proc Natl Acad Sci U S A, 1997. **94**(3): p. 849-54.
428. Bray, M.A., et al., *Nuclear morphology and deformation in engineered cardiac myocytes and tissues.* Biomaterials, 2010. **31**(19): p. 5143-50.
429. Saffitz, J.E. and A.G. Kleber, *Effects of mechanical forces and mediators of hypertrophy on remodeling of gap junctions in the heart.* Circ Res, 2004. **94**(5): p. 585-91.
430. Shanker, A.J., et al., *Matrix-protein-specific regulation of Cx43 expression in cardiac myocytes subjected to mechanical load.* Circ Res, 2005. **96**(5): p. 558-66.
431. Salameh, A., et al., *Cyclic mechanical stretch induces cardiomyocyte orientation and polarization of the gap junction protein connexin43.* Circ Res, 2010. **106**(10): p. 1592-602.
432. Yamada, K., et al., *Distinct pathways regulate expression of cardiac electrical and mechanical junction proteins in response to stretch.* Circ Res, 2005. **97**(4): p. 346-53.
433. Kensah, G., et al., *A Novel Miniaturized Multimodal Bioreactor for Continuous In Situ Assessment of Bioartificial Cardiac Tissue During Stimulation and Maturation.* Tissue Engineering, 2011. **17**(4): p. 463-473.
434. Schmelter, M., et al., *Embryonic stem cells utilize reactive oxygen species as transducers of mechanical strain-induced cardiovascular differentiation.* FASEB J, 2006. **20**(8): p. 1182-4.
435. Akhyari, P., et al., *Mechanical stretch regimen enhances the formation of bioengineered autologous cardiac muscle grafts.* Circulation, 2002. **106**(12 Suppl 1): p. I137-42.